AN INVESTIGATION INTO THE REACTIVITY AND ELECTROCHEMICAL PROPERTIES OF "HIGHER" NUCLEARITY CLUSTERS WITH NITROGEN HETEROCYCLIC LIGANDS - A CHEMICAL, ELECTROCHEMICAL AND SPECTROSCOPIC STUDY.

by Gideon Freeman

A thesis submitted for the Degree of Doctor of Philosophy.

The University of Edinburgh 1995.

Declaration

The research described herein was conducted by the author at The Department of Chemistry, The University of Edinburgh, between the dates of October 1992 and May 1995. It is the author's original work unless specific reference is made to the contrary. None of the work described herein has been submitted for a degree at any other institution.

Gideon Freeman.

To my late nana, whose pride in me meant so much.

I will never forget you.

ABSTRACT

In Chapter One we discuss the concept of the surface cluster analogy and give examples of its application in resolving the nature of chemisorbed molecules and molecular fragments on metal surfaces. This is then followed by a comprehensive review of previous studies into the reactivity of metal carbonyl clusters with nitrogen heterocyclic ligands. This highlights the substitution of carbonyl ligands for nitrogen heterocycles and the process of *ortho*metallation, and emphasises how earlier work has typically concentrated on the trinuclear clusters, with examples involving higher nuclearities being rare. Consequently the need to study such cluster's reactivity further is made apparent.

The second chapter details the synthesis of a series of disubstituted tetranuclear clusters of the general formula $M_4(\mu\text{-}H)_4(CO)_{10}(L\text{-}L)$ {M= Ru, Os; L-L= bidentate nitrogen heterocyclic ligand or $(pyridine)_2$} which have been prepared from the reaction between the parent cluster $M_4(\mu\text{-}H)_4(CO)_{12}$ and principally 2.2 equivalents of the decarbonylating reagent Me_3NO. Our studies have shown that disubstitution of the cluster is favoured whether 1.1, 2.2, or 4.2 equivalents of Me_3NO are used, and thus implies the inherent stability of the $M_4(\mu\text{-}H)_4(CO)_{10}(L\text{-}L)$ species. In particular, it is found that in its reaction with pyridine and 1.1 equivalents of Me_3NO the $M_4(\mu\text{-}H)_4(CO)_{10}(py)_2$ cluster is formed as the major product, being present in a significantly higher yield than the expected monosubstituted derivative. This reactivity is accounted for mechanistically by comparison with similarly observed substitution patterns for the $Ir_4(CO)_{12}$ cluster. Full X-ray and spectroscopic analyses are discussed in detail.

In Chapter Three the previous work of Dutton into thermal activation of the Ru_5 cluster, primarily with pyridine, is discussed and contrasted to the chemical activation process using Me_3NO utilised in this study. The $Ru_5C(CO)_{15}$ cluster has been found to react in the presence of 2.2 equivalents of Me_3NO with both 2,2'-bipyridyl and 1,10-phenanthroline to yield the $Ru_5C(CO)_{14}(L\text{-}L)$ product as the major product. Hence loss of only a single carbonyl ligand occurs to yield a 76 e bridged butterfly cluster which has been characterised both spectroscopically and by single

crystal X-ray diffraction. When a second carbonyl ligand is removed from the cluster the *ortho*metallated species $Ru_5(\mu\text{-}H)C(CO)_{13}(L\text{-}L)$ is produced, but in relatively lower yield. Again this species has been characterised by spectroscopy, and in addition for the 2,2'-bipyridyl derivative, by X-ray crystallography. In addition, it has been discovered that the $Ru_6C(CO)_{17}$ cluster undergoes cluster degradation in the presence of 2,2'-bipyridyl or 1,10-phenathroline and 2.2 equivalents of Me_3NO with the loss of an $Ru(CO)_3$ fragment in the formation of the $Ru_5C(CO)_{14}(L\text{-}L)$ cluster, which had been previously prepared directly from the $Ru_5C(CO)_{15}$ cluster. Also produced in comparable yield was the expected Ru_6 species $Ru_6C(CO)_{15}(L\text{-}L)$ which is relatively unstable and decomposes over time.

Chapter Four is concerned with the a discussion of the photochemical, electrochemical and spectroelectrochemical properties of the $Ru_4(\mu\text{-}H)_4(CO)_{10}(L\text{-}L)$ clusters discussed in Chapter Two. It has been shown that these clusters undergo a one electron reduction which is based on a predominantly ligand based orbital. The radical anion so produced is comparatively stable at room temperature for the $Ru_4(\mu\text{-}H)_4(CO)_{10}$(bpm) and $Ru_4(\mu\text{-}H)_4(CO)_{10}$(bpp) clusters which are found to slowly convert to an unidentified species whose IR spectrum indicates the presence of bridging carbonyl ligands. The 2,2'-bipyridyl species was however found to be less stable on reduction and is transformed rapidly to a species showing bridging carbonyl ligands.

Finally, Chapter Five details the experimental equipment and procedures used to carry out this research.

Glossary of Abbreviations

IR	Infra Red
ν(CO)	carbonyl stretching frequency
v	very
w	weak
m	medium
s	strong
br	broad
sh	shoulder
cm^{-1}	wavenumbers
MS	mass spectrum
amu	atomic mass units
NMR	Nuclear Magnetic Resonance
COSY	Correlation Spectroscopy
nOe	nuclear Overhauser effect
s	singlet
d	doublet
t	triplet
m	multiplet
δ	chemical shift
ppm	parts per million
J	coupling constant
Hz	hertz
EPR	Electron Paramagnetic Resonance
DPPH	2,2'-diphenyl-1-picrylhydrazyl
UV/Vis	Ultra Violet / Visible
ε	molar extinction coefficient
HOMO	Highest Occupied Molecular Orbital
LUMO	Lowest Occupied Molecular Orbital
OTTLE	Optically Transparent Thin Layer Electrode
tlc	thin layer chromatography
py	pyridine
bipy	2,2'-bipyridyl
phen	1,10-phenanthroline
dmp	2,9-dimethyl-1,10-phenanthroline
bpm	2,2'-bipyrimidine
bpp	2,3-*bis*(2-pyridyl)pyrazine
TBA	tertiary butyl ammonium
Å	Angstrom ($x10^{-10}m$)

Numbering of Compounds

$Ru_4(\mu\text{-}H)_4(CO)_{12}$	**1**
$Os_4(\mu\text{-}H)_4(CO)_{12}$	**2**
$Ru_4(\mu\text{-}H)_4(CO)_{11}(py)$	**3**
$Ru_4(\mu\text{-}H)_4(CO)_{10}(py)_2$	**4**
$Ru_4(\mu\text{-}H)_4(CO)_{10}(bipy)$	**5**
$Ru_4(\mu\text{-}H)_4(CO)_{10}(phen)$	**6**
$Ru_4(\mu\text{-}H)_4(CO)_{10}(dmp)$	**7**
$Ru_4(\mu\text{-}H)_4(CO)_{11}(bpm)$	**8**
$Ru_4(\mu\text{-}H)_4(CO)_{10}(bpm)$	**9**
$Ru_4(\mu\text{-}H)_4(CO)_{10}(bpp)$	**10**
$Os_4(\mu\text{-}H)_4(CO)_{10}(MeCN)_2$	**11**
$Os_4(\mu\text{-}H)_4(CO)_{11}(py)$	**12**
$Os_4(\mu\text{-}H)_4(CO)_{10}(py)_2$	**13**
$Os_4(\mu\text{-}H)_4(CO)_{11}(MeCN)$	**14**
$Os_4(\mu\text{-}H)_4(CO)_{10}(bipy)$	**15**
$Os_4(\mu\text{-}H)_4(CO)_{10}(phen)$	**16**
$Ru_5C(CO)_{15}$	**17**
$Ru_5(\mu\text{-}H)C(CO)_{14}(C_5H_4N)$	**18**
$Ru_5(\mu\text{-}H)C(CO)_{13}(C_5H_4N)(py)$	**19**
$Ru_5(\mu\text{-}H)C(CO)_{13}(C_5H_4N)$	**20**
$Ru_5(\mu\text{-}H)C(CO)_{12}(C_5H_4N)(py)$	**21**
"$Ru_5C(CO)_{13}(bipy)$"	**22**
$Ru_5C(CO)_{14}(bipy)$	**23**
$Ru_5(\mu\text{-}H)C(CO)_{13}(C_{10}H_7N_2)$	**24**
$Ru_5C(CO)_{14}(phen)$	**25**
$Ru_5(\mu\text{-}H)C(CO)_{13}(C_{12}H_7N_2)$	**26**
$Ru_6C(CO)_{17}$	**27**
$Ru_6C(CO)_{15}(bipy)$	**28**
$Ru_6C(CO)_{15}(phen)$	**29**

Acknowledgements

I have probably had more fun over the past three years than at any other time in my life, and I would like to thank in part Professor Brian Johnson for making this financially possible. I am also extremely grateful for the opportunity he gave me to study for a Ph.D. and for the enthusiasm he has shown over the past 3 years. Thanks also to my friends with whom I have shared so many happy and memorable times.

The past three years have not always been easy, but I have been fortunate enough to work alongside some talented people and be part of a supportive and friendly lab, to which I hope I have contributed as well as gained. Thanks in particular to Scott for improving the running of the lab and my knowledge of chemistry, and also to Jane, Tom, Ali, Nick, Garry, Lesley, Ruth, Vlad, and Ros for their help, encouragement, and friendship.

During my research I have had the privilege to call on the expertise of many people. For help in refining the crystal structures discussed in Chapter Two I would like to thank Dr. Scott Ingham, who in addition has been responsible for solving the $Ru_5C(CO)_{14}$(L-L) structures discussed in Chapter Three. Also thanks to Drs. Sandy Blake and Simon Parsons for the data collection for these structures, and to Dr. Ian Scowen (University of North London) for determining the crystal structure of the $Ru_5(\mu\text{-H})C(CO)_{13}$(bipy) cluster. I owe many thanks to Dr. Lesley Yellowlees, for not only proof reading this thesis but also for her boundless energy and enthusiasm in our discussions of the electrochemical results- thank you for making everything seem so much clearer. Thank you also to Dr. Frantisek Hartl and Maarten Baaker (University of Amsterdam) for their help during my visit to The Netherlands, and for their collaboration on the IR spectroelectrochemical studies presented in Chapter Four. I appreciate the efforts of all of the technical staff, but would particularly like to thank John Millar and Wesley Kerr for running the NMR experiments presented in this thesis.

Finally I would like to thank my family, particularly my mum and late nana, for their support and encouragement, not only over the last 7 years at university but throughout my life. I am exceptionally grateful to you both.

Always Look on the Bright Side of Life

Some things in life are bad,
They can really make you mad,
Other things just make you swear and curse.
When you're chewing on life's gristle
Don't grumble, give a whistle.
And this'll help things turn out for the best.

And....

Always look on the bright side of life, (whistle)
Always look on the bright side of life, (whistle)
If life seems jolly rotten,
There's something you've forgotten,
And that's to laugh and smile and dance and sing.
When you're feeling in the dumps,
Don't be silly chumps.
Just purse your lips and whistle, that's the thing.

And...

Always look on the bright side of life. (whistle)
Come on...
Always look on the bright side of life...

Come on guys, cheer up.

Always look on the bright side of life.

Monty Python, *"Life of Brian"*

Chapter One

1.1 Introduction

The term *cluster* is commonly defined as a metal complex with two or more metal atoms mutually bonded to each other. As such, the first clusters to be identified were metal chloro- salts of the type $W_2Cl_9^{3-}$ and $Re_3Cl_{12}^{3-}$ which led to the realisation of the existence of metal-metal bonds within complexes. A second class of clusters : the metal carbonyls, were later discovered with the emergence of the X-ray structural characterisation of $Fe_2(CO)_9$ in 1939, [1,2] and later the characterisation of $Mn_2(CO)_{10}$ in 1963, [3] which represented the first example of an unsupported metal-metal bond in this area of chemistry. Interest in the subject grew with the possibility of producing new structural types, and this area developed further with effort being focused on the reactivity of these species with small organic molecules *e.g.* alkynes, alkenes, arenes to form a large number of compounds, the nature of whose ligand co-ordinations were precisely defined by solid state X-ray molecular structures. Muetterties [4] postulated that these bonding modes may not be too dissimilar to those observed on metal surfaces as found in catalysts, and hence this led to their proposition as possible models for catalysis and chemisorption, and became known as the Surface Cluster Analogy.

1.2 The Surface Cluster Analogy

Although metal carbonyl clusters have been found to act as catalysts [5] for example $[Fe(\mu_3\text{-}CO)\ (\eta^5\text{-}C_5H_5)]_4$ in the hydrogenation of alkynes to alkenes, and $Ru_3(CO)_{12}$ in the water gas shift reaction, they have not to date found major industrial application. The analogy of clusters as models for catalysis is now no longer regarded as totally plausible, although as a model of chemisorption it has been widely applied. Indeed, a few years after his original proposal, Muetterties [6] published a detailed and critical review of the analogy with respect to chemisorption. This work is now considered below.

The geometry of a cluster and a surface are usually not comparable, although notable exceptions to this are the metal frameworks observed for some of the higher nuclearity clusters: $[Rh_{13}(CO)_{24}H_3]^{2-}$, [7] $[Os_{10}C(CO)_{24}]^{2-}$, [8] and $[Rh_{14}(CO)_{25}]^{4-}$, [9] which represent fragments of hexagonal close packed, cubic close packed, and body centred cubic lattices respectively (Figure 1.2.1). However, a flat metal surface cannot be adequately modelled by the square and triangular faces which are exhibited by these and other polyhedral clusters. It has been suggested that they could act instead as models for films or small particles on solid supports rather than as single metal crystals. However, when using spectroscopic methods to study the products resulting from chemisorption processes on poorly defined surfaces such as these, in which the geometry of the surface is random and not ordered as in crystalline samples, problems arise in the interpretation of the vibrational data. Because a range of possible sites are present on which adsorption could occur, assignments of vibrational modes can therefore be in some doubt. Hence such systems tend not to be studied.

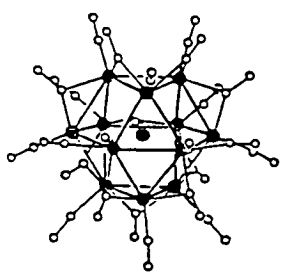

(a) $[Rh_{13}(CO)_{24}H_3]^{2-}$
h.c.p.

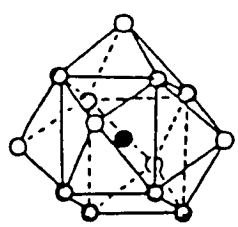

(b) $[Os_{10}C(CO)_{24}]^{2-}$
c.c.p.

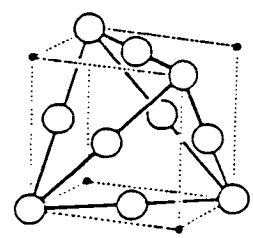

(c) $[Rh_{14}(CO)_{25}]^{4-}$
b.c.c.

Figure 1.2.1: The molecular geometries of the clusters $[Rh_{13}(CO)_{24}H_3]^{2-}$, $[Os_{10}C(CO)_{24}]^{2-}$, and $[Rh_{14}(CO)_{25}]^{4-}$.

Even though comparable geometries are possible in clusters and surfaces, further problems arise from the co-ordination number of the metal atom to its neighbours, and from the metal-ligand connectivity. The co-ordination number is usually much greater for an atom on a metal surface, typically six to nine, than for an atom in a

cluster which shows a metal-metal connectivity of two for triangular, three for tetrahedral, and four for an octahedral geometry. The co-ordination number only approaches that for the surface in some of the larger polyhedra such as $[Rh_{13}(CO)_{24}H_3]^{2-}$ with a co-ordination of five, and a maximum of seven in the cluster $[Rh_{14}(CO)_{25}]^{4-}$. This difference results from the close packing of metal atoms in the bulk and their co-ordination to atoms in the sub-layer. The metal-ligand connectivity is comparatively larger for the cluster, in the region three to five, than for the surface which is typically one or less, and again highlights some incompatibilities between the two regimes. Of particular importance is that the local atomic and electronic structure of a surface is influenced by other atoms in the layer and sub-layers, for which there is no possible cluster analogue.

Theoretical calculations have shown that a cluster of metal atoms becomes metal-like only with nuclearities in the range 13-19 for Ni and Pd and 30-51 for Ag. [10] However, these large metal-like structures show properties which are dissimilar to the bulk metal, and only approach a truly bulk metallic state with higher nuclearities.

A consideration of these factors clearly shows that a cluster and a metal surface are quite distinct in nature. Hence, it is not possible to consider a cluster to model a metal surface. However, the Muetterties analogy was not based on this, although it is often misconstrued, but rather considered the "comparison between a discrete or molecular metal cluster which has a polyhedral metal core and a periphery of ligands, and a metal surface with a similar set of ligands chemisorbed at the surface". Thus, it is suggested that there is no real difference in the metal-ligand bond formed in these two extremes. Indeed, calculations have shown that it is reasonable to approximate the adsorption of a group of atoms or a single molecule as involving the interaction with only a small group of metal atoms, although longer range interactions are important. For example, experiments have shown that the binding energy of CO on an array of Ni atoms is not greatly affected by the size of the array.[11] The co-ordination of the ligand to a cluster is thus representative of similar plausible co-ordination types on metal surfaces, and indeed appropriately substituted clusters have been prepared which show many of the known adsorbate geometries. [12]

Clusters can therefore be regarded as reasonable models of chemisorbed species on metal surfaces.

The techniques of surface analysis, have in the past been considered as somewhat imprecise. However, as technological advances have been made, and new techniques introduced, problems such as spectral resolution have been overcome, so that for example using the vibrational techniques [13] RAIRS (Reflection Absorption Infra Red Spectroscopy) or DRIFTS (Diffuse Reflectance Infra Red Spectroscopy), IR spectra can typically be recorded to 4 cm^{-1} resolution, although EELS (Electron Energy Loss Spectroscopy) can only give a *ca.* 10 cm^{-1} resolution. However the interpretation of such data is not always straightforward, and hence a number of techniques are usually combined to give complementary information. The comparison of a proposed adsorbate type and co-ordination geometry to that observed in a cluster, has often proved a valuable technique in such analyses.

Chemisorption processes at metal surfaces fall into two main classes: *associative*, in which there is no fragmentation, and *dissociative*, which results in bond cleavage of the chemisorbed fragment *e.g.* dissociation of H_2 gives M-H, and examples of these processes have been reported for clusters. Likewise mobility can be considered as *dissociative* or *non-dissociative*. The mobility of ligands has been established by NMR for clusters, for example the interconversion of $Ru_6C(CO)_{11}(\eta^6\text{-}C_6H_5Me)(\mu_3\text{-}\eta^2\text{:}\eta^2\text{:}\eta^2\text{-}C_6H_5Me)$ and $Ru_6C(CO)_{11}(\eta^6\text{-}C_6H_5Me)_2$ [14] and carbonyl scrambling in $M_3(CO)_{12}$ (M= Fe, Ru, Os). [15] The techniques of field ion microscopy and more recently the pioneering work of Bradshaw [16] on PLEEM (Photoemission Low Energy Electron Microscopy) have shown the mobility of ligands on metal surfaces. PLEEM is one of the most fascinating, innovative and important techniques to have been conceived in surface science, and has allowed the migration of molecules on metal surfaces to be observed and recorded in real time on video tape. The analogy to ligand migration on clusters is interesting but perhaps should not be considered too seriously, since examples in clusters are not that common.

Only two general examples of the analogy are cited below to typify its application, although many others have been reported, [17] and its applicability to surface science has proved to be helpful in interpreting a range of vibrational data. The view of Ertl [18] is that the analogy although imperfect, [19] works for structure and bonding but doesn't extend to reactivity and catalysis.

1.2.1 Chemisorption of Ethylene on a Pt(111) Surface

EEL spectra were recorded by Ibach *et al* [20] for the adsorption of ethylene on a Pt(111) surface at low temperature and at room temperature. Two quite distinct spectra were observed at these temperatures, and were postulated to result from a di-σ adsorbed species (a) and an ethylidene species (b) respectively (Figure 1.2.2).

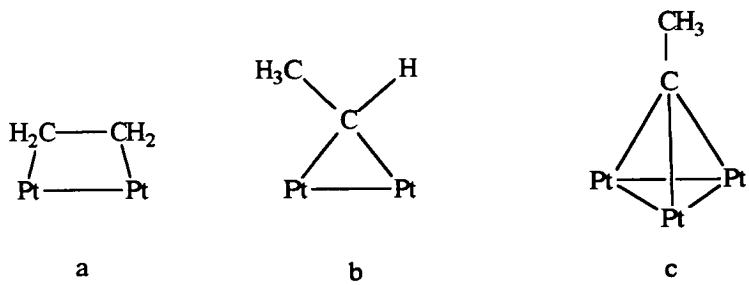

Figure 1.2.2: Proposed bonding modes of ethylene on Pt(111).

Subsequent LEED (Low Energy Electron Diffraction) studies [21] led to the room temperature species being reassigned as the ethylidyne species (c). These species were further justified by a detailed analysis of the vibrational spectra (IR and Raman) of the cluster models $Co_3(CO)_9(\mu_3\text{-}CCH_3)$ [22] and $Os_2(CO)_8(\mu_2\text{-}CH_2CH_2)$ [23] which show analogous bonding modes (Figure 1.2.3).

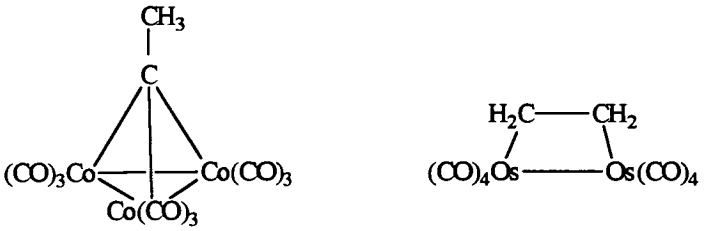

Figure 1.2.3: The model clusters $Co_3(CO)_9(\mu_3\text{-}CCH_3)$ and $Os_2(CO)_8(\mu\text{-}C_2H_4)$.

1.2.2 Co-adsorption of Benzene and CO on Rh(111)

An interesting example of the surface cluster analogy arises from the LEED pattern observed for the co-adsorption of benzene and carbon monoxide on a Rh(111) surface [24] (Figure 1.2.4), and the comparable bonding mode observed for the cluster species $M_3(CO)_9(\mu_3\text{-}C_6H_6)$ (M=Ru,Os) [25,26] and $Ru_6C(CO)_{11}(\eta^6\text{-}C_6H_6)(\mu_3\text{-}C_6H_6)$ [26a,27] (Figure 1.2.5). The benzene ligand shows co-ordination to a three-fold site and a rehybridisation of the π orbitals so as to maximise their interaction with the metal orbitals. This results in the shorter double bonds of the Kekulé benzene lying directly above the metal centres and the bending of the C-H bonds away from the metal centres. However conflicting results have been reported which suggest that the benzene molecule is adsorbed at a single rather than three-fold metal site and shows no Kekulé distortion. [28]

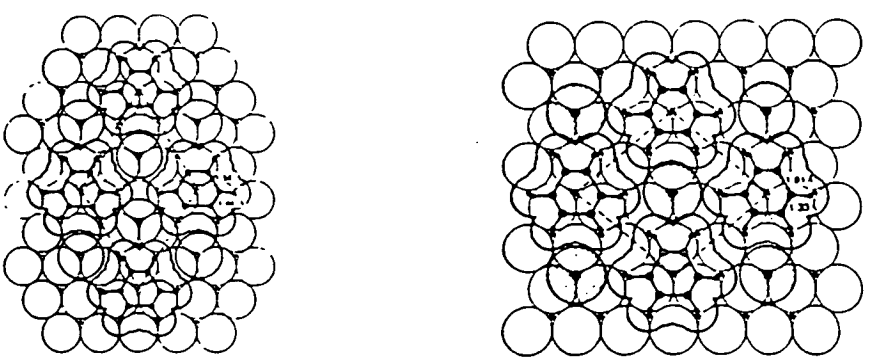

Figure 1.2.4 : The LEED pattern observed for the co-adsorption of benzene and CO on a) Rh(111)-(3x3) C_6H_6 + 2 CO surface, and b) Rh(111)-c{2(3)^{½} x4}rect - C_6H_6 + 2 CO surface.

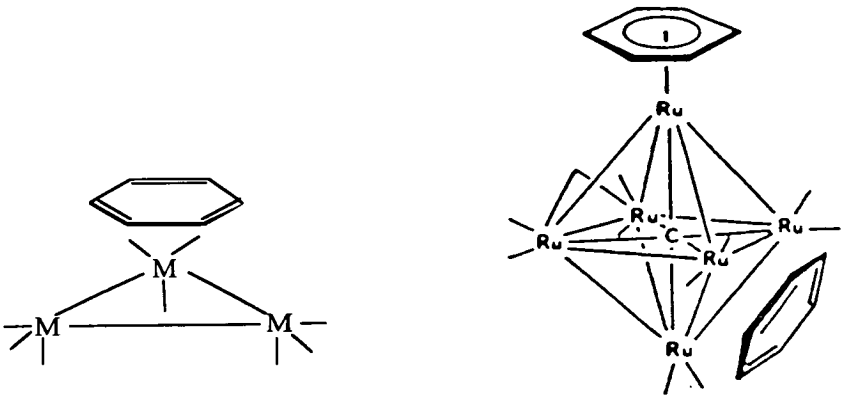

Figure 1.2.5 : The structures of $M_3(CO)_9(\mu_3\text{-}C_6H_6)$ (M=Ru,Os), and $Ru_6C(CO)_{11}(\mu_3\text{-}C_6H_6)(\eta^6\text{-}C_6H_6)$.

Although the IR spectra of the benzene ligand bound to the aforementioned clusters has been briefly reported, [29] a detailed comparison with the vibrational data for the surface species has apparently not been examined.

We wished to study the reactivity of pyridine and other nitrogen heterocycles with clusters. Interest in the pyridine system arose from the observed adsorption behaviour on Ni(001) [30]and Ag(111) [31] surfaces. These studies had shown that the pyridine molecule was bonded through its π system at low surface coverage but then gradually tilted as its concentration on the surface increased, finally σ bonding through only the nitrogen lone pair. Although pyridine has been found to bond facially through its π system to some monometallic species, [32] previous research in cluster chemistry has shown a preference for the σ bonding mode, and will now be discussed.

1.3 Metal Carbonyl Clusters and Nitrogen Heterocycles

Although some of the chemistry to be discussed in this review has been the subject of report elsewhere [33,34] these articles have discussed the area with respect to a large range of donor ligands, and so have necessarily been rather broad in their discussion. It is our intention to discuss the area of nitrogen heterocyles in somewhat greater detail and to highlight more recent research in the area.

1.3.1 Pyridines

By far the largest reported area of research of nitrogen heterocycles (the first example appearing in 1975) [35] involved the thermolysis of $Os_3(CO)_{12}$ and pyridine, either neat, or in a saturated hydrocarbon solution. Six products were successfully isolated and identified on the basis of IR, mass spectrometry, and elemental analysis, and were shown to be formed sequentially as presented below (Scheme 1.3.1).

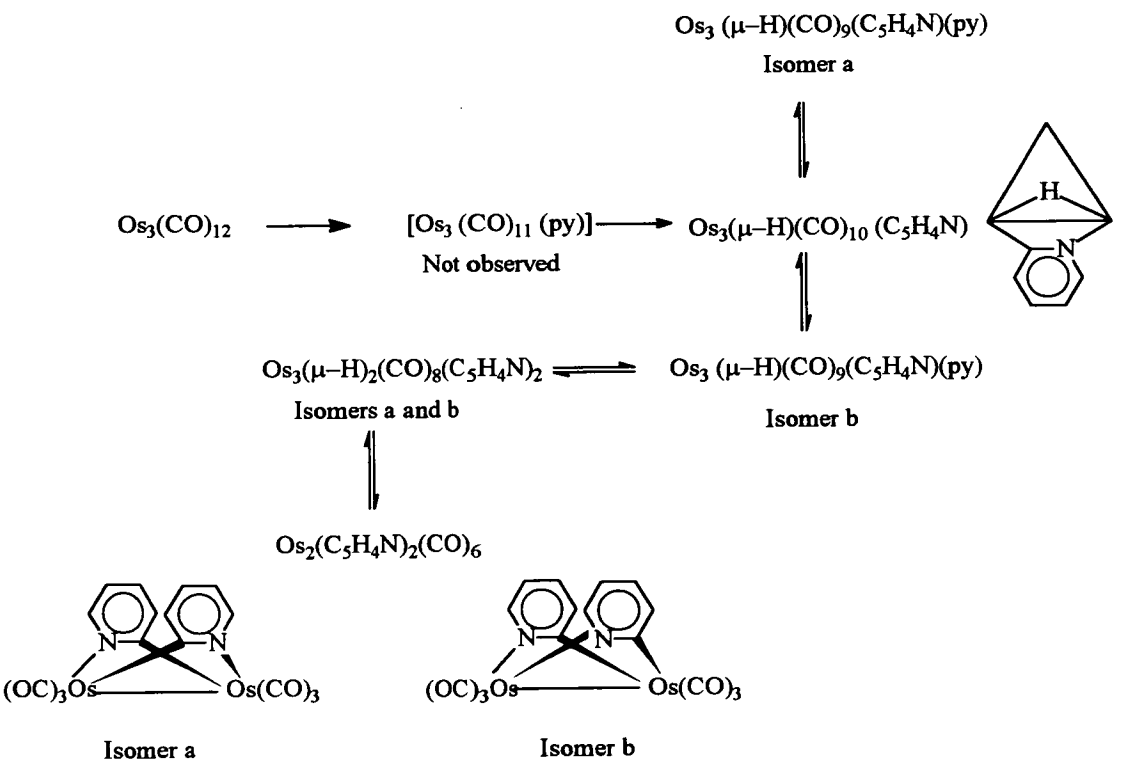

Scheme 1.3.1: Thermolysis of $Os_3(CO)_{12}$ with pyridine.

Thermolysis causes the stepwise substitution of the carbonyl ligand for pyridine and subsequent *ortho*metallation, with prolonged reaction times resulting in cluster degradation to form the substituted dimer. It is suggested that the observed isomers of $Os_3(\mu\text{-}H)(CO)_9(C_5H_4N)(py)$ result from the pyridine ligand being bound to different metal atoms, whilst the isomers of $Os_3(\mu\text{-}H)_2(CO)_8(C_5H_4N)_2$ are accounted for by the bridging of the pyridyls across different edges. This is based on X-ray crystallography, and ^1H NMR spectroscopic evidence which shows the rings to be unique. Finally, the structures of the dimers, $Os_2(CO)_6(C_5H_4N)_2$ are postulated by analogy with the known cluster $Fe_2(CO)_6(OCPh)_2$. [36] The possibility of linear *vs.* bent isomerisation is ruled out on the basis of IR which suggests that both isomers possess similar structures.

Use of the cluster $Os_3(CO)_{11}(MeCN)$, [37,38] allowed reaction with pyridine to occur under mild conditions, because of the relative ease of substitution of the labile acetonitrile ligand. Heating these two compounds together for four minutes was found to be sufficient to bring about reaction. The resulting product was shown to be $Os_3(CO)_{11}(py)$, which had previously been suggested as an intermediate in the formation of $Os_3(\mu\text{-}H)(CO)_{10}(C_5H_4N)$. That this was plausible was backed up experimentally by the further heating of the $Os_3(CO)_{11}(py)$ species in octane which produced the *ortho*metallated cluster.

Similar reactions have been carried out using $Ru_3(CO)_{12}$ in refluxing cyclohexane, [39] and $Ru_3(CO)_{11}(MeCN)$ or $Ru_3(CO)_{10}(MeCN)_2$ [40] in dichloromethane at room temperature to form the *ortho*metallated $Ru_3(\mu\text{-}H)(CO)_{10}(C_5H_4N)$ species in each case. That the reaction with $Ru_3(CO)_{11}(MeCN)$ forms this product and not $Ru_3(CO)_{11}(py)$ as for the osmium analogue, is believed to be due to the higher reactivity of ruthenium which has weaker M-CO bonds because of a smaller π back bonding effect. Prolonged heating of $Ru_3(\mu\text{-}H)(CO)_{10}(C_5H_4N)$ in the presence of excess pyridine produced a second cluster in low yield which was tentatively assigned on the basis of microanalysis, IR and mass spec. data as having undergone further

*ortho*metallation to yield $Ru_3(\mu\text{-}H)_2(CO)_8(C_5H_4N)_2$, analogous to the earlier reported osmium species. These reactions are summarised in Scheme 1.3.2.

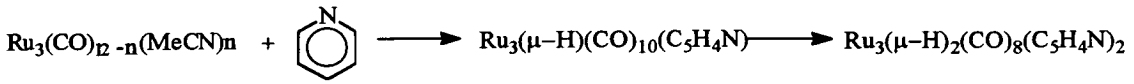

Scheme 1.3.2: The reaction of $Ru_3(CO)_{12-n}(MeCN)_n$ (n= 0,1,2) with pyridine.

The reaction between $Ru_3(CO)_{12}$ and six molar equivalents of pyridine was carried out in n-heptane over 72 hours at 120 °C, with two colourless isomers being separated and identified on the basis of ^{13}C and ^{1}H NMR as $Ru_2(CO)_6(C_5H_4N)_2$ (Scheme 1.3.3). [41] No *ortho*metallated product was detected and the NMR ruled out the presence of bridging hydrides. It would seem reasonable to suggest that the dimer perhaps represents the breakdown product of $Ru_3(\mu\text{-}H)_2(CO)_8(C_5H_4N)_2$, although this has not been investigated experimentally.

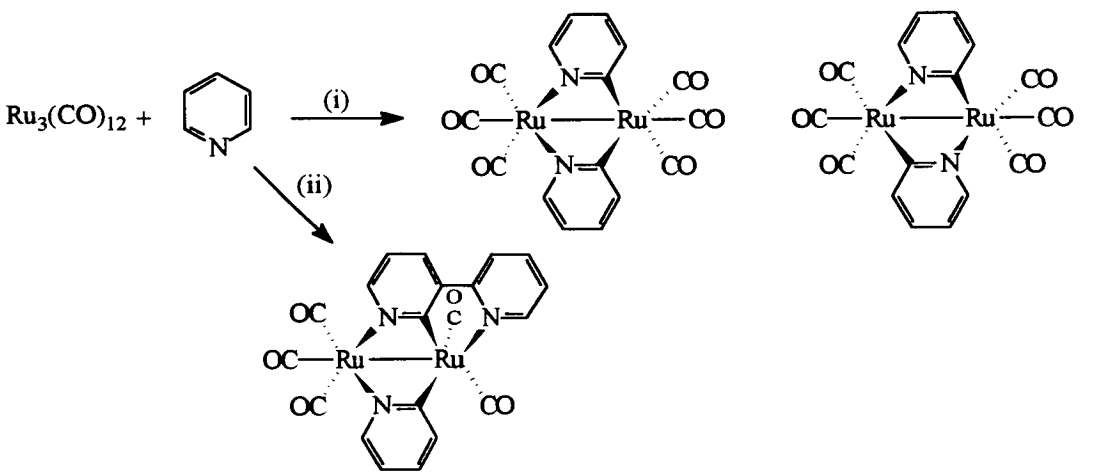

Scheme 1.3.3: The reaction between $Ru_3(CO)_{12}$ and six molar equivalents of pyridine (i) in refluxing heptane over 72 hours, and (ii) in neat pyridine at 180 °C for 6 hours.

Reaction of $Ru_3(CO)_{12}$ in neat pyridine for six hours, analogous conditions to those reported earlier for the reaction with $Os_3(CO)_{12}$ (Scheme 1.3.1), resulted in

considerable cluster breakdown and the formation of a red product. Single crystal X-ray analysis and ^{1}H NMR showed the product to be a dimer, $Ru_2(CO)_5(C_5H_4N)(C_{10}H_7N_2)$ containing both a bridging pyridyl and bipyridyl ligand (Figure 1.3.1). [41] This represents the only known such example of the coupling of pyridines to form a bipyridyl ring on clusters. These examples clearly illustrate how the reaction conditions crucially dictate the nature of the products formed.

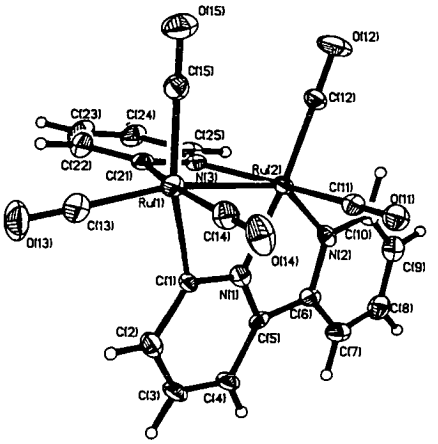

Figure 1.3.1: The molecular structure of the dimer $Ru_2(CO)_5(C_5H_4N)(C_{10}H_7N_2)$.

It has been reported by Gallup [42] that the reaction between $Os_3(CO)_9(\mu_3\text{-}\eta^2\text{:}\eta^2\text{:}\eta^2\text{-}C_6H_6)$ and 1.1 equivalents of Me_3NO in the presence of acetonitrile, leads to the formation of $Os_3(CO)_8(\mu_3\text{-}\eta^2\text{:}\eta^2\text{:}\eta^2\text{-}C_6H_6)(MeCN)$ which can then undergo a facile substitution with pyridine to form the benzene-pyridine cluster $Os_3(CO)_8(\mu_3\text{-}\eta^2\text{:}\eta^2\text{:}\eta^2\text{-}C_6H_6)(py)$, identified on the basis of ^{1}H NMR evidence (Scheme 1.3.4). Similar reactivity was also observed with phosphines.

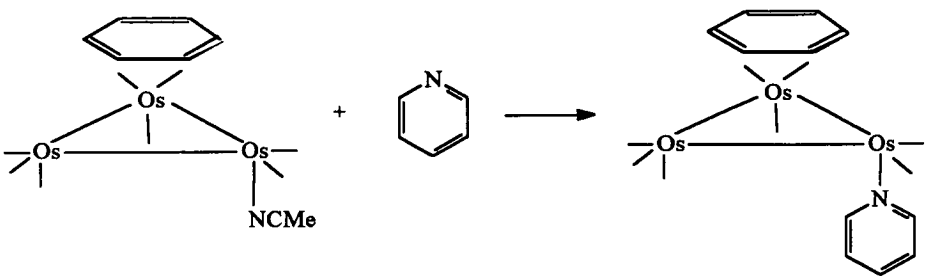

Scheme 1.3.4: Substitution reaction of $Os_3(CO)_8(\mu_3\text{-}\eta^2\text{:}\eta^2\text{:}\eta^2\text{-}C_6H_6)(MeCN)$ with pyridine.

With the exception of Dutton's [43,44] work on the $Ru_5C(CO)_{15}$ cluster, which is discussed in Chapter Three, only two other reports have been given on the formation or reaction of higher nuclearity ruthenium clusters with pyridine. Bruce *et al.* [45] showed that the reaction between the cluster $Ru_5(CO)_{13}(\mu_5\text{-}C_2PPh_2)(\mu\text{-}PPh_2)$ and pyridine in benzene at 90 °C over four hours, produced the three products outlined in Scheme 1.3.5. These show nuclearities from four to six, and pyridine bound either terminally, *ortho*metallated and bridging two metal sites, or unusually bridging three metal sites. All three species have been confirmed by X-ray crystallographic studies.

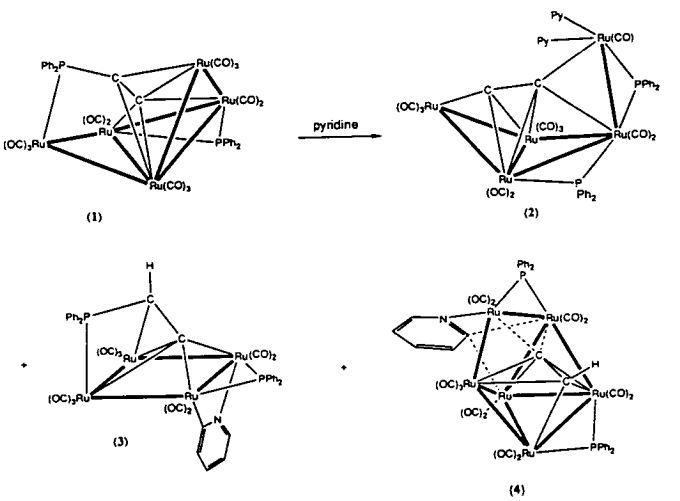

Scheme 1.3.5: The reaction between $Ru_5(CO)_{13}(\mu_5\text{-}C_2PPh_2)(\mu\text{-}PPh_2)$ and pyridine.

1) $Ru_5(CO)_{13}(\mu_5\text{-}C_2PPh_2)(\mu\text{-}PPh_2)$

2) $Ru_5(CO)_{11}(\mu_5\text{-}C_2)(\mu\text{-}PPh_2)_2(py)_2$

3) $Ru_4(CO)_{10}[\mu_4\text{-}C_2H(PPh_2)](\mu\text{-}PPh_2)(\mu\text{-}C_5H_4N)$

4) $Ru_6(CO)_{12}(\mu\text{-}CO)(\mu_6\text{-}C_2H)(\mu_3\text{-}C_5H_4N)(\mu\text{-}PPh_2)_2$

Secondly, the work of Deeming *et al.* [46] on the reaction between $Ru_3(CO)_{12}$ and the complex ruthenium (II) pyridine-2-thionato, $Ru(pyS)_2(CO)_2$ again produces some novel compounds showing the pyridine bridging two metal sites (Scheme 1.3.6). Attention to higher nuclearity clusters has instead focused mainly on unsubstituted osmium clusters. The first example was reported in 1979 with the reaction between $Os_6(CO)_{18}$ and pyridine in the presence of Me_3NO resulting in an *ortho*metallated derivative $HOs_6(CO)_{16}(C_5H_4N)$ being formed. [47]

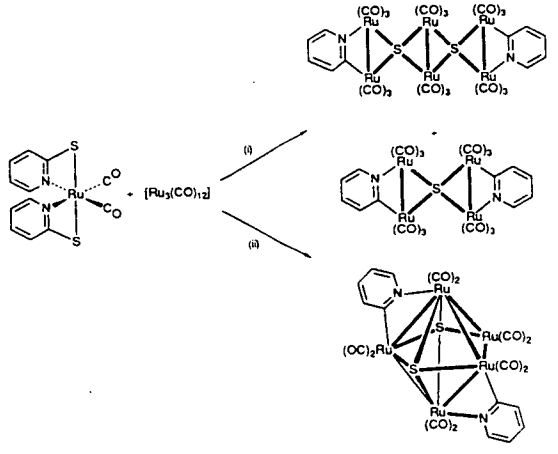

Scheme 1.3.6: Reaction of $Ru(pyS)_2(CO)_2$ with $Ru_3(CO)_{12}$, (i) in light petroleum at 150 °C in a sealed Carius tube, and (ii) in refluxing xylene.

If instead the cluster is reacted directly with pyridine, then the products formed are dependent upon the reaction conditions employed. In refluxing octane two *ortho*metallated Os_6 isomers are formed. X-ray crystallography studies have shown the metal framework to be retained for isomer (a), whilst this can only be inferred for isomer (b) on the basis of spectroscopic evidence (Scheme 1.3.7). [48] Reaction in dichloromethane in the presence of a high concentration of pyridine causes instead both reduction and decapping to occur yielding $[Os_5(CO)_{15}]^{2-}$ as the major product with some $Os_6(CO)_{17}(py)_2$ formed as a by-product (Figure 1.3.2). The structure shows that two metal-metal bonds have been broken allowing the cluster to undergo rearrangement to form a spiked trigonal bipyramidal cluster. [49] When the reaction was repeated using a low pyridine concentration then only reduction to $[Os_6(CO)_{18}]^{2-}$ was observed.

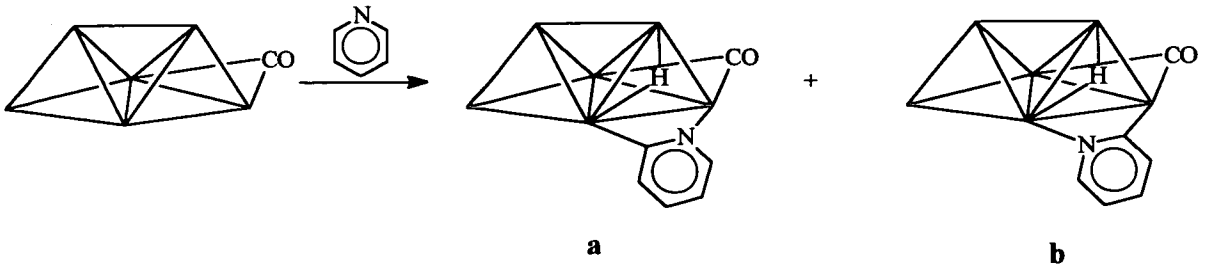

Scheme 1.3.7: Reaction of $Os_6(CO)_{18}$ and pyridine in refluxing octane.

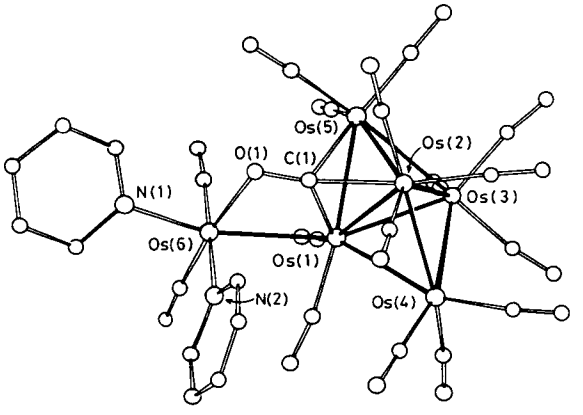

Figure 1.3.2: The molecular structure of $Os_6(CO)_{17}(py)_2$.

$Os_5(\mu\text{-}H)C(CO)_{14}(C_5H_4N)$ [50] (Figure 1.3.3) represents the first pentanuclear osmium cluster containing a bound nitrogen heterocycle to be isolated and characterised, and is analogous in structure to the ruthenium analogue reported by Dutton [43,44] . It was prepared in low yield by the pyrolysis of $Os_3(CO)_{11}(py)$, from which the major product was the dianion $[Os_{10}C(CO)_{14}]^{2-}$, and shows the *ortho*metallated pyridine bound to a bridged butterfly cluster. The structure shows the pyridyl ligand in only one of its two possible orientations, a second isomer is therefore possible but this was not characterised.

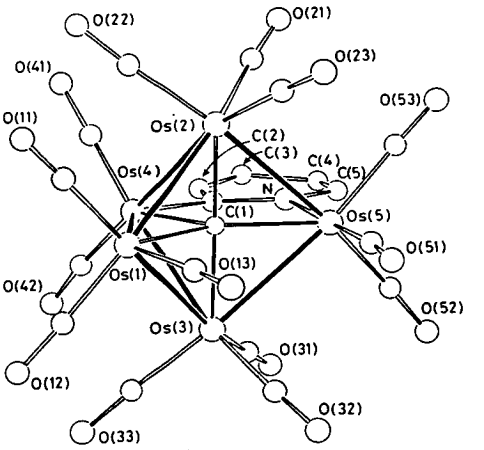

Figure 1.3.3: The molecular structure of $Os_5(\mu\text{-}H)C(CO)_{14}(C_5H_4N)$.

A further series of pentanuclear osmium clusters have been produced from the reaction between two equivalents of pyridine with the hydrido cluster $Os_5(\mu\text{-}H)_2(CO)_{15}$ in refluxing n-octane. [51] The reaction was carried out in a non-polar solvent to disfavour the deprotonation of the cluster by the basic pyridine. The products were separated by tlc and characterised on the basis of IR and ^1H NMR in the case of the two isomers $Os_5(\mu\text{-}H)_2(CO)_{15}(C_5H_5N)$ (c, d), and in addition by mass spectrometry and X-ray diffraction analysis for $Os_5(\mu\text{-}H)_3(CO)_{14}(C_5H_4N)$ (a) and $Os_5(\mu\text{-}H)_2(CO)_{14}(C_5H_5N)$ (b) (Figure 1.3.4). The structure of (a) shows that the $Os_5(\mu\text{-}H)_2(CO)_{12}$ framework, which is proposed to possess a trigonal bipyramidal structure by comparison with $Os_5(\mu\text{-}H)_2(CO)_{14}(PEt_3)$, [52] has undergone rearrangement to form an *ortho*metallated capped tetrahedron. In contrast, the polyhedral geometry of (b) is trigonal bipyramidal, showing a *di*-hydride bridge, whilst the geometry of (c) has only been tentatively assigned from its IR carbonyl pattern as being analogous to the known compound $Os_5(\mu\text{-}H)_2(CO)_{15}[P(OMe_3)]$. [53] Finally, isomer (d) is proposed to show the terminally bound pyridine ligand in the axial, rather than equatorial position.

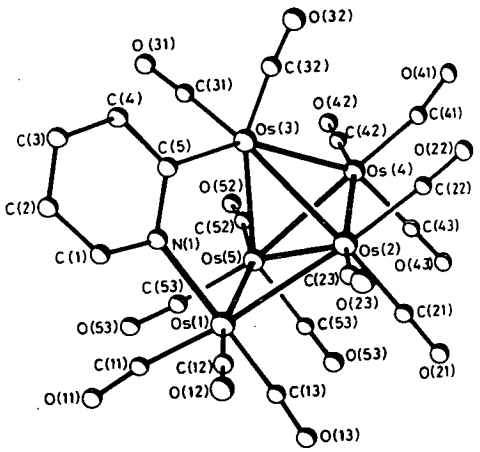

(a)

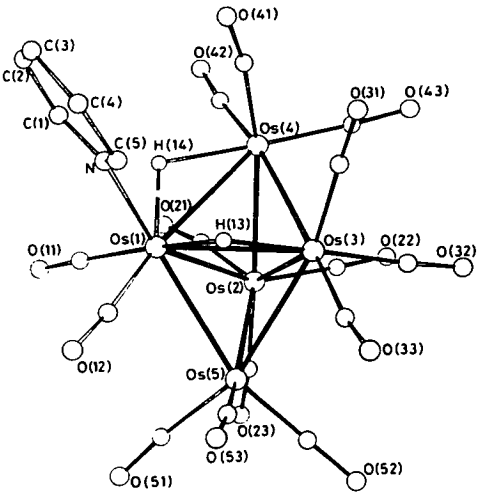

(b)

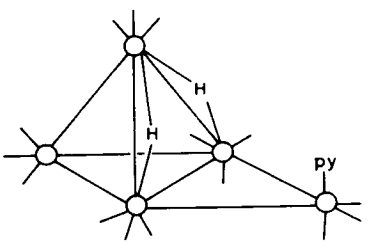

(c)

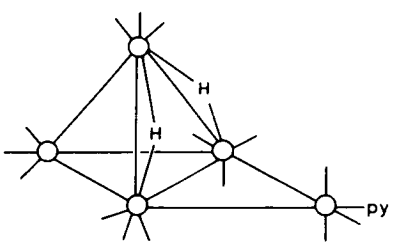

(d)

Figure 1.3.4: The molecular structures of $Os_5(\mu\text{-}H)_3(CO)_{14}(C_5H_4N)$ (a) and $Os_5(\mu\text{-}H)_2(CO)_{14}(C_5H_5N)$ (b), and the proposed structures of the $Os_5(\mu\text{-}H)_2(CO)_{15}(C_5H_5N)$ isomer (c, d).

1.3.2 Substituted Pyridines

The substituted pyridine molecules which have been reported in the literature, have fallen into three distinct categories with respect to their reactivity towards metal carbonyl clusters:

a) Methyl Substituted Pyridines (ortho, meta, para)

These undergo *ortho*metallation on reaction with $M_3(CO)_{10}(MeCN)_2$ (M= Ru, Os), [54,55] as for pyridine itself, to form clusters of the general formula $M_3(\mu\text{-}H)(CO)_{10}(C_5H_4RN)$.

b) Quinolines

The quinolines again exhibit an analogous reactivity to pyridine, forming *ortho*metallated products with $M_3(CO)_{12}$ (M= Ru, Os) and under reflux in heptane,[56,35] or at room temperature with $Ru_3(CO)_{10}(MeCN)_2$. [54] The prospect of isomerisation arises for *iso*quinoline which shows the formation of both possible isomers (Figure 1.3.5), with isomer **a** being formed in preference to **b** on reaction with $Os_3(CO)_{12}$, but *vice versa* when reacted with $Ru_3(CO)_{10}(MeCN)_2$.

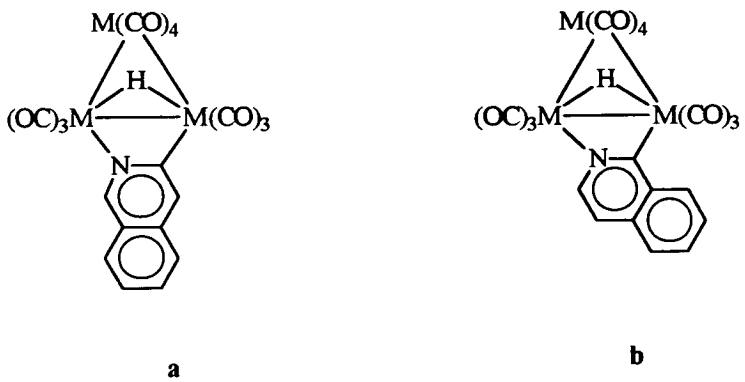

a **b**

Figure 1.3.5: The structures of the two $M_3(CO)_{10}(C_9H_6N)$, M= Ru, Os isomers **a** and **b**.

However, it has also been shown that $Ru_3(CO)_{12}$ reacts with 2,2'-biquinoline in refluxing thf over 3 hours to form a highly insoluble dark brown cluster $Ru_3(CO)_8(\mu\text{-}CO)_2$(biquin) [57] characterised by microanalysis (Scheme 1.3.8), and a comparable IR carbonyl spectrum to that observed for the 2,2'-bipyridyl derivative whose X-ray structure has been determined, [39,58] and will be discussed further in Section 1.3.5. Unusually, the structure shows that the cluster has formed bridging carbonyl bonds and that the ligand has co-ordinated to a single metal site. This is not as may have been predicted for a typical thermal reaction, from which *ortho*metallated clusters, or dimers if heating is prolonged, are often formed.

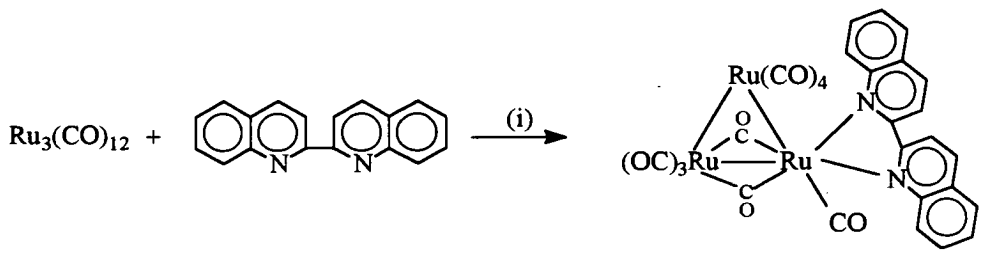

Scheme 1.3.8: Reaction of $Ru_3(CO)_{12}$ with 2,2'-biquinoline under (i) reflux in thf for 3 hours.

Finally, it has been suggested on the basis of spectroscopic evidence, that the reaction between $Ru_3(CO)_{12}$ and 1,2,3,4-tetrahydroquinoline (thq) in refluxing heptane leads to the formation of $Ru_3(\mu\text{-}H)_2(CO)_8$(quin)(dihydroquin) as the major product, in which the heterocyclic rings of the two molecules of thq have undergone partial and full dehydrogenation respectively (Scheme 1.3.9). [56]

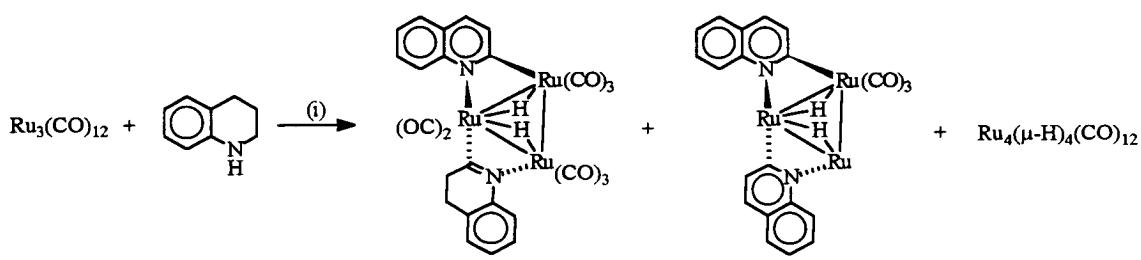

Scheme 1.3.9: Reaction between $Ru_3(CO)_{12}$ and 1,2,3,4-thq in refluxing heptane.

c) 2-Substituted Pyridines

This area represents by far the largest of all the substituted pyridines, and results from an interest in co-ordination of not only the lone pair of electrons on nitrogen but also a second donor bound in the 2- position of the ring, typically an amine, although other derivatives have been studied. This rich field of chemistry was first highlighted by Deeming *et al.* in the early 1980's. [59,60] Addition of N-benzyl 2-aminopyridine to the reactive $Os_3(CO)_{10}(C_8H_{14})_2$ cluster at room temperature caused the direct substitution of the labile cyclo-octene ligands and N-H bond cleavage in the formation of an allyl like nitrogen donor **a** (Scheme 1.3.10). Thermolysis of the product in refluxing heptane over a 45 minute period then led to the formation of two isomers **b** and **c**. Isomer **c** was *di- ortho*metallated and was shown to be formed directly from the *mono- ortho*metallated cluster on prolonged heating.

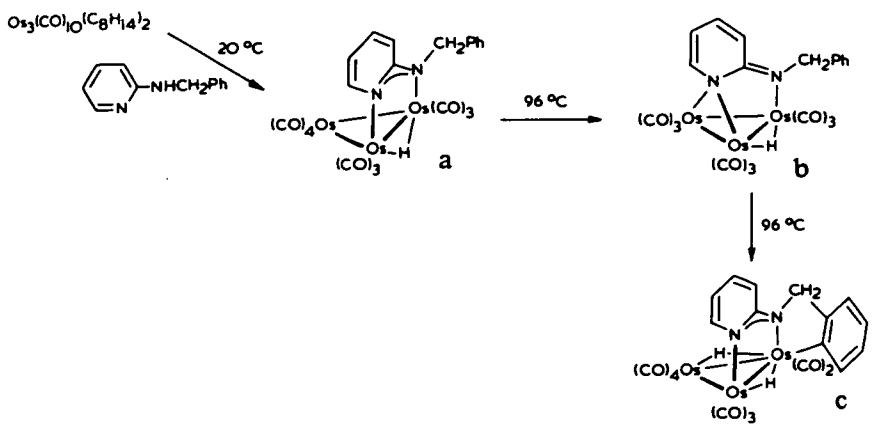

Scheme 1.3.10: Reaction of $Os_3(CO)_{10}(C_8H_{14})_2$ with C_5H_4NPh.

Similarly, reaction of $Ru_3(CO)_{12}$ with substituted 2-aminopyridines resulted in the formation of analogous species, [61] with the exception of 2-dimethyl aminopyridine. This reacted to form a cluster which possessed both terminal and bridging carbonyl ligands, and which was proposed to exhibit the structure shown in Figure 1.3.6 on the basis of IR and microanalytical evidence, and by comparison with known structures of similar pyridazine (1,2-diazine) [62] and napthyridine derivatives [58] (Figures 1.3.20 and 1.3.21).

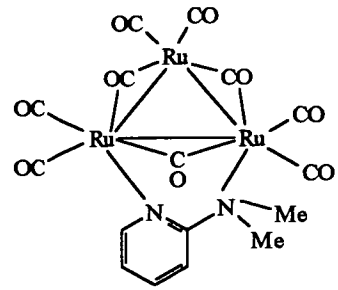

Figure 1.3.6: The proposed structure of $Ru_3(\mu\text{-}CO)_3(CO)_7(2\text{-}NMe_2\text{-}C_5H_4N)$.

However if $Os_3(CO)_{12}$ was reacted with 2-aminopyridine in octane in a sealed and evacuated Carius tube under forcing conditions (183 °C, 69 hours), two colourless isomers were formed: $Os_2(CO)_6(C_5H_4N\text{-}NH)_2$ [60] (Figure 1.3.7), identified on the basis of ^1H NMR and microanalysis as analogous to the pyridine derivatives formed under similar conditions (Scheme 1.3.1).

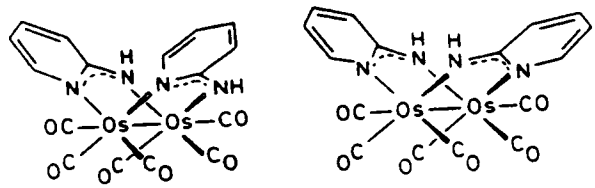

Figure 1.3.7: The proposed structures of the $Os_2(CO)_6(C_5H_4N\text{-}NH)_2$ isomers.

A recent publication reported that the amino-methylpyridine derivative $Ru_3(\mu\text{-}H)(CO)_9(ampy)$ reacted with hydrogen in refluxing toluene to produce the unexpected and unusual dimer $Ru_6(\mu\text{-}H)_6(\mu_3,\eta^2\text{-}ampy)_2(CO)_{14}$, which was proposed on the basis of its ^1H NMR spectrum, and by comparison with a single crystal X-ray diffraction study of its phosphine derivative [63] (Scheme 1.3.11).

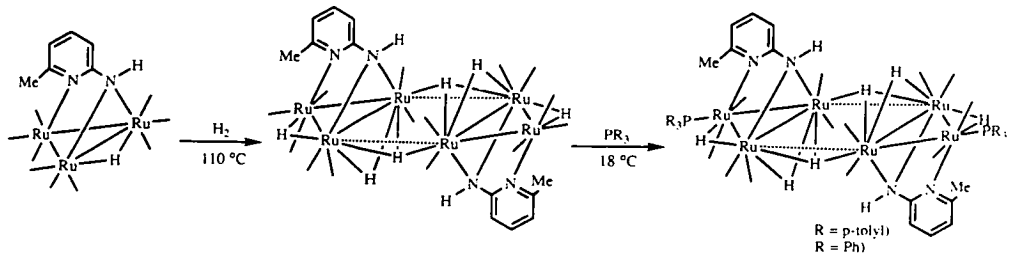

Scheme 1.3.11: Reaction between $Ru_3(\mu\text{-}H)(CO)_9(ampy)$ and hydrogen in refluxing toluene, and the subsequent formation of the phosphine derivatives.

In contrast to the previous examples, if the 2-amino group was replaced by Me, Cl or CN then bonding to these groups was not observed on reaction with $Os_3(CO)_{11}(MeCN)$, even under prolonged reflux in benzene (18 hours), instead only *ortho*metallation of the pyridine ring occurred. [64] However, if the functional side group was -OH (2- pyridone), -SH (pyridine-2-thiol), or $-NH_2$ (2-aminopyridine), then co-ordination to both the pyridine's lone pair and the side group were observed.[64] Further thermolysis resulted in decarbonylation of the cluster and the formation of a bridge to the S or N atoms only (Scheme 1.3.12). Despite refluxing the solution in heptane at 200 °C, the pyridone donor failed to convert to the bridging species.

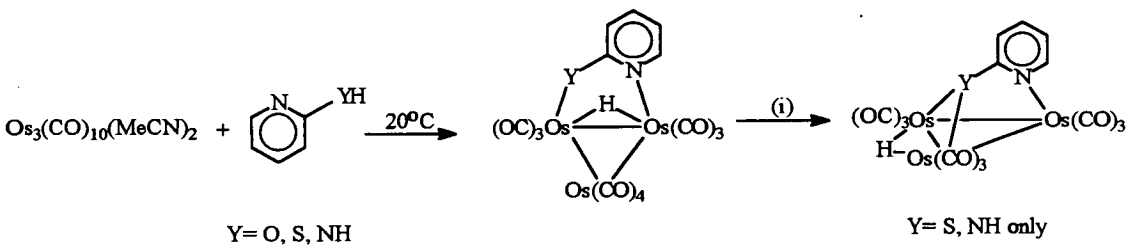

Scheme 1.3.12: Reaction of $Os_3(CO)_{10}(MeCN)_2$ with C_5H_4N-YH at 20 °C, followed by heating in (i) heptane at 68 °C for Y= S, and at 160 °C for Y= NH.

Reaction of 2-pyridone in nonane in a Carius tube at 145 °C for 80 hours resulted in the formation of two colourless Os_2 isomers $Os_2(CO)_6(C_5H_4ON)_2$ [60] which were analogous in structure to those reported for the reaction with 2-aminopyridine (Figure 1.3.7).

Similarly, the reaction between six equivalents of 2-pyridone and $Ru_3(CO)_{12}$ in refluxing toluene gave the dimer $Ru_2(CO)_6(C_5H_4NO)_2$. [61] Reaction with only three equivalents of ligand however, yielded an insoluble yellow solid which was proposed to be the polymer $[Ru_2(CO)_4(C_5H_4NO)_2]_n$ on the basis of its low solubility. On further reaction with L= CO, MeCN, or PPh_3 the dimers $Ru_2(CO)_4L_2(C_5H_4NO)_2$ were formed. Similar polymers have been proposed for the products resulting from the reaction between $Ru_3(CO)_{12}$ and carboxylic acid. [65,66]

Replacement of the side group with an aldehyde function to give pyridine-2-carboxaldehyde, and reaction with $Os_3(CO)_{10}(MeCN)_2$ was found to give the *ortho*metallated cluster $Os_3(\mu\text{-}H)(CO)_{10}(C_5H_4N\text{-}CO)$ [64] which unusually showed only co-ordination to the aldehyde and not to the lone pair on nitrogen. Heating in heptane at 90 °C for 1 hour was found to be sufficient to cause the loss of this aldehydic carbonyl to form the pyridine cluster derivative $Os_3(\mu\text{-}H)(CO)_{10}(C_5H_4N)$ discussed earlier. The only other reported example of a pyridine not bound through its lone pair to a metal carbonyl cluster resulted from the reaction between $Os_3(\mu\text{-}H)_2(CO)_{10}$ with 2-pyridyldimethylsilane $[2\text{-}(CH_3)_2SiH(C_5H_4N)]$. [67] Co-ordination was observed to the silicon only, and seems to be a consequence of the steric hindrance of the methyl groups on the silicon which prevent the nitrogen lone pair co-ordinating (Figure 1.3.8).

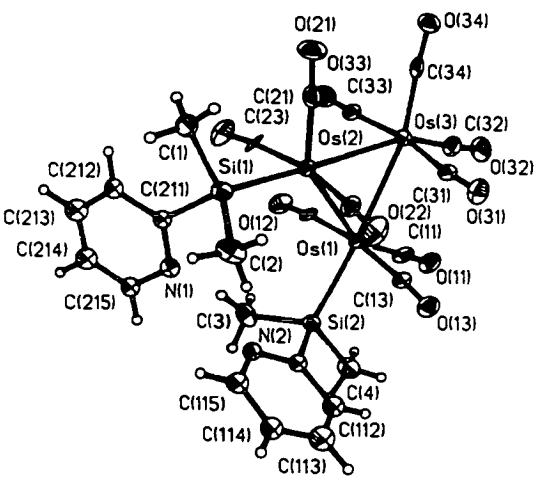

Figure 1.3.8: The molecular structure of $Os_3(\mu\text{-}H)_2(CO)_{10}[2\text{-}(CH_3)_2\{SiH(C_5H_4N)\}_2]$.

Treatment of $Os_3(CO)_{10}(MeCN)_2$ with 2-pyridyl-diphenylphosphine at room temperature led to the formation of the cluster: $Os_3(CO)_{10}(C_5H_4N\text{-}\mu PPh_2)$, [68] which is analogous to the pyridyl amines discussed earlier. Thermolysis of this product in heptane led to the formation of several species which are detailed below in Scheme 1.3.13. The major reaction product was **a**: $Os_3(\sigma\text{-}Ph)\{\mu_3\text{-}PPh(C_5H_4N)\}(CO)_9$, which was formed in 60 % yield, and shows the transfer of a phenyl group to the osmium framework. Its formulation was determined both crystallographically and spectroscopically. Product **b** was formed in 6% yield whilst **c** and **d** were formed in only trace amounts.

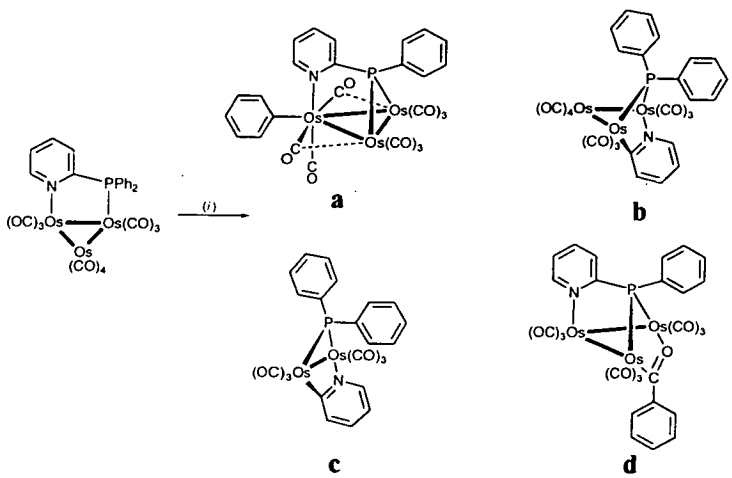

Scheme 1.3.13: Thermolysis reaction of $Os_3(CO)_{10}(C_5H_4N\text{-}\mu PPh_2)$ in (i) heptane at 98 °C, over 4 hours.

Reaction of $Os_3(CO)_{10}X_2$ (X= MeCN or H) with 2- ethenylpyridine results in the cleavage of both a C-H and an Os-Os bond to form a rather unusual and unique trinuclear "chain" cluster which was bound to both pyridine's lone pair and to the π cloud of the alkene (Figure 1.3.9). [69]

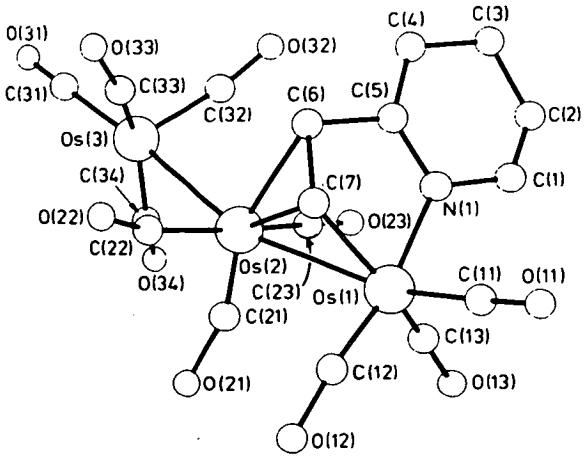

Figure 1.3.9: The molecular structure of $Os_3(\mu\text{-}H)(CO)_{10}(C_5H_4NCH{=}CH)$.

Likewise, metal-metal bond cleavage has also been observed in the reaction between $Ru_3(CO)_{12}$ and 8-quinolol and related ligands in refluxing thf (Figure 1.3.10). [70]

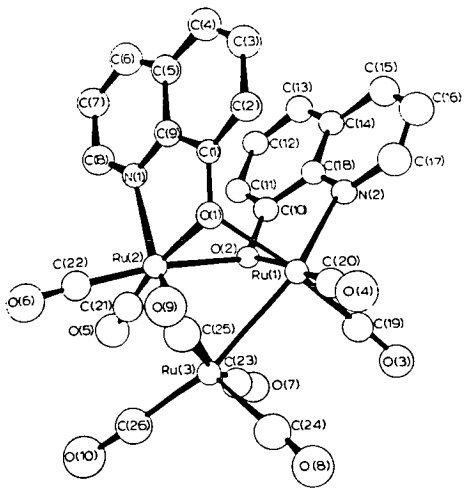

Figure 1.3.10: The molecular structure of $Ru_3(CO)_8(C_9H_6NO)_2$.

Finally, an interesting series of compounds have been identified which show metal-metal bond cleavage to occur but with the retention of their nuclearity. They were prepared from the reaction between $Ru_3(CO)_{12}$ and *di-* or *tri-*(2-pyridyl) phosphine at room temperature. The reaction was carried out in thf in the presence of $[N(PPh_3)_2]Cl$, which acted as a catalyst, to form products which showed cleavage of phosphorus-pyridyl and phosphorus-benzyl bonds (Figure 1.3.11). [71] Reaction with *tri-*(2-pyridyl) phosphine gave only product **1a**, which exhibited migration of a pyridyl

from the phosphine to a bridging metal site. Reaction with the *di*-(2-pyridyl) phosphine gave two products in approximately similar yields: **2a** which is analogous to **1a** in structure, and product **2b** which shows migration of the phenyl to a carbonyl ligand which has become bridging. It was proposed that these species were formed *via* an $Ru_3(CO)_{10}(\mu\text{-L})$ intermediate, for which an osmium analogue is known, [68] and a mechanism was suggested to account for the observed substitution patterns.

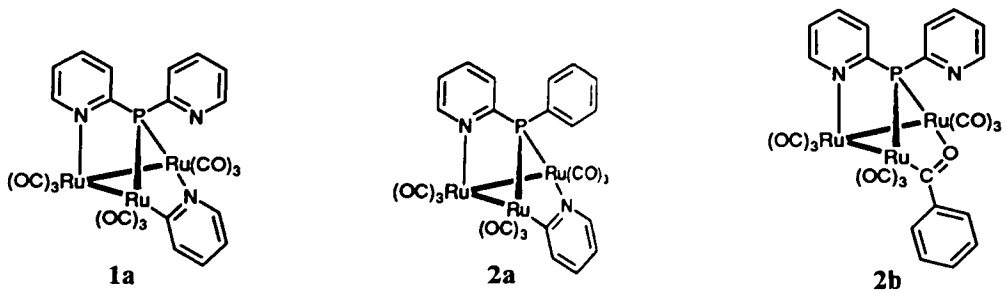

Figure 1.3.11: The structures of **1a**: $Ru_3(CO)_9(\mu\text{-}2\text{-}C_5H_4N)\{(\mu_3\text{-}P(2\text{-}C_5H_4N)_2\}$, **2a**: $Ru_3(CO)_9(\mu\text{-}2\text{-}C_5H_4N)\{(\mu_3\text{-}PPh(2\text{-}C_5H_4N)\}$, **2b**: $Ru_3(CO)_9(\mu\text{-}PhCO)\{(\mu_3\text{-}P(2\text{-}C_5H_4N)_2\}$.

1.3.3 Pyrroles and Pyrazoles

From a review of the literature, it appears that only the reaction between $Os_3(CO)_{12}$ and its more reactive derivative $Os_3(CO)_{10}(MeCN)_2$ with pyrroles have been studied.

The reaction between $Os_3(CO)_{10}(MeCN)_2$ and 2-formyl pyrrole shows similarities to the reaction with pyridine-2-carboxaldehyde. Again the aldehydic C-H bond was cleaved and an acyl bridge formed, rather than the direct reaction with the ring occurring, and on refluxing for 15 minutes in n-decalin decarbonylation resulted.[72] The products of this reaction are summarised in Scheme 1.3.14 and were proposed on the basis of spectroscopic evidence, and an X-ray crystal structure determination of the Me derivative. [73] The decarbonylation products were also shown to form in the direct reaction between $Os_3(CO)_{12}$ and pyrrole in refluxing decalin in addition to $Os_3(\mu\text{-H})(CO)_{10}(C_4H_3N)$ (Scheme 1.3.15). [72,74]

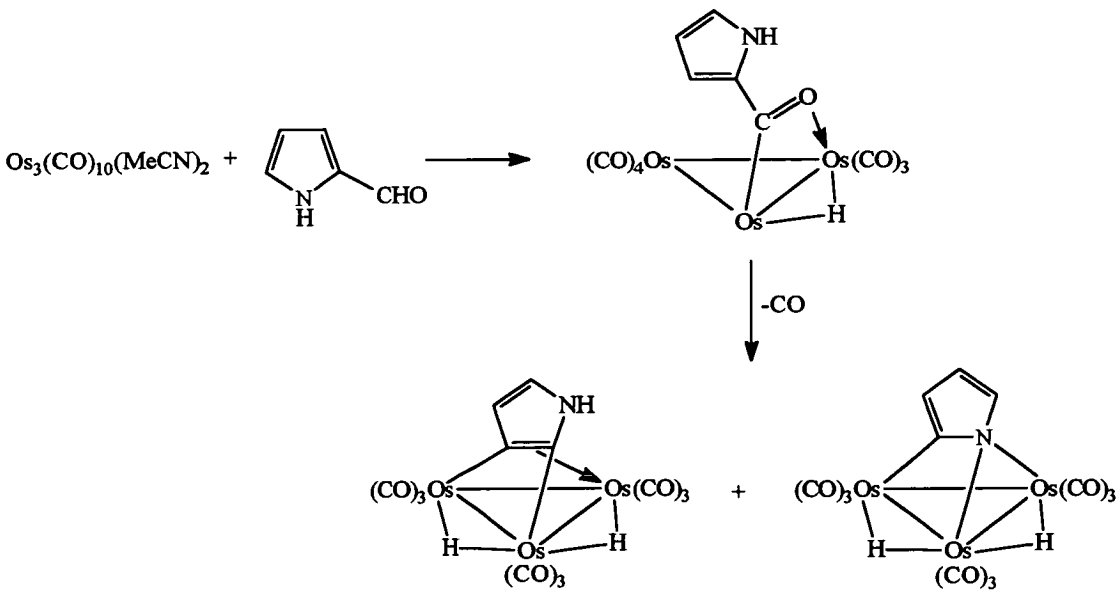

Scheme 1.3.14: Reaction of $Os_3(CO)_{10}(MeCN)_2$ with 2-formyl pyrrole, followed by subsequent decarbonylation resulting from thermolysis in refluxing decalin.

Cluster **a** was shown to isomerise to give **b** as determined by NMR spectroscopy. In addition, deuterium exchange experiments demonstrated that the resulting proton transfer to carbon was from the metal and not the nitrogen. Such an isomerisation is not possible for the methyl derivative which yields only the equivalent of isomer **a** on reaction with $Os_3(CO)_{12}$ in refluxing decalin.

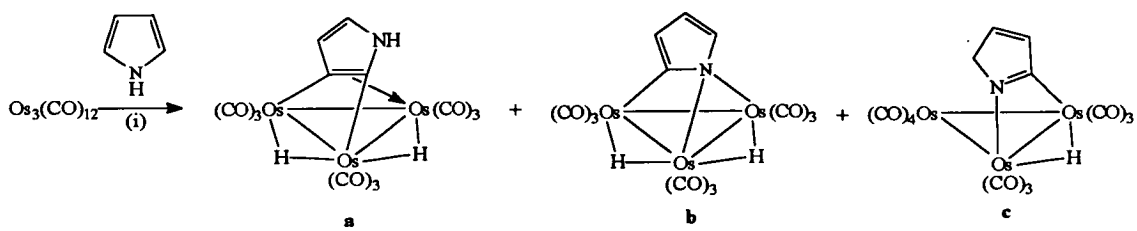

Scheme 1.3.15: Reaction of $Os_3(CO)_{12}$ and pyrrole, (i) in refluxing n-decane over 4 hours.

Treatment of $Os_3(CO)_{12}$ with indole [75] did not exhibit the same chemistry. Instead a disubstituted, *di-ortho*metallated Os_3 cluster, comparable to a known pyridine derivative [35,55] was formed as the major product (Scheme 1.3.16). The product was identified by the similarity of its IR carbonyl spectrum to that of its pyridine analogue, and from further ^1H NMR and X-ray crystallography studies. Its structure represents in effect the trapping of an unstable tautomer of indole. A second product was also formed in minute quantity and characterised as showing an analogous bonding mode to isomer a from the reaction with pyrrole, presented in the figure above.

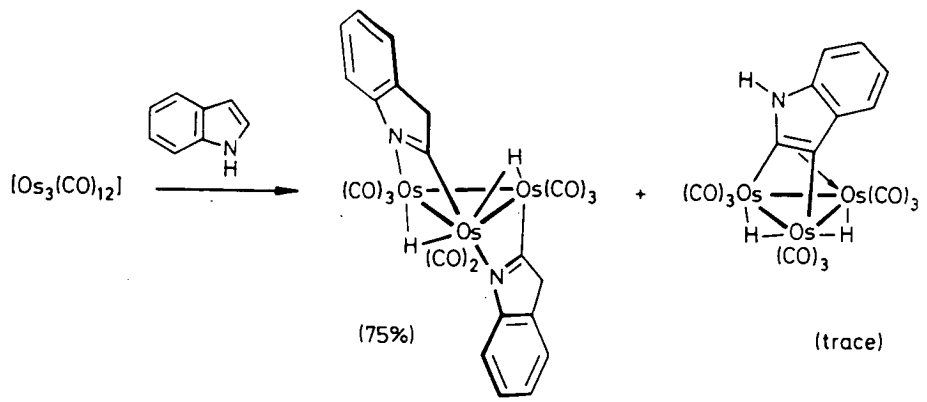

Scheme 1.3.16: Reaction of $Os_3(CO)_{12}$ with indole in refluxing decane over 4 hours.

Reaction of $Os_3(CO)_{10}(MeCN)_2$ with N-methyl pyrrole or N-methyl indole in refluxing cyclohexane produced a *mono*- hydrido species [76] in contrast to the reaction with $Os_3(CO)_{12}$. A rather different bonding mode to those observed previously was shown by X-ray crystallography (Figure 1.3.12). The ligand was co-ordinated through only a single carbon atom of the heterocyclic ring which bridged one edge of the Os_3 triangle.

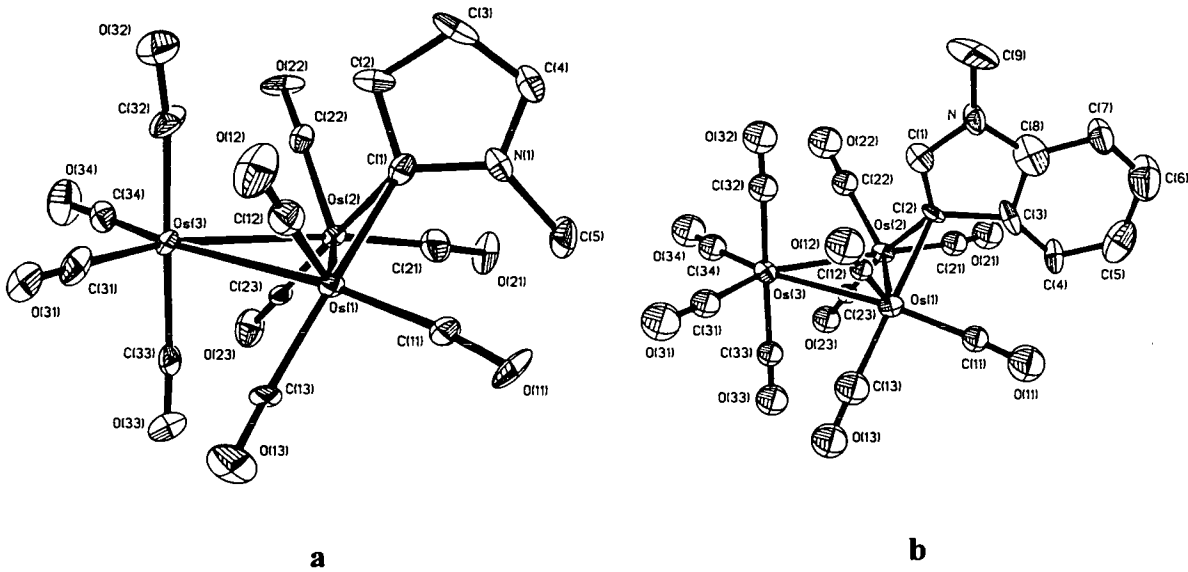

Figure 1.3.12: The molecular structures of **a**: the N-methyl pyrrolyl cluster $Os_3(\mu\text{-}H)(CO)_{10}(\mu\text{-}C_4H_3NMe)$, **b**: the N-methyl indolyl cluster $Os_3(\mu\text{-}H)(CO)_{10}(\mu\text{-}C_6H_4C_2HNMe)$.

The reaction of imidazole and its N-methyl derivative with $Os_3(CO)_{10}(MeCN)_2$ in refluxing benzene over one hour yielded two isomers (Figure 1.3.13). These were characterised by microanalysis and spectroscopy, in particular ^1H NMR spectrum, and in addition for the major isomer of the imidazole bound cluster, also by a single crystal X-ray diffraction study. [77]

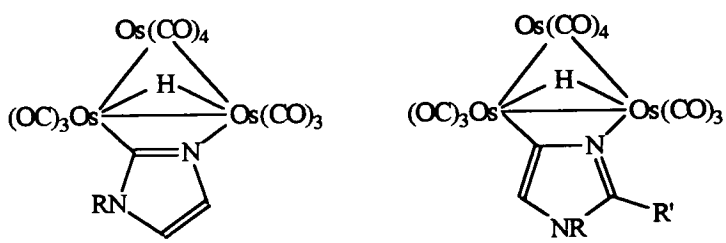

R= H, Me

Imidazole — R= H, R'= H
N-methyl imidazole — R= CH_3 , R'= H

Figure 1.3.13: The structures of the imidazole clusters: $Os_3(\mu\text{-}H)(CO)_{10}(C_3H_3N_2)$, and the N-methyl imidazole clusters: $Os_3(\mu\text{-}H)(CO)_{10}(C_4H_5N_2)$, **a**= minor isomer, **b**= major isomer.

Pyrazole reacted in a similar manner to form two isomers which were distinguished on the basis of ^{1}H NMR evidence. [77] The major isomer showed cleavage of the N-H bond to have occurred to give co-ordination to both nitrogens (Figure 1.3.14), which was obviously not sterically possible for the imidazoles.

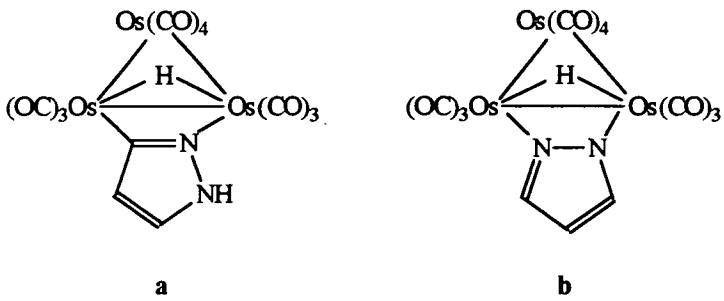

Figure 1.3.14: Structures of **a** the minor and **b**: the major isomers of the pyrrole clusters $Os_3(\mu\text{-}H)(CO)_{10}(C_3H_3N_2)$.

However, reaction of $Ru_3(CO)_{12}$ with pyridazine and its methyl derivatives in refluxing heptane was found to produce only dimers of the general formula $Ru_2(CO)_6(C_3R_3N_2)_2$ which did not show *ortho*metallation (Figure 1.3.15). [78]

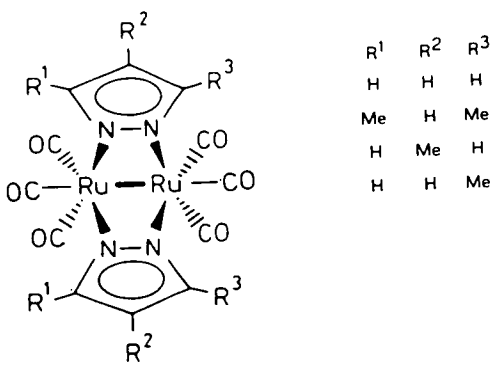

Figure 1.3.15: Structure of the $Ru_2(CO)_6(C_3R_3N_2)_2$ dimers.

Reaction of $Os_3(CO)_{10}(MeCN)_2$ with benzimidazole in refluxing benzene yielded two isomers, both of which were trinuclear. [77] The minor cluster product **a**, showed *ortho*metallation of the pyrrole ring only, whilst the major isomer **b** showed *ortho*metallation between the pyrrole and benzene rings (Figure 1.3.16). From the

reaction between the $Ru_3(CO)_{12}$ cluster and this ligand however, only isomer a was observed. [57]

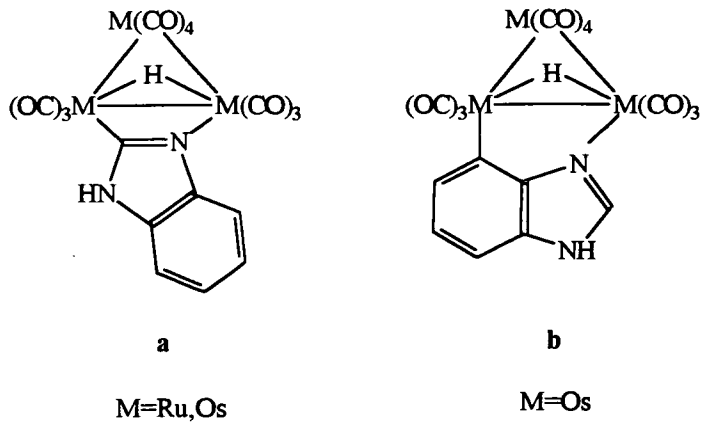

Figure 1.3.16: The structures of the isomers of the benzimidazole clusters $M_3(\mu\text{-}H)(CO)_{10}(C_7H_5N_2)$.

The ligand 2-azopyridine exists predominantly as its benzotetrazole tautomer and has been found to react with $Os_3(\mu\text{-}H)_2(CO)_{10}$ to produce the *di*-nitrogen bound trinuclear cluster presented in Figure 1.3.17. [33] Whilst reaction with $Ru_3(CO)_{12}$ and a similar ligand: benzotriazole in refluxing benzene gave instead a dimer showing co-ordination of the nitrogens only (Figure 1.3.18). [57]

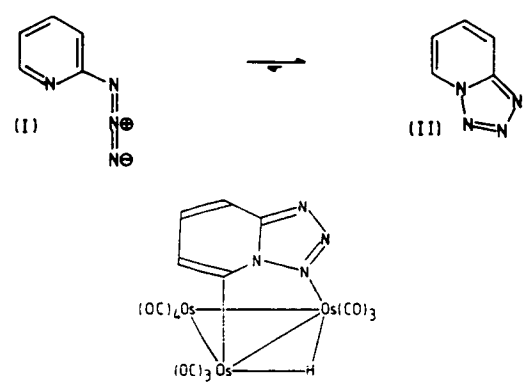

Figure 1.3.17: The tautomerisation of 2-azopyridine (I) to benzotetrazole(II), and the structure of the $Os_3(\mu\text{-}H)(CO)_{10}(C_5H_3N_4)$ product from its reaction with $Os_3(\mu\text{-}H)_2(CO)_{10}$.

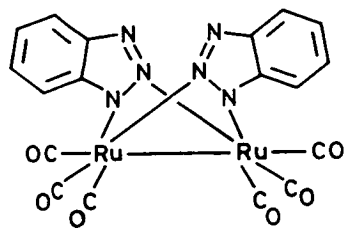

Figure 1.3.18: Structure of $Ru_2(CO)_6(C_6H_4N_3)_2$.

1.3.4 Diazines

The cluster $Ru_3(CO)_{10}$ (1,2-diazine) was first prepared by Cotton *et al.* [62,79] by the thermal reaction between $Ru_3(CO)_{12}$ and 1,2-diazine in thf at 50 °C, and it was shown by a single crystal X-ray diffraction study to possess three bridging carbonyl ligands (Figure 1.3.19).

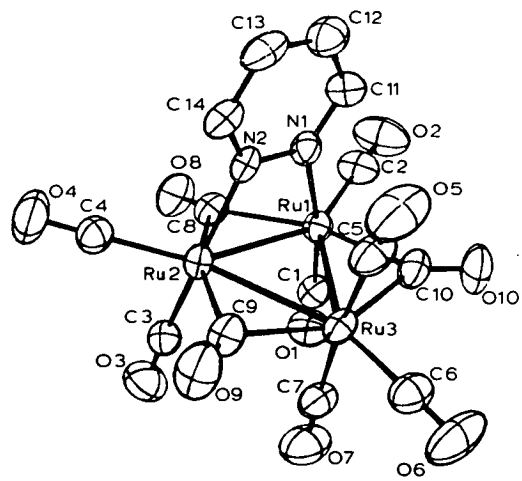

Figure 1.3.19: The molecular structure of $Ru_3(\mu\text{-}CO)_3(CO)_7(C_4H_4N_2)$.

In contrast, the cluster formed by treating the reactive *bis*-acetonitrile cluster $Ru_3(CO)_{10}(MeCN)_2$ with the ligand at room temperature shows only terminal carbonyl ligands, and has been found by ^1H NMR to possess a similar edge bridging ligand bonding through both nitrogens and is not *ortho*metallated. [54] Its structure is presented in Figure 1.3.20 for comparison, and is analogous to the osmium derivative,

which has been synthesised by the addition of two equivalents of Me_3NO to a THF solution of $Os_3(CO)_{12}$ at room temperature in the presence of the ligand. [80] The reaction between $Os_3(CO)_{10}$(cyclo-octene)$_2$, a more reactive derivative of the parent carbonyl cluster $Os_3(CO)_{12}$, and 1,2-diazine was found instead to result in *ortho*metallation at 50 °C, with only one of the two nitrogens bonding to the cluster.[55] An attempt to prepare the ruthenium analogue in this way proved unsuccessful. [54]

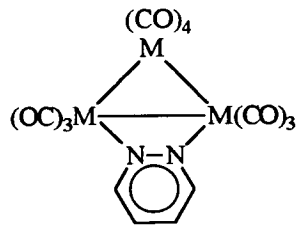

Figure 1.3.20: Structure of $M_3(CO)_{10}(C_4H_4N_2)$, (M= Ru, Os).

Although 1,2-diazine can form an N-N bridge on reaction with $M_3(CO)_{12}$ clusters (M= Ru, Os), a similar co-ordination is not possible for the 1,3- and 1,4-diazines, which react instead with $Ru_3(CO)_{10}(MeCN)_2$ [54] or $Os_3(CO)_{10}$(cyclo-octene)$_2$ [55] to give *ortho*metallated products.

1.3.5 Other Bidentate Ligands

1,8-napthyridine reacts with $Ru_3(CO)_{12}$ in a similar manner to the 1,2-diazine, forming the *tri*-carbonyl bridged cluster in refluxing hexane. [57] Further reaction with tetrafluoroboric acid produces the species $[Ru_3(\mu\text{-}H)(CO)_{10}(C_8H_6N_2)]^+[BF_4]^-$ which possesses only terminal carbonyls and an *ortho*metallated metal-metal bond. This anion can be deprotonated by the mild base triethylamine to reform the bridged carbonyl cluster (Figure 1.3.21).

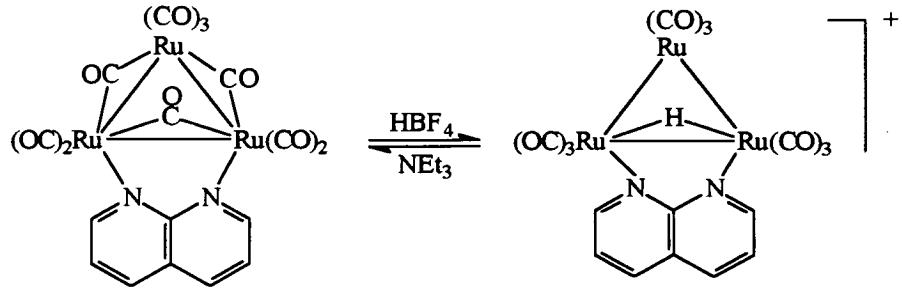

Figure 1.3.21: The chemical interconversion of the 1,8-napthyridine clusters $Ru_3(CO)_{10}(C_8H_6N_2)$ and $[Ru_3(\mu\text{-}H)(CO)_{10}(C_8H_6N_2)]^+$.

Treatment of the reactive cluster $Os_3(CO)_{10}$(cyclo-octene)$_2$ with 2,2'-bipyridyl at room temperature was found to produce the *ortho*metallated cluster $Os_3(\mu\text{-}H)(CO)_9(C_{10}H_7N_2)$ whose X-ray structure is shown in Figure 1.3.22. [55]

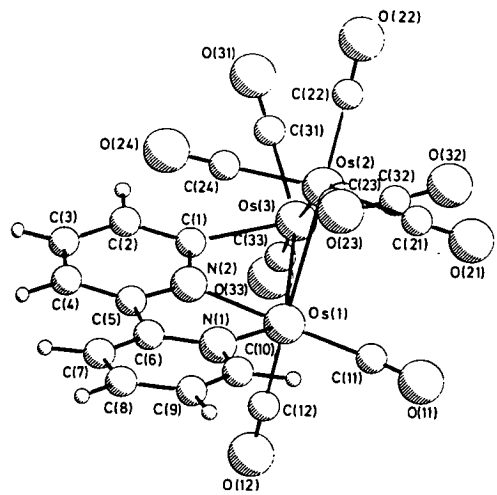

Figure 1.3.22: The molecular structure of $Os_3(\mu\text{-}H)(CO)_9(C_{10}H_7N_2)$.

The ruthenium cluster $Ru_3(CO)_{10}(MeCN)_2$ undergoes a similar reaction, forming the $Ru_3(CO)_{10}$(bipy) cluster which converts to the *ortho*metallated species in refluxing toluene over 15 minutes. [54] However, the structure proposed in the literature (Figure 1.3.23, **a**) would result in a poor overlap between the lone pair of electrons on nitrogen and the metal orbitals because of the relative orientation of the lone pairs.

In addition there would appear to be steric hindrance resulting from the proximity of the ring proton H(1) to the metal framework. By comparison with the osmium analogue, the structure presented in Figure 1.3.23, **b** seems more plausible. Similarly, the $Ru_3(CO)_{10}$(bipy) derivative would be assigned as bound to a single metal atom to minimise steric repulsion.

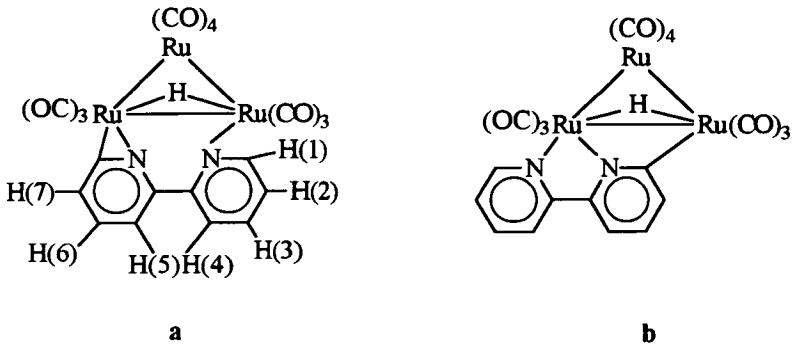

Figure 1.3.23: Structures of $Ru_3(\mu\text{-}H)(CO)_{10}(C_{10}H_7N_2)$ **a**: as proposed in the literature, and **b**: as proposed by a consideration of steric repulsion and by analogy with the reported osmium derivative whose molecular structure has been determined.

In contrast to the *ortho*metallation reaction between $Os_3(CO)_{12}$ and 2,2'-bipyridyl, [55] reaction with the ruthenium analogue $Ru_3(CO)_{12}$ in refluxing cyclohexane results in the formation of $Ru_3(\mu\text{-}CO)_2(CO)_8$(bipy) [39] which shows a structure comparable to $Fe_3(CO)_{12}$ [81] (Figure 1.3.24). Rather than spanning a metal-metal edge, the ligand is co-ordinated terminally. Likewise, refluxing the cluster with 1,10-phenanthroline, 2,2'-biquinoline or 2,2'-bipyrimidine in THF yields similar products.

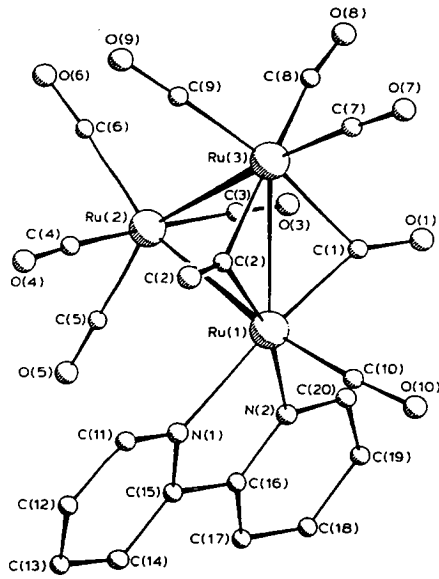

Figure 1.3.24: The molecular structure of $Ru_3(\mu\text{-}CO)_2(CO)_8(bipy)$.

1.4 Concluding Remarks

The work reviewed herein shows the range of compounds which have been previously synthesised. Research has shown a tendency for the clusters to undergo *ortho*metallation upon heating the $M_3(CO)_{12}$ (M= Ru, Os) clusters and ligand together, although some exceptions have been found which result in the formation of $Fe_3(CO)_{12}$ like structures. Indeed, *ortho*metallation need not be brought about by vigorous heating, often the more reactive acetonitrile or *bis* cyclo-octene derivatives will react similarly at room temperature or under much milder thermal conditions. Little attention has however been focused on "higher" nuclearity clusters, with the majority of those studied being confined to trinuclear clusters. With the exception of Dutton's work on $Ru_5C(CO)_{15}$, which is discussed in Chapter Three, only a few osmium and unusual ruthenium clusters have been briefly studied (Scheme 1.3.5-1.3.7, 1.3.11 and Figures 1.3.2-1.3.4). Other ligands, in particular benzene and its derivatives, but also alkynes and alkenes, have been reported for a range of cluster nuclearities for both ruthenium and osmium.

In the chapters which follow, we shall build upon this chemistry with a discussion of the reactivity of $Ru_4(\mu\text{-}H)_4(CO)_{12}$, $Os_4(\mu\text{-}H)_4(CO)_{12}$, $Ru_5C(CO)_{15}$, and $Ru_6C(CO)_{17}$ towards nitrogen heterocycles (L-L). Furthermore, the electronic spectroscopy, electrochemistry, and spectroelectrochemistry observed for the $Ru_4(\mu\text{-}H)_4(CO)_{10}$(L-L) derivatives will be discussed, thus expanding upon an area which has previously focused on the unsubstituted clusters.

1.5 References

1. H.M. Powell, R.V.G. Ewens, *J. Chem. Soc.*, 1939, 286.
2. F.A. Cotton, *Prog. Inorg. Chem.*, 1976, **21**, 1.
3. L.F. Dahl, R.E. Rundle, *Acta Cryst.*, 1963, **16**, 419.
4. E.L. Muetterties, *Bull. Soc. Chim. Belg.*, 1975, **84**, 959.
5. See *e.g.* E.L. Muetterties, M.J. Krause, *Angew. Chem. Int. Ed. Engl.*, 1983, **22**, 135, and references cited therein.
6. E.L. Muetterties, T.N. Rhodin, E. Band, C.F. Brucker, W.R. Pretzer, *Chem. Rev.*, 1979, **79**, 91.
7. V.G. Albano, A. Ceriotto, P. Chini, G. Ciani, S. Martinego, W.M. Anker, *J. Chem. Soc., Chem. Commun.*, 1975, 859..
8. P.F. Jackson, B.F.G. Johnson, J. Lewis, W.J.H. Nelson, M. McPartlin, *J. Chem. Soc., Dalton Trans.*, 1982, 2099.
9. G. Ciani, A. Sironi, S. Martinego, *J. Chem. Soc., Dalton Trans.*, 1982, 1099.
10. R. Baetzold, *Adv. Catal.*, 1976, **25**, 1.
11. J.C. Robertson, C.W. Wilmsen, *J. Vac. Sci. Technol.*, 1972, **9**, 901.
12. G.A. Samorjai, B.E. Bent, *Adv. Colloid Interface Sci.*, 1989, **29**, 223.
13. N. Sheppard, C. de la Cruz, *React. Kinet. Catal. Lett.*, 1987, **35**, 21.
14. D. Braga, F. Grepioni, E. Parsini, P.J. Dyson, B.F.G. Johnson, D. Reed, D.S. Shepherd, P.J. Bailey, J. Lewis, *J. Organomet. Chem.*, 1993, **462**, 301.
15. a) F.A. Cotton, D.L. Hunter, *Inorg. Chim. Acta.*, 1974, **11**, L9; b) L. Milone, S. Aime, E.W. Randall, E. Rosenberg, *J. Chem. Soc., Chem. Commun.*, 1975, 452; c) A. Forster, B.F.G. Johnson, J. Lewis, T.W. Matheson, B.H. Robinson, G.W. Jackson, *J. Chem. Soc., Chem. Commun.*, 1974, 1042.
16. B. Rausenberger, W. Swietch, C.S. Rastomjee, M. Mundschau, W. Engel, E. Zeitler, A.M. Bradshaw, *Chem. Phys. Lett.*, 1993, **215**, 109.
17. See *e.g* a) I.A. Oxton, D.B. Powell, N. Sheppard, K. Burgess, B.F.G. Johnson, J. Lewis, *J. Chem. Soc., Chem. Commun.*, 1982, 719; b) U.A. Jayasooriya, C.E. Anson, O. Al-Jowder, G. D'Alfonso, P.L. Stanghellini, R. Rosetti, *Surface Science*, 1993, **294**, 131; c) C.E. Anson, N. Sheppard, D.B. Powell, B.R. Bender, J.R. Norton, *J. Chem. Soc., Faraday Trans.*, 1994, **90**, 1449; d) C.E. Anson, B.T. Keiller, I.A. Oxton, D.B. Powell, N. Sheppard, *J. Chem. Soc., Chem. Commun.*, 1983, 470; e) C.E. Anson, B.J. Bandy, M.A. Chesters, B.T. Keiller, I.A. Oxton, N. Sheppard, *J.Electron Spec. and Related Phenom.*, 1983, **29**, 315.
18. G. Ertl, in *Metal Clusters in Catalysis*, (Editors: B.C. Gates, L. Guczi, H. Knözinger), Elsevier, Amsterdam 1986 p.577.

19. M. Moskovits, *Acc. Chem. Res.* , 1979, **12**, 229.

20. H. Ibach, S. Lehwald, *J. Vac. Sci. Technol.*, 1978, **15**, 407.

21. L. Kesmodel, L. Dubois, G.A. Somorjai, *J. Chem. Phys.*, 1979, **70**, 2180.

22. P. Skinner, M.W. Howard, I.A. Oxton, S.F.A. Kettle, D.B. Powell, N. Sheppard, *J. Chem. Soc. Faraday Trans.*, 1981, **77**, 1203.

23. C.E. Anson, N. Sheppard, D.B. Powell, J.R. Norton, W. Fischer, R.L. Keiter, B.F.G. Johnson, J. Lewis, A.K. Bhattacharrya, S.A.R. Knox, M.L. Turner, *J. Am. Chem. Soc.*, 1994, **116**, 3058.

24. a) R.F. Lin, G.S. Blackman, M.A. van Hove, G.A. Somorjai, *Acta Crystallogr., Sect. B*, 1987, **43**, 368; b) M.A. van Hove, R.F. Lin, G.A. Somorjai, *J. Am. Chem. Soc.*, 1986, **108**, 2532.

25. a) B.F.G. Johnson, J. Lewis, M. Martinelli, A.H. Wright, D. Braga, F. Grepioni, *J.Chem. Soc., Chem. Commun*, 1990, 364; b) D. Braga, F. Grepioni, B.F.G. Johnson, J. Lewis, C.E. Housecroft, M. Martinelli, *Organometallics*, 1991, **10**, 1260.

26. a) M.P. Gomez-Sal, B.F.G. Johnson, J. Lewis, P.R. Raithby, A.H. Wright, *J. Chem. Soc., Chem. Commun.*, 1985, 1682; b) M.A. Gallup, M.P. Gomez-Sal, C.E. Housecroft, B.F.G. Johnson, J. Lewis, S.M. Owen, P.R. Raithby, A.H. Wright, *J. Am. Chem. Soc.*, 1992, **114**, 2502.

27. P.J. Dyson, B.F.G. Johnson, J. Lewis, M. Martinelli, D. Braga, F. Grepioni, *J. Am. Chem. Soc.*, 1993, **115**, 9062.

28. a) E. Bertl, G. Rosina, F.P. Netzer, *Surf. Sci.*, 1987, **183**, 1; b) M. Neumann, J.U. Mack, E. Bertl, F.P. Netzer, *Surf. Sci.*, 1985, **162**, 395; c) F.P. Netzer, G. Rosina, E. Bertl, H. Saalfeld, *Surf. Sci.*, 1987, **184**, L397.

29. B.F.G. Johnson, J. Lewis, C. Housecroft, M. Gallup, M. Martinelli, D. Braga, F. Grepioni, *J. Mol. Catal.*, 1992, **74**, 61.

30. N.J. DiNardo, P. Avouris, J.E. Demuth, *J. Chem Phys.*, 1984, **81**, 2169.

31. J.E. Demuth, K. Christmann, P.N. Sanda, *Chem. Phys. Lett.*, 1980, **76**, 201.

32. See *e.g.* a) K.H. Pannell, B.L. Kalostra, C. Párkányi, *J. Heterocyclic Chem.*, 1978, **15**, 1057; b) S.G. Davies, M.R. Shipton, *J. Chem. Soc. Perkin Trans. I*, 1991, 501; c) E.J. Wucherer, E.L. Muetterties, *Organometallics*, 1987, **6**, 1696; d) E.J. Wucherer, E.L. Muetterties, *Organometallics*, 1987, **6**, 1691; e) R.H. Morris, J.M. Ressner, *J. Chem. Soc., Chem. Commun.*, 1983, 909; f) C. Elschenbroich, J. Koch, J. Kroker, M. Wünsch, W. Massa, G. Baum, G. Stork, *Chem. Ber.*, 1988, **121**, 1983; g) H.W. Choi, M.S. Sollberger, *J. Organomet. Chem.*, 1983, **243**, C39; h) P.L. Timms, *Angew. Chem. Int. Ed. Engl.*, 1975, **14**, 273.

33. K. Burgess, *Polyhedron*, 1984, **3**, 1175.

34. M.I. Bruce, M.P. Cifuentes, M.G. Humphrey, *Polyhedron*, 1991, **10**, 277.

35. C.C Yin, A.J. Deeming, *J. Chem. Soc., Dalton Trans.*, 1975, 2091.

36. E.O. Fischer, V. Kiener, *J. Organomet. Chem.*, 1970, **23**, 215.

37. B.F.G. Johnson, J. Lewis, D.A. Pippard, *J. Chem. Soc., Dalton Trans.*, 1981, 407.

38. P.A. Dawson, B.F.G. Johnson, J. Lewis, J. Puga, P.R. Raithby, M.J. Rosales, *J. Chem. Soc., Dalton Trans.*, 1982, 233.

39. M.I. Bruce, M.G. Humphrey, M.R. Snow, E.R.T. Tieknik, R.C. Wallis, *J. Organomet. Chem.*, 1986, **314**, 311.

40. G.A. Foulds, B.F.G. Johnson, J. Lewis, *J. Organomet. Chem.*, 1985, **296**, 147.

41. B.R. Cockerton, A.J. Deeming, *J. Organomet. Chem.*, 1992, **426**, C36.

42. M. Gallup, Ph.D. Thesis, University of Cambridge, 1988.

43. T. Dutton, Ph.D. Thesis, University of Cambridge, 1989.

44. T. Dutton, B.F.G. Johnson, J. Lewis, S.M. Owen, P.R. Raithby, *J. Chem. Soc., Chem. Commun.*, 1988, 1423.

45. a) C.J. Adams, M.I. Bruce, B.W. Skelton, A.H. White, *J. Organomet. Chem.*, 1993, **445**, 211; b) C.J. Adams, M.I. Bruce, B.W. Skelton, A.H. White, *J. Organomet. Chem.*, 1992, **423**, 97.

46. K.I. Hardcastle, B.R. Cockerton, A.J. Deeming, M. Karim, *J. Chem. Soc., Dalton Trans.*, 1992, 1607.

47. G.R. John, B.F.G. Johnson, J. Lewis, *J. Organomet. Chem.*, 1979, **181**, 143.

48. M-A. Pearsall, Ph.D. Thesis, University of Cambridge, 1984.

49. B.F.G. Johnson, J. Lewis, M. McPartlin, M-A. Pearsall, A. Sironi, *J. Chem. Soc., Chem. Commun.*, 1984, 1089.

50. P.F. Jackson, B.F.G. Johnson, J. Lewis, W.J.H. Nelson, M. McPartlin, *J. Chem. Soc., Dalton Trans.*, 1982, 2099.

51. B.F.G. Johnson, J. Lewis, W.J.H. Nelson, M-A. Pearsall, P.R. Raithby, M.J. Rosales, M. McPartlin, A. Sironi, *J. Chem. Soc., Dalton Trans.*, 1987, 327.

52. B.F.G. Johnson, J. Lewis, P.R. Raithby, M.J. Rosales, *J. Organomet. Chem.*, 1983, **259**, C9.

53. G.R. John, B.F.G. Johnson, J. Lewis, W.J.H. Nelson, M. McPartlin, *J. Organomet. Chem.*, 1979, **171**, C14.

54. G.A. Foulds, B.F.G. Johnson, J. Lewis, *J. Organomet. Chem.*, 1985, **294**, 123.

55. A.J. Deeming, J.D.J. Backer-Dirks, M.B. Hursthouse, R. Peters, *J. Chem. Soc., Dalton Trans.*, 1982, 787.

56. R.H. Fish, T.J. Kim, J.L. Stewart, J.H. Bushweller, R.K. Rosen, J.W. Dupon, *Organometallics*, 1986, **5**, 2193.

57. J.A. Cabeza, L.A. Oro, A. Tiripicchio, M. Tiripicchio-Cameilini, *J. Chem. Soc., Dalton Trans.*, 1988, 1437.

58. T. Venäläinen, J. Pursianen, T.A. Pakkanen, *J. Chem. Soc., Chem. Commun.*, 1985, 1348.

59. A.J. Deeming, R. Peters, *J. Organomet. Chem.*, 1980, **202**, C39.

60. A.J. Deeming, R. Peters, J.D.J. Backer-Dirks, M.B. Hursthouse, *J. Chem. Soc., Dalton Trans.*, 1982, 1205.

61. P.L. Andreu, J.A. Cabeza, V. Riera, Y. Jeannin, D. Miguel, *J. Chem. Soc., Dalton Trans.*, 1990, 2201.

62. F.A. Cotton, J.D. Jamerson, *J. Am. Chem. Soc.*, 1976, **98**, 5396.

63. J.A. Cabeza, I. del Río, J.M. Fernández-Colinas, A. Llamazares,V. Riera, *J. Organomet. Chem.*, 1995, **494**, 169.

64. K. Burgess, B.F.G. Johnson, J. Lewis, *J. Organomet. Chem.*, 1982, **233**, C55.

65. G.R. Crooks, B.F.G. Johnson, J. Lewis, J.G. Williams, G. Gamlen, *J. Chem. Soc.* A, 1969, 2761.

66. M. Rotem, I. Goldberg, U. Shmueli, Y. Shvo, *J. Organomet. Chem.*, 1986, **314**, 185.

67. H.G. Ang, B. Chang, W.L. Kwik, E.S.H. Sim, *J. Organomet. Chem.*, 1994, **474**, 153.

68. A.J. Deeming, M.B. Smith, *J. Chem. Soc., Dalton Trans.*, 1993, 3383.

69. K. Burgess, H.D. Holden, B.F.G. Johnson, J. Lewis, M.B. Hursthouse, N.P.C. Walker, A.J. Deeming, P.J. Manning, R. Peters, *J. Chem. Soc., Dalton Trans.*, 1985, 85.

70. J.A. van Doorn, P.W.N.M. van Leeuwen, *J. Organomet. Chem.*, 1981,**222**, 299.

71. A.J. Deeming, M.B. Smith, *J. Chem. Soc., Dalton Trans.*, 1993, 2041.

72. A.J. Arce, Y. De Sanctis, A.J. Deeming, *J. Organomet. Chem.*, 1986, **311**, 371.

73. A.J. Deeming, A.J. Arce, Y. De Sanctis, M.W. Day, K.I. Hardcastle, *Organometallics*, 1989, **8**, 1408.

74. C.C. Yin, A.J. Deeming, *J. Chem. Soc., Dalton Trans.*, 1982, 2563.

75. K.I. Hardcastle, H. Minassian, A.J. Arce, Y. De Sanctis, A.J. Deeming, *J. Organomet. Chem.*, 1989, **368**, 119.

76. A.J. Arce, J. Manzur, M. Marquez, Y. De Sanctis, A.J. Deeming, *J. Organomet. Chem.*, 1991, **412**, 177.

77. J.R. Shapley, D.E. Samkoff, C. Bueno, M.R. Churchill, *Inorg. Chem.*, 1982, **21**, 634.

78. F. Neumann, G. Süss-Fink, *J. Organomet. Chem.*, 1989, **367**, 175.

79. F.A. Cotton, B.E. Hanson, J.D. Jamerson, *J. Am. Chem. Soc.*, 1977, **99**, 6588.

80. F.A. Cotton, B.E. Hanson, *Inorg. Chem.*, 1977, **16**, 2820.

81. a) C. H Wei, L.F. Dahl, *J. Am. Chem. Soc.*, 1969, **91**, 1351; b) F.A. Cotton, J.M. Troup, *J. Am. Chem. Soc.*, 1974, **96**, 4155.

Chapter Two

The Reactions of $M_4(\mu\text{-}H)_4(CO)_{12}$ (M= Ru, Os) with Nitrogen Heterocyclic Ligands

2.1 Introduction

No previous work has been reported in the literature to date of the reactivity of the $M(\mu\text{-}H)_4(CO)_{12}$ (M= Ru **1**, Os, **2**) clusters towards nitrogen heterocycles. Research into the ruthenium cluster's reactivity has been based mainly on its reaction with phosphines although some work has been reported on the deprotonation of the cluster. [1] Examples of *mono-*, *di-*, *tri-*, and tetrasubstitution have all been reported in the literature [2] but we shall limit our discussion to only the *mono-* and the disubstituted products since their formulations have been verified by single crystal X-ray studies and are most relevant to the later discussion of the experimental results.

2.1.1 Monosubstitution

The $Ru_4(\mu\text{-}H)_4(CO)_{12}$ cluster **1** is known to react with monodentate tertiary phosphines under reflux conditions *via* a step-wise substitution of the carbonyl ligands to produce the corresponding $Ru_4(\mu\text{-}H)_4(CO)_{12-n}L_n$ (n= 1-4) clusters with the major product being determined by the ratio of cluster to ligand. [2] The only crystallographic report of a monosubstituted derivative is that for $Ru_4(\mu\text{-}H)_4(CO)_{11}[P(OMe)_3]$, however only a preliminary set of X-ray data has been published [3] and to date a full paper has not been reported. The structure shows four long Ru-Ru bonds (2.93 Å) and two shorter Ru-Ru bonds (2.76 Å) which are opposite each other and are presumed to be due to unbridged Ru-Ru bonds. Its proposed structure is given in Figure 2.1.1. The longer bonds represent hydride bridged metal-metal bonds, M (μ-H) M, which are closed two electron three centre bonds. These bonds have less bonding electron density between the metal atoms than normal two centre, two electron bonds have and are consequently longer. The observed differences in metal-metal bond lengths is a common feature of $Ru_4(\mu\text{-}H)_4$ systems and is often used

to infer the position of bridging hydrides when they cannot be found directly from crystallographic data.

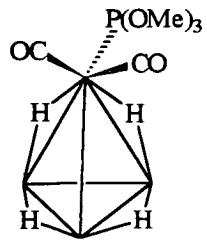

Figure 2.1.1: The proposed structure of $Ru_4(\mu\text{-}H)_4(CO)_{11}[P(OMe)_3]$.

This compound has also subsequently been synthesised by near UV irradiation of a solution of the parent cluster **1** in the presence of the phosphine ligand, [4] and by substitution initiated by sodium diphenyl ketyl. [5] NMR studies have shown that the hydrides are highly fluxional in solution and give rise to a doublet due to splitting of the hydride resonance by phosphorus. [6]

2.1.2 Disubstitution

The possible co-ordination geometries which can exist for the disubstitution of $Ru_4(\mu\text{-}H)_4(CO)_{12}$ **1** are: a) terminal co-ordination in which both donor ligands bond to a single metal atom; b) terminal co-ordination in which both donor ligands bond to different metal atoms; and c) bridging co-ordination in which the ligand spans two metal atoms. All of these geometries have been reported.

The 1:1 substitution reaction of **1** with PPh_3 under reflux in hexane has been found to produce not only the monosubstituted product but also some of the *di-* and trisubstituted products and large amounts of unreacted starting material. Reaction with an excess of ligand was generally found to produce only the *di-* and trisubstituted

products at 70 °C but at higher temperatures gave almost exclusively the tetrasubstituted derivative. [2b]

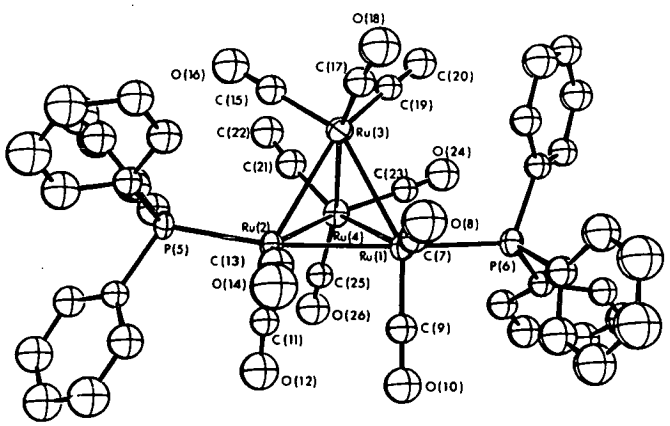

Figure 2.1.2: The structure of $Ru_4(\mu\text{-}H)_4(CO)_{10}(PPh_3)_2$. The position of the bridging hydrides are inferred from the Ru-Ru bond lengths but are not shown. Mean Ru-Ru (long) 2.966(16) Å and mean Ru-Ru (short) 2.772(16) Å.

The structure of the disubstituted product is given in Figure 2.1.2 and shows that the two phosphines have co-ordinated to separate metal centres thus reducing their steric repulsion, and shows the same hydride distribution as observed for the parent cluster. [7] Direct reaction of cluster **1** with the bidentate diphos ligand ($PPh_2CH_2CH_2PPh_2$) at 60 °C [8] however, was found to yield the cluster $Ru_4(\mu\text{-}H)_4(CO)_{10}$(diphos) whose structure shows the ligand terminally co-ordinated as previously, but, because the alkyl chain between the phosphines is sufficient to minimise any steric repulsion between them, the donors co-ordinate to only a single metal atom (Figure 2.1.3).

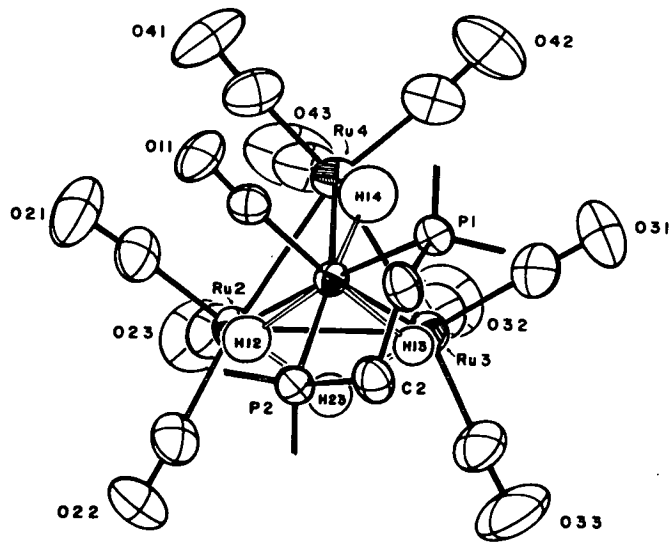

Figure 2.1.3: The solid state structure of $Ru_4(\mu\text{-}H)_4(CO)_{10}$(diphos) in which the hydrides were directly located by crystallography. Phenyl rings and hydrogen atoms on C(1) and C(2) have been omitted for clarity. Mean Ru-Ru (long) 2.970(3) Å and mean Ru-Ru (short) 2.791(7) Å.

An NMR study of the cluster has shown that the hydrides are scrambled over the metal framework and has been interpreted as arising from the movement of the hydrides from bridging to terminal to bridging positions. [9] Although this exchange is observed in solution, the solid state structure of the cluster shows the hydrides to be in a single fixed configuration which differs from the parent cluster.

There are only three simple geometries which can exist for an $M_4(\mu\text{-}H)_4$ molecular core containing only bridging hydride ligands and these are shown in Figure 2.1.4.

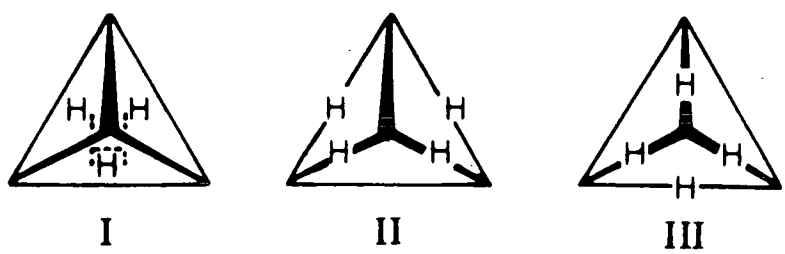

Figure 2.1.4: The possible geometries of an $Ru_4(\mu\text{-}H)_4$ molecular core containing only bridging hydrides. **I**= Facially bridging hydrides; **II**= two edge bridging and two base bridging hydrides; **III**= three edge bridging and one base bridging hydride.

In the figure, **I** represents the structure found in $Re_4(\mu\text{-}H)_4(CO)_{12}$ [10] and $Co_4(\mu\text{-}H)_4(\eta^5\text{-}C_5H_5)_4$ [11] in which the hydrides are found to bridge facially, and **II** represents the hydride arrangement found in for example $Ru_4(\mu\text{-}H)_4(CO)_{12}$ **1** [7] and $Ru_4(\mu\text{-}H)_4(CO)_{11}[P(OMe)_3]$, [3] whilst **III** is known for the $Ru_4(\mu\text{-}H)_4(CO)_{10}$(diphos) cluster (Figure 2.1.3) and has been shown to be the geometry observed in the nitrogen heterocyclic derivatives of **1** discussed herein.

The reaction between the $Ru_4(\mu\text{-}H)_4(CO)_{12}$ cluster and diphos has been repeated using chemical rather than thermal activation. Using 2.2 equivalents of Me_3NO at 25 °C a new phosphine bridging isomer was produced (Figure 2.1.5). [12] This isomer was found to convert back to the terminal isomer in solution over a period of a few days or when heated at 60 °C for 2-3 hours (the conditions used previously to form the terminal isomer). These results perhaps imply that the terminal isomer is the thermodynamic product and the bridged isomer the kinetic product. Variable temperature ^1H NMR studies have shown coalescence of the hydride resonances occurring between 27 °C and -102 °C. [12] The hydride ligands although chemically dissimilar, have become equivalent as a result of fast exchange, but again the crystal structure shows only a single fixed geometry.

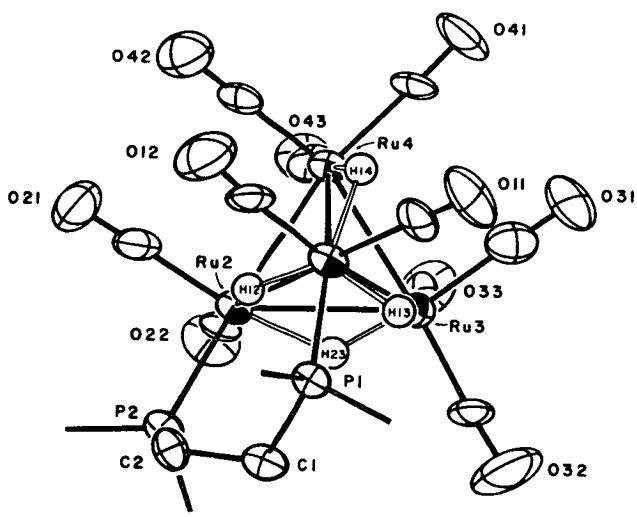

Figure 2.1.5: The molecular structure of $Ru_4(\mu\text{-}H)_4(CO)_{10}(\mu\text{-diphos})$ which shows configuration **III**. The phenyl groups and methylene hydrogens on C(1) and C(2) have been omitted for clarity. Mean Ru-Ru (long) 2.989(5) Å and mean Ru-Ru (short) 2.781(2) Å.

In summary, the phosphine derivatives have been found to undergo *mono-*, *di-*, *tri-*, and tetrasubstitution. Disubstitution is observed for the 1:1 phosphine:cluster reaction with PPh_3 and NMR studies have indicated that the hydrides are highly fluxional in solution. In contrast, the solid state molecular structures imply that only a single hydride distribution is present in which the hydrides are found to bridge Ru-Ru edges and exhibit either geometry **II** or **III** (Figure 2.1.4). On the basis of the diphos reactions, it would appear that terminal co-ordination of the ligand to a single metal atom gives the most thermodynamically stable product. Reference will be made to these compounds where appropriate in the following sections which discuss the reaction of $M_4(\mu\text{-}H)_4(CO)_{12}$ (M= Ru, Os) with the series of nitrogen heterocyclic ligands presented in Figure 2.1.6.

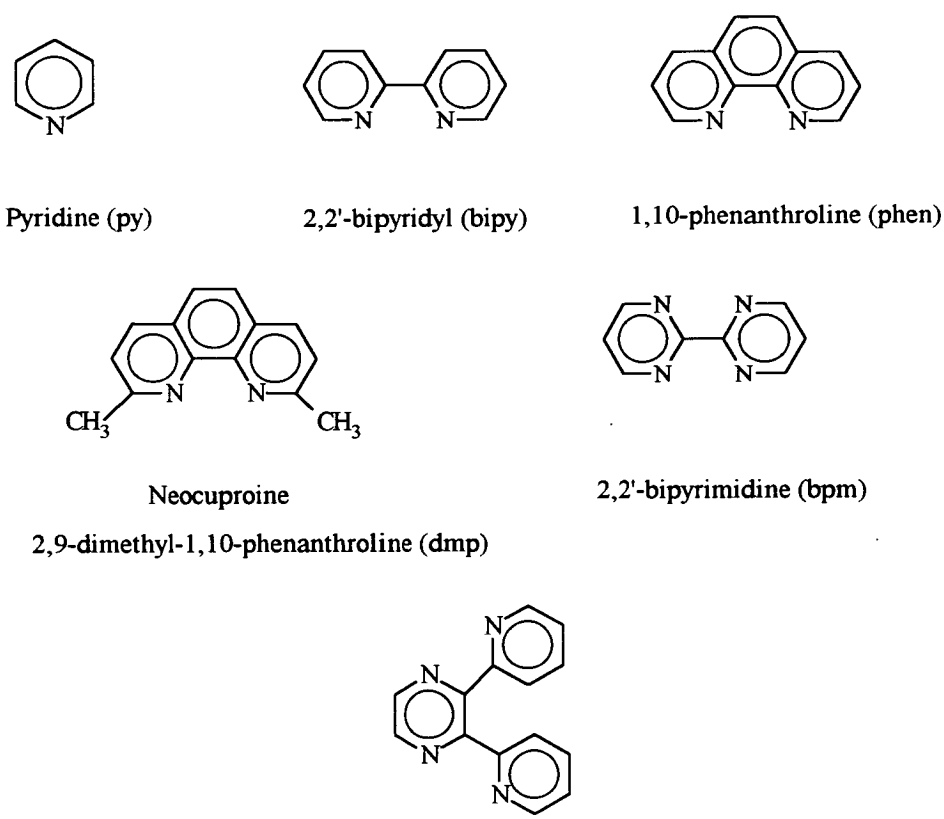

Figure 2.1.6: The series of nitrogen heterocyclic ligands investigated.

Reactions of $Ru_4(\mu\text{-}H)_4(CO)_{12}$ with Nitrogen Heterocycles

2.2 Reaction of $Ru_4(\mu\text{-}H)_4(CO)_{12}$ with Pyridine

A dichloromethane solution of the $Ru_4(\mu\text{-}H)_4(CO)_{12}$ cluster **1** in the presence of an excess of pyridine was activated at -78 °C by the dropwise addition of 1.1 equivalents of trimethylamine-N-oxide (Me_3NO) and left to react slowly as it warmed to room temperature. The solution changed from orange at room temperature to deep yellow at -78 °C before addition of Me_3NO, and some precipitation was observed upon cooling. A deep orange/red solution was produced upon warming to room temperature from which three products were chromatographically separated using hexane/dichloromethane (7:3 v/v) as eluent. In order of elution these products were identified as unreacted cluster **1**, $Ru_4(\mu\text{-}H)_4(CO)_{11}(py)$ **3**, and $Ru_4(\mu\text{-}H)_4(CO)_{10}(py)_2$ **4** on the basis of IR, mass spectrometry, and in addition for **4** by ^1H NMR and X-ray crystallography (Scheme 2.2.1).

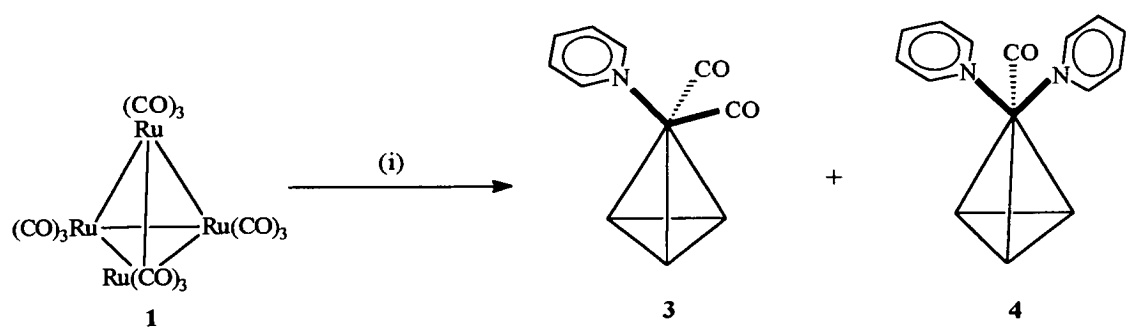

1 3 4

Scheme 2.2.1: Formation of $Ru_4(\mu\text{-}H)_4(CO)_{11}(py)$ **3** and $Ru_4(\mu\text{-}H)_4(CO)_{10}(py)_2$ **4** from $Ru_4(\mu\text{-}H)_4(CO)_{12}$: (i)1.1 equivalents Me_3NO at -78° C. Hydride ligands have been omitted for clarity.

Results and Discussion

The unreacted cluster **1** was easily identified on the basis of its IR carbonyl spectrum and was present in approximately the same yield as **4**. Compound **3** was

characterised on the basis of its mass spectrum which showed the parent ion peak at M^+= 796 (calc 795) amu followed by the subsequent loss of carbonyl ligands. The remaining product 4 was initially formulated as $Ru_4(\mu\text{-}H)_4(CO)_{10}(py)_2$ on the basis of its mass spectrum which showed a strong parent ion peak at 847 (calc 846) amu followed by the loss of ten carbonyls. The IR spectrum shows peaks in the region 2075-1958 cm^{-1} indicating that only terminal carbonyls are present in the molecule. To avoid the overlap of the $CHCl_3$ peak with one of the cluster's resonances, the ^1H NMR was recorded in CD_2Cl_2. Three resonances are observed at δ values of 8.39 (4H), 7.75 (2H), and 7.29 (4H) ppm and can be readily assigned to the *ortho-*, *meta-*, and *para-* protons respectively on the basis of their integrals and couplings. In addition, two relatively broad singlet resonances at -14.30 (2H) and -21.45 (2H) corresponding to the bridging hydrides on the cluster are observed. It is apparent that the hydrides do not show the same distribution in solution as in the solid state. Thus, instead of the expected 3:1 hydride ratio a ratio of 2:2 is observed, which implies the presence of two distinct magnetic environments. One possible explanation of this behaviour is that in solution the hydrides are distributed as in structure **II** (Figure 2.1.4), with two hydrides bridging the edges and two bridging the base of the tetrahedron. Furthermore these hydrides are not static. The relative broadness of their resonances implies that they are fluxional, and thus may undergo exchange with each other or with their equivalent partner only *i.e.* exchange between edge bridging hydrides only, and exchange of basal bridging hydrides only. However, this proposal is only speculative and further variable temperature NMR experiments ought to be carried out to establish the nature of the exchange more fully.

Finally, it is important to note that the *ortho* proton is shifted to higher frequency relative to the other protons in the ring. This can be explained on the basis of the electronegativity of the nitrogen and the effective charge distribution which is set up in the ring (Figure 2.2.1).

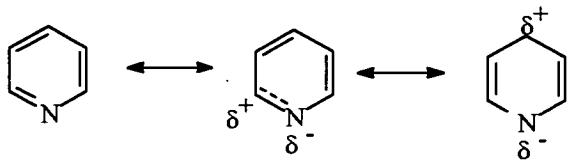

Figure 2.2.1: The resonance structures of pyridine.

The resonance structures of pyridine show quite clearly that a slight positive charge is set up on the *ortho* and *para* positions as a result of the nitrogen withdrawing electron density. This effect is felt most strongly at the adjacent carbon sites *i.e.* in the *ortho* positions and hence results in these protons being shifted to a higher frequency relative to the other protons. This effect is analogous to that seen for aldehydic and ketonic protons. A second key feature of the *ortho* proton is that it shows a somewhat smaller three bond coupling than the other ring protons.

X-ray Structure Determination

Single crystals of $Ru_4(\mu\text{-}H)_4(CO)_{10}(py)_2$ **4**, suitable for X-ray analysis, were grown from a solution of dichloromethane and hexane at 5 °C. The solid state molecular structure of **4** is presented in Figure 2.2.2 together with some relevant bond lengths (Table 2.2.1). The structure confirms that the tetrahedral Ru_4 framework remains intact and is co-ordinated to only ten terminal carbonyl ligands with two pyridine rings σ bonded to the cluster as predicted by spectroscopy. The structure also shows that disubstitution has occurred at a single metal centre rather than at two distinct sites as in $Ru_4(\mu\text{-}H)_4(CO)_{10}(PPh_3)_2$. It is interesting to note that the disubstituted product is produced despite removing only one carbonyl from the cluster using Me_3NO, and that it is formed in higher yields than the monosubstituted derivative. The possible mechanism of this cluster activation will be considered after discussing the crystallographic data in depth.

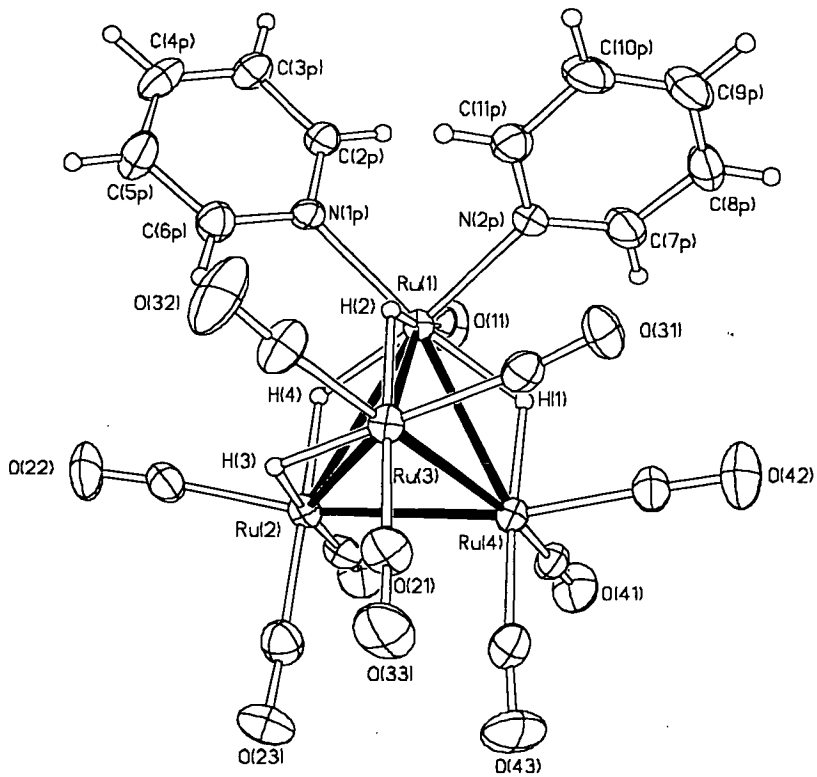

Figure 2.2.2: The thermal ellipsoid plot at 30% probability depicting the molecular structure of $Ru_4(\mu\text{-}H)_4(CO)_{10}(py)_2$ **4** at 298K.

Ru(1)-Ru(2) 2.9509(10)	mean Ru-C 1.89	Ru(2)-H(4) 1.75(3)
Ru(1)-Ru(3) 3.0166(11)	Ru(1)-N(1P) 2.141(7)	Ru(3)-H(2) 1.76(3)
Ru(1)-Ru(4) 2.9501(10)	Ru(1)-N(2P) 2.133(7)	Ru(3)-H(3) 1.74(3)
Ru(2)-Ru(3) 2.9426(10)	Ru(1)-H(1) 1.75(3)	Ru(4)-H(1) 1.75(3)
Ru(2)-Ru(4) 2.7751(11)	Ru(1)-H(2) 1.77(3)	mean C-O 1.14
Ru(3)-Ru(4) 2.8013(10)	Ru(1)-H(4) 1.74(3)	N(2P)-Ru(1)-N(1P) 90.5(3)
Ru(1)-C(11) 1.849(10)	Ru(2)-H(3) 1.75(3)	

Table 2.2.1: Selected bond lengths (Å) and angles (°) for $Ru_4(\mu\text{-}H)_4(CO)_{10}(py)_2$.

The hydrides in the structure of **4** were determined from low angle scattering data and quite clearly show the structural geometry **III** previously described for the

$Ru_4(\mu\text{-}H)_4(CO)_{10}$(diphos) cluster. The Ru-Ru distances fall into two distinct classes: the two non-hydrido bridged Ru-Ru bonds which are short- Ru(2)-Ru(4)= 2.775(1) Å and Ru(3)-Ru(4)= 2.801(1) Å, average value= 2.79 Å and the four remaining long Ru-Ru bonds which are bridged by the hydride ligands, average value= 2.96 Å. As discussed earlier this distribution of bond lengths is a classic feature of these $Ru_4(\mu\text{-}H)_4$ systems and comparable metal-metal bond lengths to those reported for $Ru_4(\mu\text{-}H)_4(CO)_{10}$(diphos) [7] are observed. The Ru-C distances range from 1.849(10)-1.942(11) Å and average 1.90 Å, with the shortest Ru-C distance being observed for Ru(1)-C(11). This presumably results from the increased electron density at the substituted metal centre which causes an increase in π back bonding. The carbonyl ligands are all terminally bonded and show a variation in the C-O length of 1.117(11)-1.1159(11) Å, average = 1.14 Å. The pyridine ligands show no great distortion of bond lengths and lie at an angle of 90.5 ° relative to one another. Furthermore, the rings are twisted with respect to each other, thus minimising the repulsion between the hydrogen atoms of the two rings. No graphitic packing is observed as in other Ru and Os clusters containing either terminal or facially bonded aromatic ring systems, [13] but this is perhaps to be expected since the orientation of the rings do not favour a stacking arrangement.

Conclusions

With only 1.1 equivalents of Me_3NO the removal of only one carbonyl ligand from the cluster would be predicted and hence the monosubstituted product $Ru_4(\mu\text{-}H)_4(CO)_{11}$(py) **3** ought to be observed as the major product. However, the results have shown that the disubstituted cluster $Ru_4(\mu\text{-}H)_4(CO)_{10}(py)_2$ **4** is prevalent. This suggests that the co-ordination of one pyridine ligand results in cluster activation and makes the loss of a second carbonyl favourable. There are two possible explanations which can be given to rationalise this behaviour:

a) The mechanism outlined below in Scheme 2.2.2 is proposed by direct comparison with a report in the literature on the carbonyl substitution reactions of $Ir_4(CO)_{12}$. [14]

This mechanism has not only been used to account for the products obtained from substitution reactions of $Ir_4(CO)_{12}$ but also for metal carbonyl dimers [15] and trimers [16] and is in accord with the observed kinetic data for these systems. It is thought that steps (i)-(iii) and (iv)-(vi) occur in a concerted fashion. The most pertinent feature of the scheme is step (iv). Heterolytic bond cleavage results in the preferential formation of an 18 electron centre on the $M(CO)_3$ site, and a 16 electron metal centre on the $M(CO)_2(py)$ site as a result of its stabilisation by the stronger σ donating ability of the nitrogen heterocycle. Attack of the second pyridine must occur at the 16 electron centre and consequently at the site of initial substitution, thus leading to the formation of the observed reaction product.

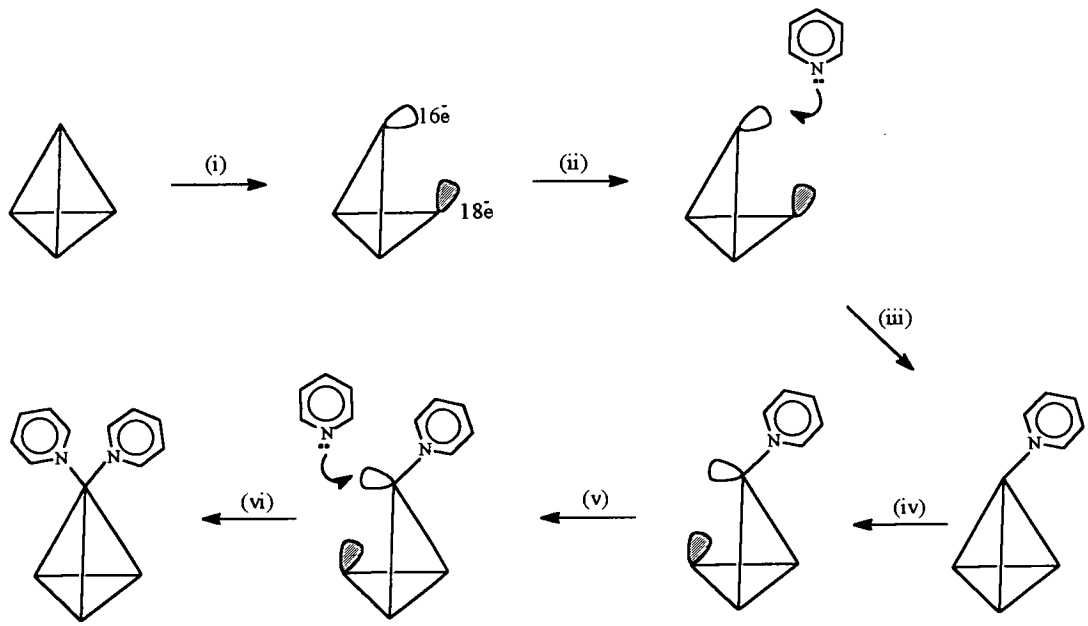

Scheme 2.2.2: The proposed mechanism for the disubstitution of $Ru_4(\mu\text{-}H)_4(CO)_{12}$.

(i) Heteronuclear metal-metal bond cleavage.

(ii) Addition of ligand to the unsaturated 16 electron metal centre.

(iii) Dissociation of CO followed by metal-metal bond formation.

(iv) Heteronuclear bond cleavage resulting in the formation of the 16 electron metal centre partially stabilised by the higher electron density from the ligand.

(v) Addition of ligand to the unsaturated 16 electron metal centre.

(vi) Dissociation of CO followed by metal-metal bond formation.

warming slightly before ultimately turning deep red/brown on reaching room temperature. It is postulated that the green solution may represent the monosubstituted cluster intermediate on route to the final disubstituted product $Ru_4(\mu\text{-}H)_4(CO)_{10}$(bipy) **5**. This is discussed further for the 2,2'-bipyrimidine derivative which showed a similar green intermediate which has been tentatively assigned on the basis of its IR spectrum (Section 2.6).

The crude reaction products were separated using either tlc with dichloromethane/hexane (7:3 v/v) as eluent or by column chromatography using first dichloromethane/hexane (1:9 v/v) to remove unreacted cluster followed by gradient elution to extract the red substituted product **5**. Column chromatography was used for the reaction involving 1.1 equivalents of Me_3NO because a large amount of insoluble decomposition products were present and a spot tlc test had shown that the major isolateable product was the unreacted cluster. Both reactions gave the same products, although 2.2 equivalents of Me_3NO was found to reduce the level of unreacted starting material, and consequently increase the final product yield.

Results and Discussion

Cluster **5** was initially proposed to possess an analogous structure to the *bis* pyridine derivative **4** because of the similarity in their IR spectra. The mass spectrum shows a molecular peak at 845 (calc 844) amu followed by a series of carbonyl loss peaks, which is consistent with the formulation $Ru_4(\mu\text{-}H)_4(CO)_{10}$(bipy). The ^1H NMR shows four resonances which arise from the aromatic protons at δ values of 8.92 (2H), 8.11 (2H), 7.76 (2H) and 7.44 (2H) ppm and two rather broad singlets for the hydride peaks, indicating their fluxional nature, at δ -15.00 (2H) and -21.45 (2H) ppm (Figure 2.3.1).

Due to its proximity to the nitrogen, the resonance arising from protons H_{2b} and H_{11b} is shifted furthest to high frequency to 8.92 ppm, leaving the other doublet at 8.11 ppm to be attributed to H_{5b} and H_{8b}. On the basis of the observed coupling constants protons H_{3b} and H_{10b} must give rise to the resonance at 7.44 ppm (showing

a small ^3J coupling to H_{2b}/H_{11b} and a larger ^3J coupling to H_{4b}/H_{9b}), and hence protons H_{4b} and H_{9b} are responsible for the signal at 7.76 ppm. This assignment was later confirmed by a decoupling experiment.

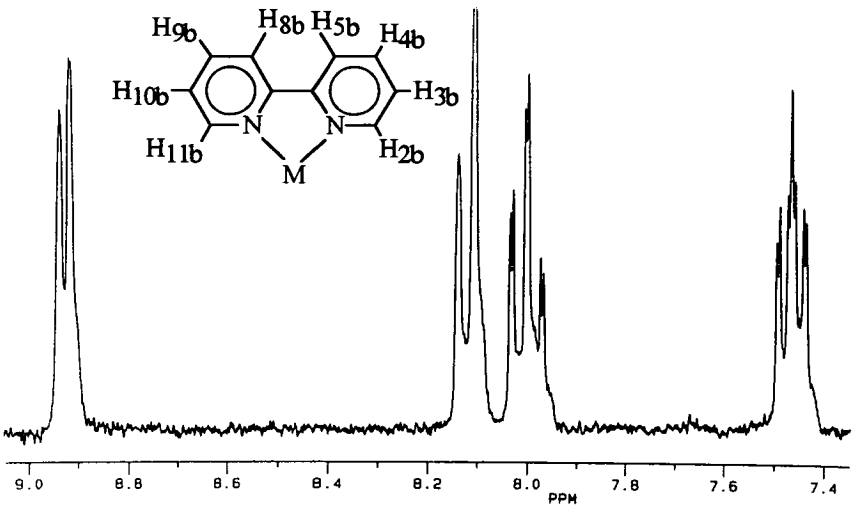

Figure 2.3.1: The ^1H NMR spectrum of $Ru_4(\mu\text{-}H)_4(CO)_{10}$(bipy) **5** run in $CDCl_3$.

X-ray Structure Determination

The characterisation of compound **5** was completed by an X-ray diffraction study on crystals grown from a dichloromethane/hexane solution at 5 °C. The structure, given in Figure 2.3.2, shows the chelating ligand bonding through the lone pair on nitrogen to a single metal centre with a bite angle of 77.4 (2) °. The tetrahedral cluster geometry is distorted as a result of the lengthening of the hydride bridged Ru-Ru bonds relative to the unbridged bonds, and show average bond lengths of 2.964 Å and 2.787 Å respectively. All ten carbonyl ligands are terminally bonded, as previously inferred from the IR data, and show an average length of 1.13 Å. The shortest metal-carbon bond of 1.844 (7) Å is seen to the substituted Ru(3) site because it possesses the greatest electron density and thus shows the greatest π back bonding character.

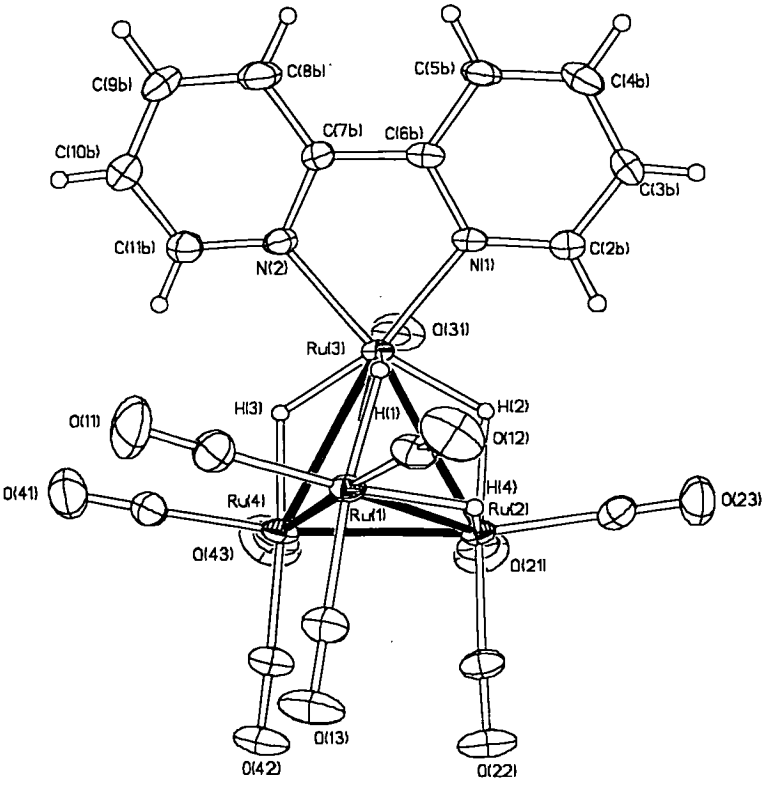

Figure 2.3.2: The thermal ellipsoid plot at 30% probability depicting the molecular structure of $Ru_4(\mu\text{-}H)_4(CO)_{10}$(bipy) **5** at 298K.

Ru(1)-Ru(2) 2.9253(7)	Ru(3)-Ru(4) 2.9462(7)	Ru(1)-H(4) 1.76(3)	Ru(3)-H(3) 1.76(3)
Ru(1)-Ru(3) 3.0229(7)	Ru(3)-C(31) 1.844(7)	Ru(2)-H(2) 1.77(3)	Ru(4)-H(3) 1.76(3)
Ru(1)-Ru(4) 2.7954(8)	Ru(3)-N(1) 2.095(5)	Ru(2)-H(4) 1.77(3)	mean Ru-C 1.90
Ru(2)-Ru(3) 2.9637(7)	Ru(3)-N(2) 2.090(5)	Ru(3)-H(1) 1.76(3)	mean CO 1.13
Ru(2)-Ru(4) 2.7795(8)	Ru(1)-H(1) 1.76(3)	Ru(3)-H(2) 1.75(3)	N(1)-Ru(3)-N(2) 77.4(2)

Table 2.3.1: Selected bond lengths (Å) and angles (°) for $Ru_4(\mu\text{-}H)_4(CO)_{10}$(bipy).

This co-ordination geometry is well known for monometallic species and has been reported for both $Ru_3(\mu\text{-}CO)_2(CO)_8$(bipy) [17] and $Os_3(\mu\text{-}H)(CO)_9(C_{10}H_7N_2)$, [18] which are discussed in Chapter One.

Conclusion

The cluster $Ru_4(\mu\text{-}H)_4(CO)_{12}$ shows a similar reactivity with 2,2'-bipyridyl to pyridine, forming the terminally bonded disubstituted cluster whether 1.1 or 2.2 equivalents of Me_3NO are used to remove the carbonyl ligands.

2.4 Reaction of $Ru_4(\mu\text{-}H)_4(CO)_{12}$ with 1,10-Phenanthroline

Having prepared the bipyridyl derivative, further derivatives incorporating other similar electrochemically active ligands were then synthesised so that both the electrochemistry and the electronic spectroscopy of the resulting compounds could be investigated. The results of that research are discussed in detail in Chapter Four.

Results and Discussion

The reaction between $Ru_4(\mu\text{-}H)_4(CO)_{12}$ 1 and 1,10-phenanthroline (phen) was carried out in the presence of Me_3NO as previously described. The resulting orange/red solution was separated by tlc using hexane/dichloromethane (1:1 v/v) initially as eluent to give a favourable product separation, and finally neat dichloromethane to advance the major product band from the baseline. The reaction proceeded cleanly producing only one major orange/red product which was initially characterised from its IR carbonyl spectrum as $Ru_4(\mu\text{-}H)_4(CO)_{10}$(phen) **6**. This was confirmed by the mass spectrum which shows the molecular ion peak at 870 (calc 868) amu followed by a series of carbonyl losses and a peak at 688 amu which corresponds to the loss of the ligand (calc 688 amu). The ^1H NMR (Figure 2.4.1) shows the predicted pattern with resonances observed at δ shifts of 9.22 (1H), 8.48 (2H), 8.02 (2H) and 7.79 (2H) ppm for the aromatic protons and two broad singlet hydride resonances at -15.65 (2H) and -21.03 (2H) ppm. The similarity in the hydride resonance pattern of this cluster to both the pyridine and bipyridyl derivatives indicates an analogous fluxional exchange must be occurring.

The observed proton resonances are readily assigned- the α protons H_{1p} and H_{12p} gives rise to the doublet of doublets at 9.22 ppm, which is shifted to higher frequency relative to the other protons because it is adjacent to the electronegative nitrogen atom. The doublet of doublets at 8.48 ppm arises from H_{3p} and H_{10p} and hence shows a large ^3J coupling and a smaller ^4J coupling. Protons H_{2p}/H_{11p} couple to both H_{3p}/H_{10p} and H_{1p}/H_{12p} and thus give rise to the doublet of doublets at 7.79 ppm showing two large ^3J couplings. Finally, because H_{6p} is magnetically equivalent to H_{7p} it gives rise to a singlet and not a doublet at 8.02 ppm.

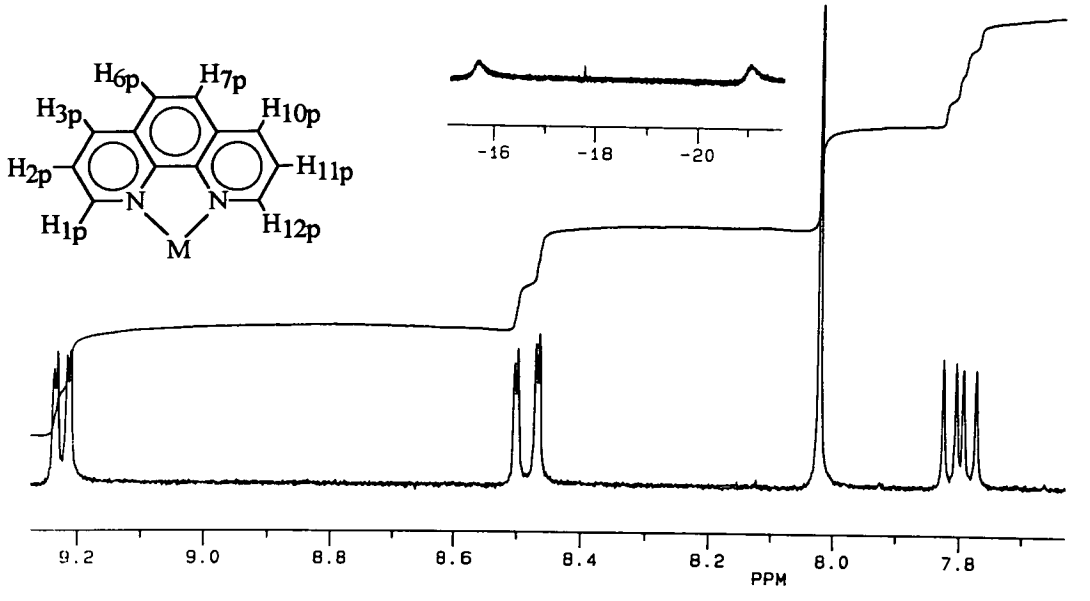

Figure 2.4.1 : The ^1H NMR of $Ru_4(\mu\text{-}H)_4(CO)_{10}$(phen) **6** recorded in $CDCl_3$.

X-ray Structure Determination

Having characterised the product satisfactorily from the spectroscopic data its identification was then confirmed by an X-ray crystallographic study. The structure shows a slightly distorted Ru_4 core which is edge bridged by three hydride ligands with the fourth hydride spanning the basal Ru(3)-Ru(4) bond as represented by the type **III** structure (Figure 2.1.4). The hydrides were found from a Fourier difference map of the low angle diffraction data, and span the longer metal-metal bonds as expected, exhibiting bond lengths in the range 2.7788(7)-3.0168(8) Å. The phenanthroline ligand shows a bite angle of 78.86(14) ° which is similar to the

77.4(2)° angle observed for the bipyridyl derivative. Again the metal-carbon bond of the ligand substituted site, Ru(1)-C(11) is comparatively shorter than the others due to the increased electron density and hence π back bonding to this site. This metal-carbon bond is almost identical in length to the analogous bond in the bipyridyl derivative **5**, and suggests that there is no great difference in the extent of π back bonding between the two. Again no graphitic packing is observed but this is thought to be due to the cluster's geometry as discussed earlier.

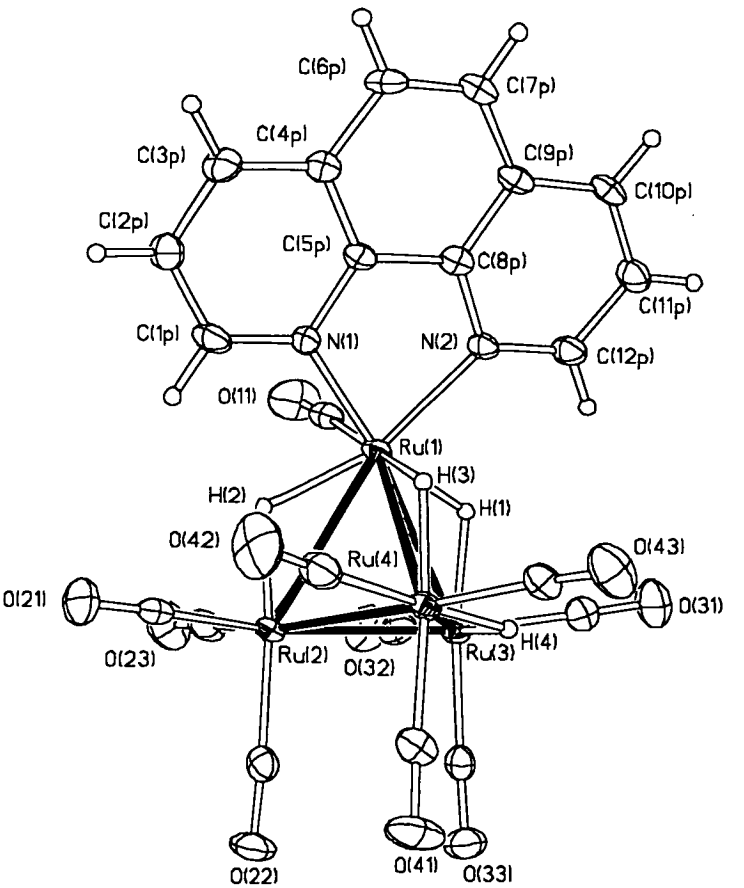

Figure 2.4.2 : The thermal ellipsoid plot at 50% probability depicting the molecular structure of $Ru_4(\mu\text{-}H)_4(CO)_{10}$(phen) **6** at 150K.

Ru(1)-Ru(2) 2.9335(7)	Ru(3)-Ru(4) 2.9366(8)	Ru(1)-H(2) 1.73(2)	Ru(4)-H(3) 1.74(2)
Ru(1)-Ru(3) 2.9618(8)	Ru(1)-C(11) 1.843(5)	Ru(1)-H(3) 1.75(2)	Ru(4)-H(4) 1.75(3)
Ru(1)-Ru(4) 3.0168(8)	Ru(1)-N(1) 2.096(4)	Ru(2)-H(2) 1.74(2)	mean Ru-C 1.90
Ru(2)-Ru(3) 2.7788(7)	Ru(1)-N(2) 2.100(4)	Ru(3)-H(1) 1.74(3)	mean C-O 1.14
Ru(2)-Ru(4) 2.7971(9)	Ru(1)-H(1) 1.73(2)	Ru(3)-H(4) 1.74(3)	N(1)-Ru(1)-N(2) 78.86(14)

Table 2.4.1: Selected bond lengths (Å) and angles (°) of $Ru_4(\mu\text{-}H)_4(CO)_{10}(phen)$.

Conclusions

Whether the reaction was carried out using 1.1 or 2.2 equivalents of Me_3NO two carbonyl ligands were removed and substituted by the ligand. However, utilisation of 2.2 equivalents of Me_3NO was found to increase the yield of $Ru_4(\mu\text{-}H)_4(CO)_{10}(phen)$ **6** and significantly reduce the relative amount of unreacted cluster. In addition to the apparent thermodynamic stability of the disubstituted product there is a contribution from the chelate effect which favours this substitution pattern. Attempts to synthesise the tetrasubstituted compound $Ru_4(\mu\text{-}H)_4(CO)_8(phen)_2$ using 4.2 equivalents of Me_3NO to activate the cluster have proven unsuccessful with only the disubstituted product **6** and decomposition products being formed. Hence the co-ordination of a second ligand appears to be disfavoured using this route. It can only be tentatively suggested that this may result from the proposed activation of the substituted site (Scheme 2.2.2, notes a, b) which would favour the bonding of the ligand to the metal centre with one phenanthroline ligand already co-ordinated. Steric as well as electronic factors would therefore rule out the proposed co-ordination of the second ligand to this site, although it would be of interest to investigate whether pyridine or a smaller monodentate ligand would attack at the disubstituted site.

2.5 Reaction of $Ru_4(\mu\text{-}H)_4(CO)_{12}$ with Neocuproine

Neocuproine, the 2,9-dimethyl substituted derivative of phenanthroline (Figure 2.1.6), was reacted with $Ru_4(\mu\text{-}H)_4(CO)_{12}$ **1** in an attempt to form the monosubstituted cluster as the major product by introducing a degree of steric hindrance around the nitrogen donor sites.

Results and Discussion

The reaction was carried out initially using 1.1 equivalents of Me_3NO and was later repeated using 2.2 equivalents to yield the same products. It was found that the levels of unreacted cluster were however reduced using 2.2 equivalents of Me_3NO and henceforth these conditions have been employed.

The major orange/red product was isolated from the reaction mixture by chromatography and displays the same distinctive carbonyl IR pattern of the previously identified disubstituted clusters **4**, **5** and **6**. Mass spectrometry reveals a strong parent ion peak at 870 amu followed by the loss of several carbonyls which is consistent with the formulation $Ru_4(\mu\text{-}H)_4(CO)_{10}$(dmp) **7** (calc 868 amu), and this was later corroborated by both ^1H NMR and X-ray crystallographic studies.

The ^1H NMR spectrum (Figure 2.5.1) shows four resonances which are readily assigned. Protons H_{2p} and H_{11p} give rise to the doublet at 8.26 ppm which is comparable to the signal observed for the equivalent proton in the phenanthroline derivative. H_{5p}/H_{7p} exhibit a singlet resonance at 7.82 ppm, and protons H_{3p} and H_{10p} give rise to the doublet at 7.66 ppm. A sharp singlet at 3.14 ppm with an integral of six corresponds to the methyl protons and the two singlet hydride resonances appear as broad peaks at -16.04 and -21.03 ppm indicative of a fluxional exchange. On cooling the sample to 223K the hydride region was seen to change and give rise to two broad singlets at -16.43 and -22.22 ppm. This is in agreement with the scrambling of two base bridging and two edge bridging hydrides (structure **II** {Figure 2.1.4}) as previously suggested.

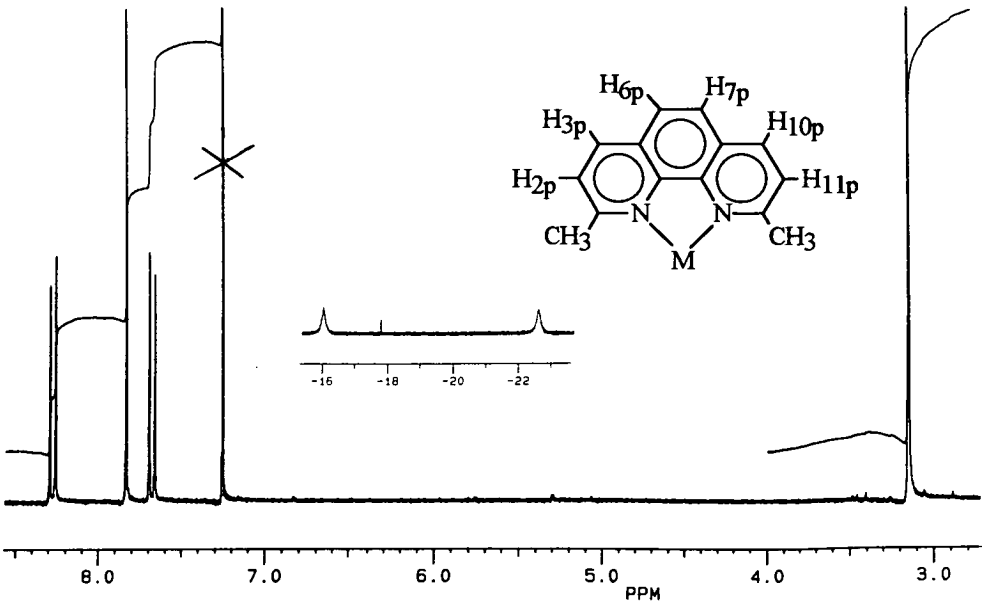

Figure 2.5.1: The ^1H NMR of $Ru_4(\mu\text{-}H)_4(CO)_{10}(dmp)$ **7** run in $CDCl_3$.

X-ray Structure Determination

The single crystal X-ray diffraction study of **7** quite clearly shows that the steric hindrance of the methyl groups has been insufficient to cause only monosubstitution as hoped (Figure 2.5.2). The ligand has instead been forced to tilt somewhat in order to minimise the steric repulsion between the methyl groups of the ligand and the cluster framework. As a result the co-ordination of the nitrogens is now unsymmetrical, showing ruthenium-nitrogen bond lengths of 2.165 (3) and 2.132(3) Å. In contrast, the phenanthroline derivative which has no steric constraints is co-ordinated symmetrically to the cluster. The distribution of the hydride ligands is analogous to the previously discussed nitrogen heterocyclic derivatives, showing three edge bridging bonds and one basal bridged bond. Again a lengthening of the bridged bonds is observed, which show an average length of 2.99 Å compared to 2.77 Å for the unbridged edges. The ten terminal carbonyl ligands average 1.14 Å in length, and the metal-carbon bond to atom C(11) of the substituted ruthenium atom Ru(1) is the shortest with a bond length of only 1.840 (4) Å compared to an average of 1.90 Å.

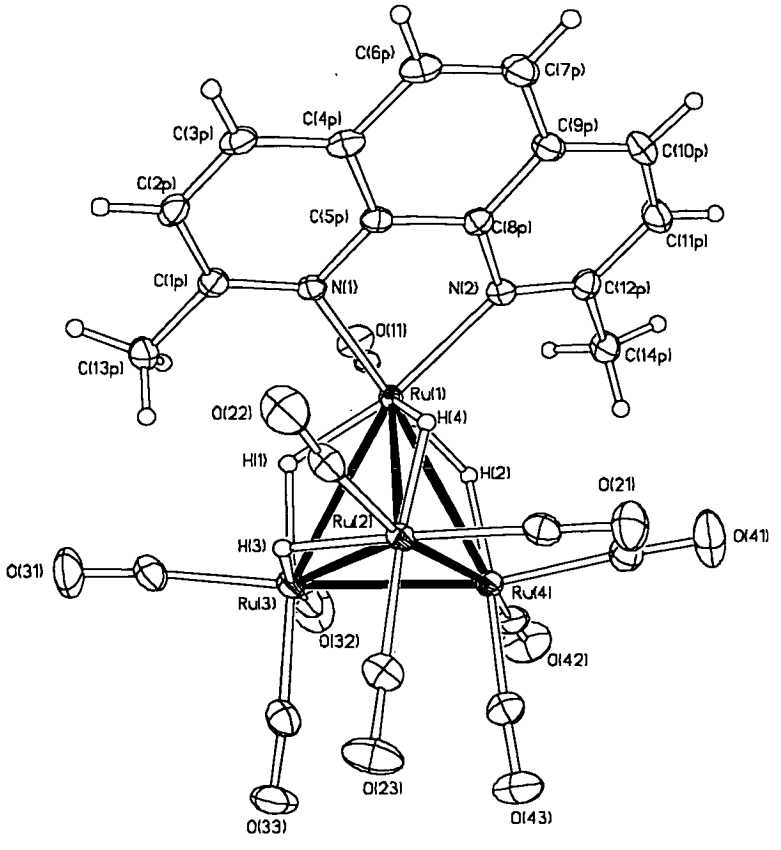

Figure 2.5.2: The thermal ellipsoid plot at 50% probability depicting the molecular structure of $Ru_4(\mu\text{-}H)_4(CO)_{10}$(dmp) 7.

Ru(1)-Ru(2) 3.054(2)	Ru(1)-N(1) 2.165(3)	Ru(2)-H(3) 1.740(14)	mean C-O 1.14
Ru(1)-Ru(3) 3.006(2)	Ru(1)-N(2) 2.132(3)	Ru(2)-H(4) 1.739(14)	N(1)-Ru(1)-N(2) 78.43(14)
Ru(1)-Ru(4) 2.981(2)	Ru(1)-C(11) 1.840(4)	Ru(3)-H(1) 1.740(14)	N(1)-Ru(1)-Ru(3) 112.56(10)
Ru(2)-Ru(3) 2.933(1)	Ru(1)-H(1) 1.738(14)	Ru(3)-H(3) 1.743(14)	N(2)-Ru(1)-Ru(4) 107.16(9)
Ru(2)-Ru(4) 2.784(2)	Ru(1)-H(2) 1.739(14)	Ru(4)-H(2) 1.743(14)	
Ru(3)-Ru(4) 2.758(2)	Ru(1)-H(4) 1.743(14)	mean Ru-C 1.90	

Table 2.5.1: Selected bond lengths (Å) and angles (°) of $Ru_4(\mu\text{-}H)_4(CO)_{10}$(dmp).

Conclusion

In hindsight, perhaps the best strategy to procure the monosubstitution of the cluster may have been to synthesise the 2,Bu^t-1,10-phenanthroline ligand (Figure 2.5.2) in which co-ordination to one nitrogen site would be hindered by the bulky tertiary butyl group whilst leaving the second nitrogen site available for bonding.

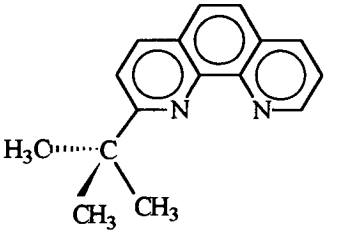

Figure 2.5.2: The 2,Bu^t-1,10- phenanthroline ligand.

2.6 Reaction of $Ru_4(\mu\text{-}H)_4(CO)_{12}$ with 2,2'- Bipyrimidine

Results and Discussion

The reaction between $Ru_4(\mu\text{-}H)_4(CO)_{12}$ **1** and the bipyrimidine ligand in the presence of 2.2 equivalents of Me_3NO showed similar trends to those observed previously during the reaction with the bipyridyl ligand. The reaction solution changed colour from orange/yellow at -78 °C to green upon gradual warming. On further warming the solution became progressively darker, ultimately producing a deep red solution at room temperature.

A sample of the green intermediate solution was kept in a dry ice/acetone bath at -78 °C before being quickly transferred into a solution IR cell and the spectrum

recorded immediately to minimise its conversion to the final red product. The spectrum was virtually identical to the $Ru_4(\mu\text{-}H)_4(CO)_{11}(py)$ product **3**, and hence the green intermediate was assigned as $Ru_4(\mu\text{-}H)_4(CO)_{11}(bpm)$ **8**. It would therefore appear that a stepwise substitution of the carbonyl ligands is occurring as the cluster progressively reacts with the bpm ligand upon warming (Scheme 2.6.1).

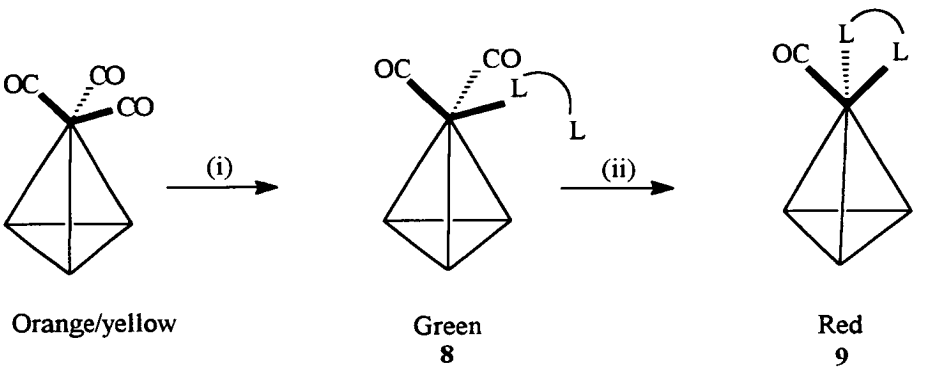

Scheme 2.6.1: The proposed reaction course of the $Ru_4(\mu\text{-}H)_4(CO)_{12}$ cluster with 2,2'-bipyrimidine (L-L) on route to the final product **9**.

(i) 2.2 equivalents of Me_3NO at -78 °C followed by gradual warming.

(ii) Warming to room temperature.

A similar colour change was observed for the reaction with the bipyridyl ligand, and it may be that this mechanism is pertinent to all the reactions discussed herein. However, the proposed intermediate $Ru_4(\mu\text{-}H)_4(CO)_{10}(\eta^1\text{: L-L})$ may not always differ greatly in colour to the final product, and therefore its formation would not be so apparent.

It was not possible to record mass spectroscopic or NMR data on **8** because of its transient nature, and hence it can only be tentatively assigned on the basis of the IR evidence. Product **9**: $Ru_4(\mu\text{-}H)_4(CO)_{10}(bpm)$ has however been fully characterised. Its IR carbonyl pattern is almost identical to those previously observed for the disubstituted clusters and shows that the compound possesses only terminal carbonyl

ligands. The mass spectrum exhibits a molecular ion peak at 848 (calc 846) amu followed by the loss of carbonyls and is backed up by microanalysis of the recrystallised product.

The ^1H NMR spectrum is relatively simple and shows only three resonances at 9.16 (2H), 9.07 (2H) and 7.62 ppm which can be readily assigned on the basis of their structure and chemical shifts to protons H_{2b}/H_{8b} , H_{4b}/H_{6b} and H_{3b}/H_{7b} respectively. The hydride resonances are very weak and broad indicating that they are perhaps more fluxional than those observed for the previous clusters, but are just detectable at -15.9 ppm and -21.5 ppm.

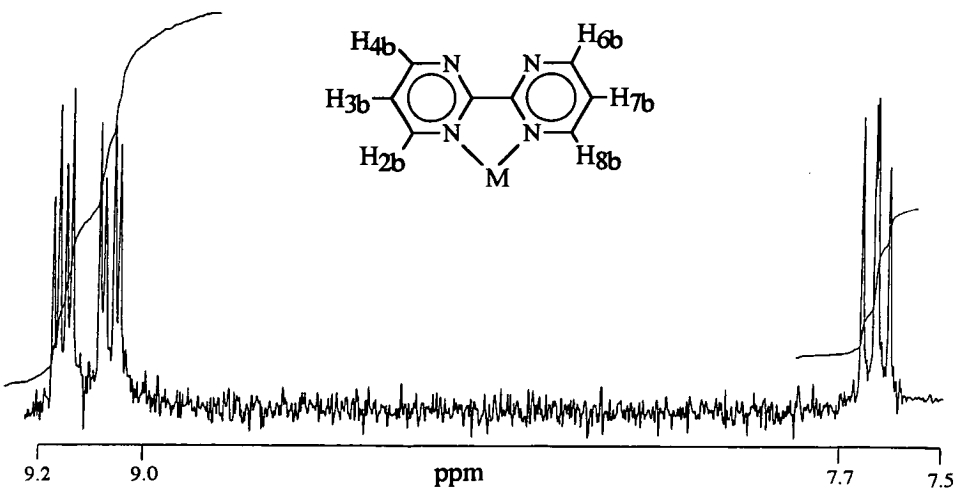

Figure 2.6.1: The ^1H NMR spectrum of $Ru_4(\mu\text{-}H)_4(CO)_{10}$(bpm) **9** in $CDCl_3$.

X-ray Structure Determination

The solid state molecular structure of **9** is given in Figure 2.6.2 and shows that the ligand has been successfully σ bonded to the tetrahedral cluster through two of its nitrogen sites leaving the remaining two sites available for further potential co-ordination. The bite angle of the ligand is 77.4(3) ° and the metal-nitrogen bonds show lengths of 2.099(8) Å and 2.117(8) Å which are considerably shorter than those observed for the derivatives discussed earlier. Because of the higher electron density in the aromatic rings due to the presence of the four nitrogens (*cf.* previous bidentate

ligands) there is an enhanced π back bonding effect at Ru(2) which results in the shortening of the M-C bond Ru(2)-C(21) to 1.834(11) Å relative to the others. The position of the hydrides clearly represents the type **III** arrangement shown in Figure 2.1.4. Those metal-metal bonds which are bridged by the hydrides show significantly longer bonds than the unbridged sites: 2.965 Å (average) *cf.* 2.773 Å (average).

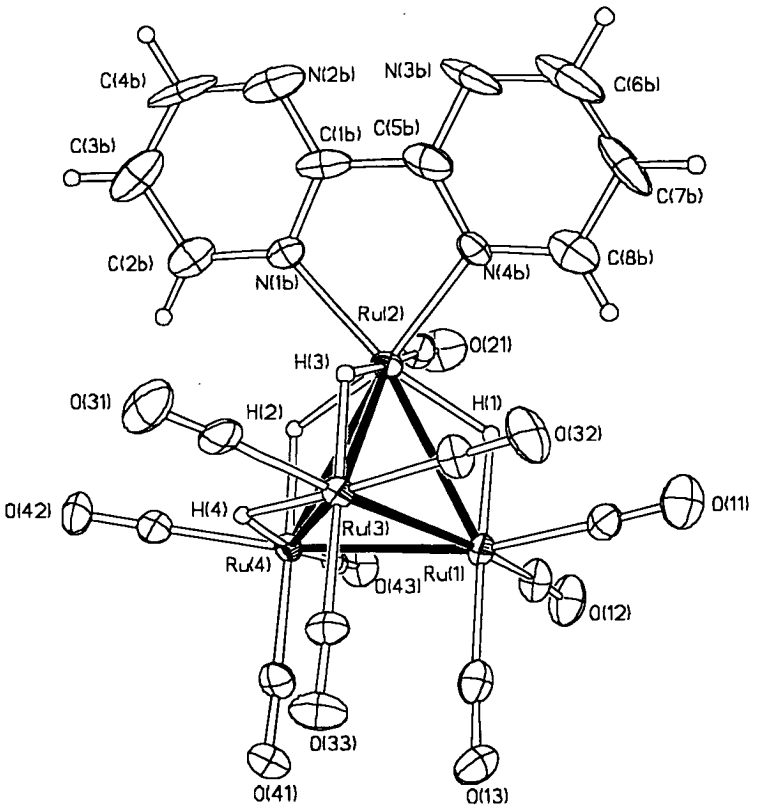

Figure 2.6.2: The thermal ellipsoid plot at 50% probability of the molecular structure of $Ru_4(\mu\text{-}H)_4(CO)_{10}$(bpm) **9** at 150K.

Ru(1)-Ru(2) 2.9441(12)	Ru(3)-Ru(4) 2.9309(12)	Ru(2)-H(2) 1.74(3)	Ru(4)-H(4) 1.74(3)
Ru(1)-Ru(3) 2.7872(13)	Ru(2)-C(21) 1.834(11)	Ru(2)-H(3) 1.75(3)	mean Ru-C 1.89
Ru(1)-Ru(4) 2.7597(11)	Ru(2)-N(1b) 2.099(8)	Ru(3)-H(3) 1.75(3)	mean C-O 1.14
Ru(2)-Ru(3) 3.0345(12)	Ru(2)-N(4b) 2.117(8)	Ru(3)-H(4) 1.75(3)	N(1b)-Ru(2)-N(4b) 77.4(3)
Ru(2)-Ru(4) 2.9489(13)	Ru(2)-H(1) 1.74(3)	Ru(4)-H(2) 1.75(3)	

Table 2.6.1: Selected bond lengths (Å) and angles (°) for $Ru_4(\mu\text{-}H)_4(CO)_{10}$(bpm).

2.7 Reaction of $Ru_4(\mu\text{-}H)_4(CO)_{12}$ with 2,3-Bis(2-Pyridyl)Pyrazine

Results and Discussion

The chemical activation of the $Ru_4(\mu\text{-}H)_4(CO)_{12}$ cluster **1** using 2.2 equivalents of Me_3NO in the presence of the bpp ligand saw the reaction solution change in colour from orange to dark red. The reaction mixture was separated using tlc with hexane/dichloromethane as eluent (3:7 v/v) to isolate one major red product which has been characterised spectroscopically only. Despite repeated attempts, crystals suitable for X-ray diffraction have not been obtained. The distinctive carbonyl IR pattern was indicative of the formulation $Ru_4(\mu\text{-}H)_4(CO)_{10}$(bpp) **10**, and this was confirmed by mass spectrometry which showed the parent ion peak (M^+= 925, calc 922 amu) followed by the loss of ten carbonyls. The ^1H NMR spectrum is somewhat complex (Figure 2.7.1) but has been assigned on the basis of a series of irradiation experiments which are shown in Figure 2.7.2.

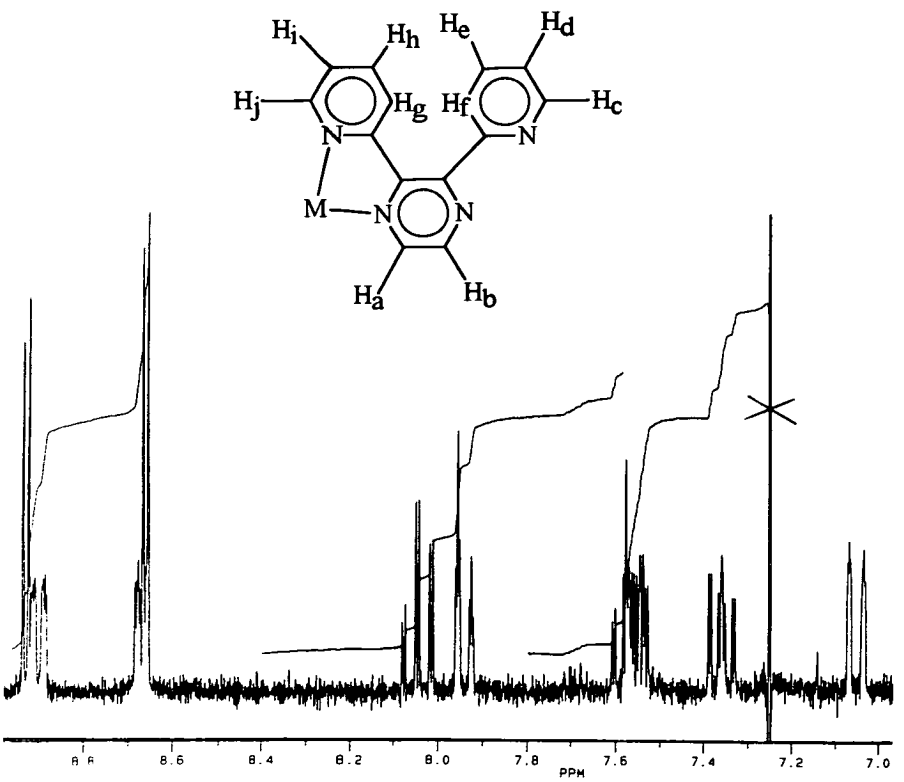

Figure 2.7.1: ^1H NMR of $Ru_4(\mu\text{-}H)_4(CO)_{10}$(bpp) **10** in $CDCl_3$.

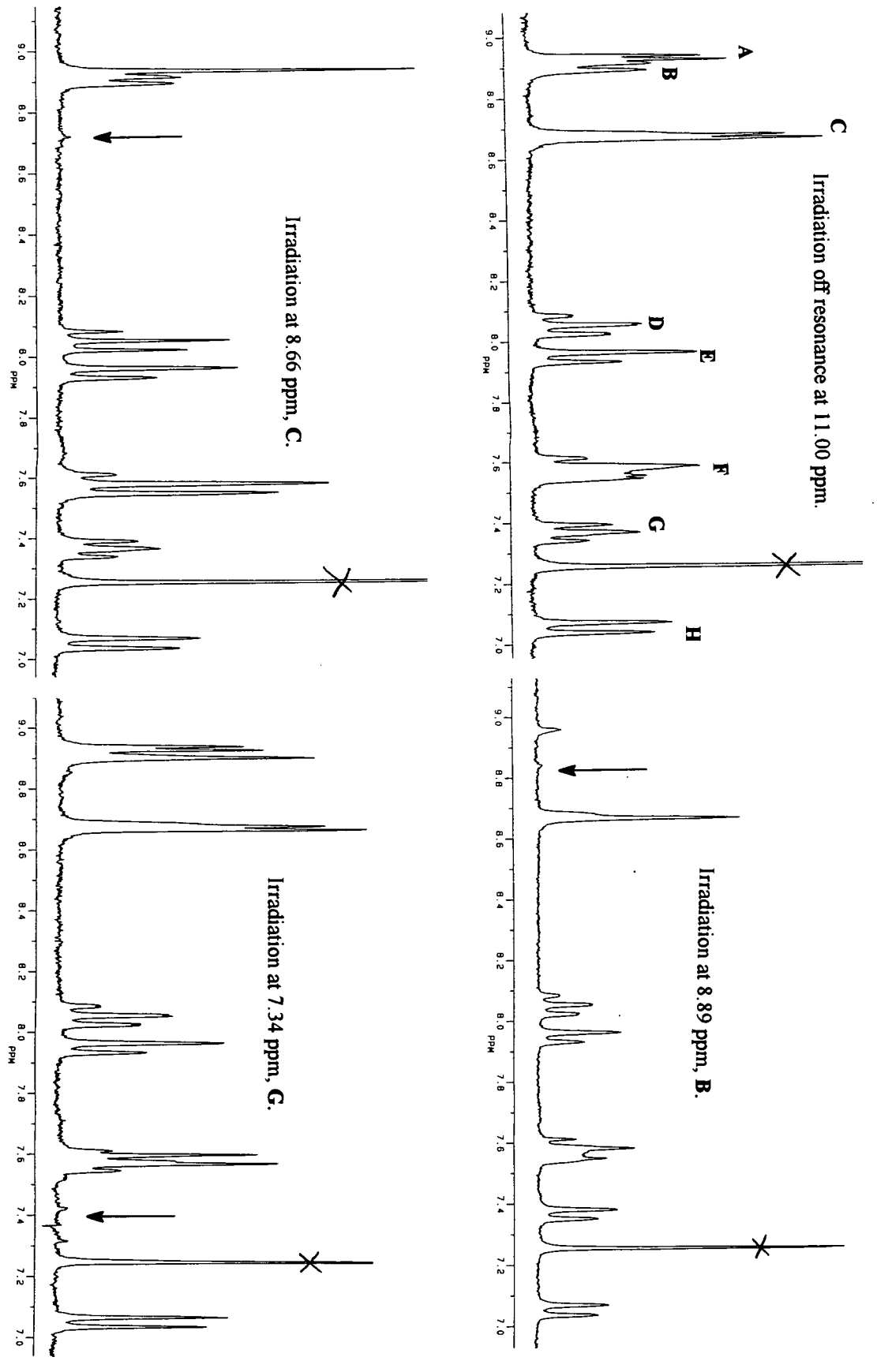

Figure 2.7.2: Irradiation experiments run on $Ru_4(\mu\text{-}H)_4(CO)_{10}$(bpp) **10**.

Clearly the doublet resonances at 8.93 ppm and 8.66 ppm, must be due to protons H_a and H_b which become inequivalent upon co-ordination and are shifted to higher frequency relative to the free ligand's resonance at 8.50 ppm (s). H_a is predicted to be shifted furthest because it is adjacent to the bound nitrogen and hence should be relatively more electron deficient. The resonance at 8.89 ppm (ddd) is assigned to H_j on the basis of its chemical shift and the observed couplings, and similarly H_c to the resonance at 8.89 ppm which is partially obscured by the signal arising from H_b.

Interpretation of ^1H NMR Irradiation Experiments

The resonances observed in the irradiation experiment (Figure 2.7.2) have been labelled **A-H** for ease of reference. They are rather broad and do not exhibit the fine structure shown in Figure 2.7.1, but this is a consequence of the way in which the experimental parameters were set up and is not the result of a fluxional process.

Irradiation at 8.89 ppm, B (H_j)

The attempted irradiation of H_j was not completely clean. Because the resonance lies so close to H_a this has also been partially irradiated and hence appears as a singlet of greatly reduced intensity, and in addition, resonance **C**, assigned to H_b, is transformed from a doublet to a singlet. Since H_a and H_b only couple to each other this unintended irradiation will not affect the other resonances. Clearly resonance **G** must be due to H_i and this explains the collapse of the triplet (actually a dddd from inspection of Figure 2.7.1) to a doublet upon the loss of coupling to H_j.

Irradiation at 7.34 ppm, G (H_i)

The coupling to resonance **B** is lost upon irradiation of H_i (d→s) confirming it to be H_j and the loss of a large ^3J coupling to resonance **F** is observed, narrowing it considerably, and infers it must be due to H_h. Furthermore, integration shows that there are in fact two protons responsible for the complex multiplet **F**.

Irradiation at 8.66 ppm, C (H_b and H_c)

Resonance **C** is a combination of both the signals for protons H_b and H_c and hence irradiation of it affects the coupling observed to both nuclei. However, since H_b couples only to H_a it is simple to deduce the resonances affected by irradiating H_c.

Resonance **A** (H_a) is transformed from a doublet to a singlet as expected and the loss of a large coupling from **F** and a small one from **D** is observed. Hence **F** must be due to H_d and H_h and the loss of coupling from **D** implies it may be due to H_e, and this would seem reasonable from its triplet of doublets pattern.

The 7.8 Hz splitting observed to the doublet resonance **E** implies that it must be coupled to proton H_e and it is therefore assigned to proton H_f , leaving the remaining doublet **H** to be assigned to proton H_g .

Resonance	δ/ppm	Proton
A	8.92	H_a
B	8.89	H_j
C	8.67	H_b & H_c
D	8.04	H_e
E	7.94	H_f
F	7.56	H_d & H_h
G	7.34	H_i
H	7.04	H_g

Table 2.7.1: The ^{1}H NMR assignment of $Ru_4(\mu\text{-}H)_4(CO)_{10}$(bpp) **10**.

The successful synthesis of the bipyrimidine and bpp $Ru_4(\mu\text{-}H)_4(CO)_{10}$(L-L) derivatives led to the idea of attempting to link a second cluster to the vacant lone pair of electrons on the co-ordinated ligand. To achieve such linkages these clusters were reacted with the reactive species $M_3(CO)_{10}(MeCN)_2$ (M=Ru, Os). However, the

reactions had varied success, and due to lack of time this project was not studied in greater depth.

2.8 Reaction of $Os_4(\mu\text{-}H)_4(CO)_{12}$ with Nitrogen Heterocycles

To date no previous reports have appeared in the literature regarding the reaction between the $Os_4(\mu\text{-}H)_4(CO)_{12}$ cluster **2** with nitrogen heterocyclic ligands. Initial attempts to react the cluster directly with the ligand in the presence of 2.2 equivalents of Me_3NO proved unsuccessful, and instead the method of Chen *et al.*, [19] was followed. Thus a solution of the more reactive $Os_4(\mu\text{-}H)_4(CO)_{10}(MeCN)_2$ cluster derivative **11** was prepared and used in the reaction with the ligands under mild thermal conditions.

2.8.1 Reaction of $Os_4(\mu\text{-}H)_4(CO)_{10}(MeCN)_2$ with Pyridine

The major reaction product resulting from the thermal reaction between $Os_4(\mu\text{-}H)_4(CO)_{12}$ and pyridine over a one hour period was found to be the monosubstituted derivative $Os_4(\mu\text{-}H)_4(CO)_{11}(py)$ **12**. This was confirmed by its mass spectrum which showed the molecular ion peak at 1152 (calc 151) amu followed by the sequential loss of several carbonyl ligands. The ^1H NMR confirmed the presence of the pyridine ligand, showing a doublet resonance at 8.72 ppm, and two triplet resonances at 7.93 ppm and 7.63 ppm of relative intensity 2:1:2 which are readily assigned to the *ortho*, *para*, and *meta* protons respectively. Only one rather broad hydride resonance was evident in the spectrum at -17.9 ppm although a very weak and broad peak at *ca.* -24.3 ppm is also just apparent. That only a single hydride resonance was observed suggests a greater fluxionality of the hydrides in the osmium cluster. Also isolated from the reaction mixture were $Os_4(\mu\text{-}H)_4(CO)_{10}(MeCN)_2$ and $Os_4(\mu\text{-}H)_4(CO)_{10}(py)_2$ **13** as identified on the basis of mass spectroscopy.

Furthermore, $Os_4(\mu\text{-}H)_4(CO)_{11}(MeCN)$ **14** was prepared by a similar route, using 1.1 equivalents of Me_3NO in the presence of acetonitrile and identified on the

basis of mass spectroscopic evidence. Refluxing a dichloromethane solution of the cluster in the presence of pyridine over 18 hours was found to be sufficient to cause its reaction to produce the $Os_4(\mu\text{-}H)_4(CO)_{10}(py)_2$ cluster, which has been characterised by IR and mass spectroscopy, and the formation of two other unidentified species.

2.8.2 Reaction of $Os_4(\mu\text{-}H)_4(CO)_{10}(MeCN)_2$ with 2,2'-Bipyridyl

The same procedure as outlined for the synthesis of the *bis-* pyridine derivative **13** was followed in the preparation of the bipyridyl analogue, except that the solution was heated under reflux for 18 hours.

Its ^1H NMR spectrum shows a broad singlet resonance at 9.27 ppm which is attributed to the α proton H_a (Figure 2.8.1), whilst protons H_b and H_c give rise to doublet of doublets at 7.46 and 8.17 ppm and the doublet resulting from H_d appears at 8.06 ppm. This is comparable to the assignment of the ruthenium analogue. Furthermore, its mass spectrum shows the molecular ion peak at 1203 (calc 1200) amu, and the subsequent loss of several carbonyl ligands.

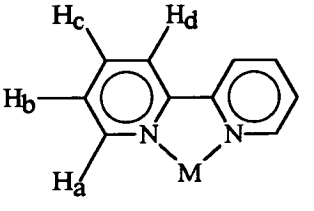

Figure 2.8.1: Labelling scheme for the $Os_4(\mu\text{-}H)_4(CO)_{10}$(bipy) cluster **15**.

The appearance of the α proton as a broad singlet rather than a doublet of doublets as expected, is thought to arise from the fluxionality of the hydrides around the cluster thus causing a change in the magnetic environment. Because the α proton lies closest in space to the hydrides it would feel this change most and thus lead to its resonance

broadening. The protons furthest from the hydrides are then unaffected and hence show sharper resonances. That this broadening is only observed for the osmium and not the ruthenium analogue perhaps indicates a differing rate of fluxionality of the hydrides in the latter, which is in agreement with the observation of the doublet hydride resonances for the osmium derivative *cf.* the broad singlets of the ruthenium derivative.

2.8.3 Reaction of $Os_4(\mu\text{-}H)_4(CO)_{10}(MeCN)_2$ with 1,10-Phenanthroline

A dichloromethane solution of $Os_4(\mu\text{-}H)_4(CO)_{10}(MeCN)_2$ **11** was found to react with 1,10- phenanthroline on refluxing for 20 minutes, as shown by both IR spectroscopy and its colour change from orange/yellow to brown. Product separation was carried out by tlc using 1:1 (v/v) hexane/dichloromethane as eluent, although it was found to be necessary to repeat the process using a 3:2 (v/v) hexane/dichloromethane solution to separate some of the unreacted cluster from the major red/brown compound. This species has been characterised on the basis of spectroscopy alone, as attempts to grow single crystals suitable for X-ray diffraction studies proved unsuccessful. Its IR spectrum indicates the presence of terminal carbonyl ligands only, and resembles that of the $Ru_4(\mu\text{-}H)_4(CO)_{10}(phen)$ analogue, and its mass spectrum exhibits the parent ion peak at 1225 (calc. 1224) amu, corresponding to $Os_4(\mu\text{-}H)_4(CO)_{10}(phen)$ **16**. The ^1H NMR shows four resonances at 9.55, 8.55, 8.07, and 7.80 ppm, all of relative integral two. The resonances can be readily assigned on the basis of their couplings as previously discussed for the ruthenium analogue. The singlet resonance at 9.55 ppm is attributed to the α proton is however rather broad and is again thought to result from the movement of the hydride ligands as discussed earlier.

The hydrides resonances were observed as two sets of doublets between -18.13 and -21.28 ppm and were assigned on the basis of their integrals. In contrast, the ruthenium analogue shows only two broad singlet resonances, and thus apparently shows a more rapid exchange of the hydrides.

2.9 Concluding Remarks

The research discussed in this chapter has shown that the $Ru_4(\mu\text{-}H)_4(CO)_{12}$ cluster reacts with pyridine and a number of bidentate and tetradentate nitrogen heterocycles to form the disubstituted clusters $Ru_4(\mu\text{-}H)_4(CO)_{10}L_2$, which show the ligand co-ordinated at a single metal site. It was found to be the major product whether 1.1 or 2.2 equivalents of Me_3NO were used to remove the carbonyl ligands, and has therefore been suggested as the thermodynamically favoured final product. Furthermore, attempted tetrasubstitution of the cluster using 4.2 equivalents of Me_3NO led only to the formation of this product. The monosubstituted derivative was however identified as a minor product from the reaction with pyridine and 1.1 equivalents of Me_3NO, and was tentatively assigned to the intermediate green species observed during the reaction with 2,2'-bipyrimidine, which ultimately produced the disubstituted cluster. The formation of these disubstituted cluster derivatives is summarised in Scheme 2.9.1. Similar reactions involving the $Os_4(\mu\text{-}H)_4(CO)_{12}$ cluster and Me_3NO proved unsuccessful and instead the more reactive $Os_4(\mu\text{-}H)_4(CO)_{10}(MeCN)_2$ species had to be utilised. Again comparable disubstituted cluster were synthesised. It is suggested that the differing rate of hydride fluxionality in the osmium clusters *cf.* the ruthenium clusters, result in the broadening of the resonance of the α proton because it lies closest to the hydrides in space and thus shows the greatest effect on its magnetic environment.

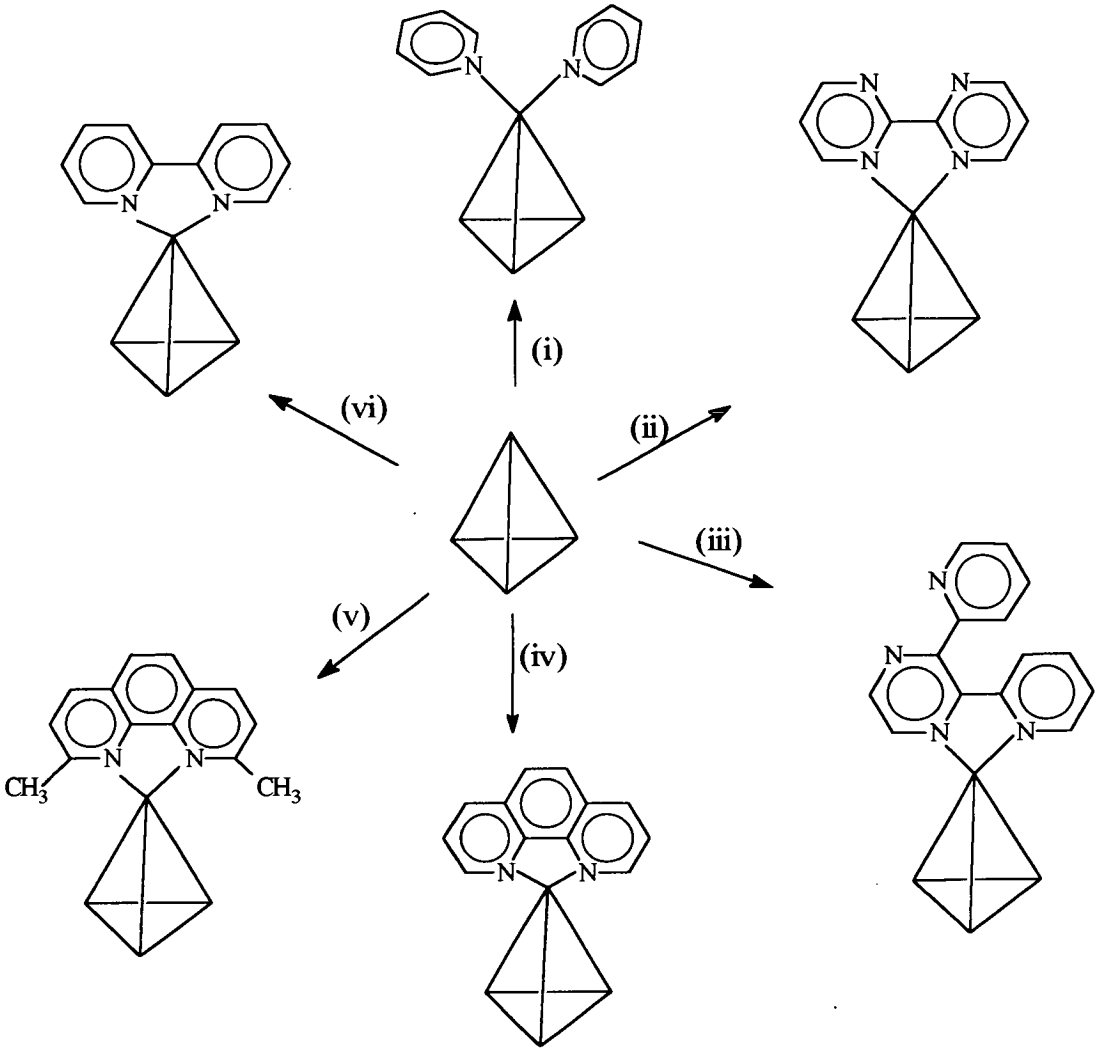

Reaction of $Ru_4(\mu\text{-}H)_4(CO)_{12}$ at -78 °C with 2.2 equivalents of Me_3NO with L=

(i) pyridine (py)
(ii) 2,2'-bypyrimidine (bpm)
(iii) 2,3-bis-(2-pyridyl)pyrazine
(iv) 1,10-phenanthroline (phen)
(v) 2,9-dimethyl-1,10-phenanthroline (dmp)
(vi) 2,2'-bipyridyl (bipy)

Scheme 2.9.1: The disubstituted products from the reaction of $Ru_4(\mu\text{-}H)_4(CO)_{12}$ with a series of nitrogen heterocycles.

2.10 References

1. a) J.W. Koepke, J.R. Johnson, S.A.R Knox, H.D. Kaesz, *J. Am. Chem. Soc.*, 1975, **97**, 3947; b) K.E. Inkrott, S.G. Shore, *J. Am. Chem. Soc.*, 1978, **100**, 3594; c) P.F. Jackson, B.F.G. Johnson, J. Lewis, M. McPartlin, W.J.H. Nelson, *J. Chem. Soc., Chem. Commun.*, 1978, 920.
2. a) G. Wilkinson, F.G.A. Stone, E.W. Abel (Editors), Comprehensive Organometallic Chemistry, Pergamon Press, New York, 1982, **4**, 891.

   b) F. Piacenti, M. Bianchi, P. Frediani, E. Benedetti, *Inorg. Chem.*, 1971, **10**, 2759.
3. R.D. Wilson, R. Bau, *J. Am. Chem. Soc.*, 1976, **98**, 4687 (Note 24).
4. J.L. Graaf, M.S. Wrighton, *J. Am. Chem. Soc.*, 1980, **102**, 2123.
5. M.I. Bruce, J.G. Matisons, B.K. Nicholson, *J. Organomet. Chem.*, 1983, **247**, 321.
6. S.A.R Knox, H.D. Kaesz, *J. Am. Chem. Soc*, 1971, **93**, 4594.
7. R.D. Wilson, S.M. Wu, R.A. Love, R. Bau, *Inorg. Chem*, 1978, **17**, 1271.
8. M.R. Churchill, R.A. Lashewycz, *Inorg. Chem*, 1978, **17**, 1950.
9. J.R. Shapley, S.I. Richter, M.R. Churchill, R.A. Lashewycz, *J. Am. Chem. Soc*, 1977, **99**, 7384.
10. R.D. Wilson, R. Bau, *J. Am. Chem. Soc*, 1976, **98**, 4687.
11. G. Huttner, H. Lorenz, *Chem. Ber.*, 1975, **108**, 973.
12. M.R. Churchill, R.A. Lashewycz, J.R. Shapley, S.I. Richter, *Inorg. Chem*, 1980, **19**, 1277.
13. a) S.L. Ingham, B.F.G. Johnson, J.G.M. Nairn, *J. Chem. Soc., Chem. Commun.*, 1995, 189; b) D. Braga, P.J. Dyson, F. Grepioni, B.F.G. Johnson, *Chem. Rev.*, 1994, **94**, 1585.
14. B.F.G. Johnson, Y.V. Roberts, *Inorg. Chim. Acta.*, 1993, **205**, 175.
15. B.F.G. Johnson, *J. Organomet. Chem.*, 1991, **415**, 109.
16. a) B.F.G. Johnson, *Inorg. Chim. Acta.*, 1986, **115**, L 39;
    b) B.F.G. Johnson, Y.V. Roberts, *J. Cluster Sci.*, 1993, **4**, 231.
17. a) T. Venäläinen, J. Purisainen, T. Pakkanen, *J. Chem. Soc., Chem. Commun.*, 1985, 1348; b) M.I. Bruce, M.G. Humphrey, M.R. Snow, E.R.T. Tieknik, R.C. Wallis, *J. Organomet. Chem.*, 1986, **314**, 311.
18. A.J. Deeming, R. Peters, M.B. Hursthouse, J.D.J. Backer-Dirks, *J. Chem. Soc, Dalton Trans.*, 1982, 787.
19. H. Chen, B.F.G. Johnson, J. Lewis, D. Braga, F. Grepioni, E. Parisini, *J. Chem. Soc., Dalton Trans.*, 1991, 215.

Chapter Three

The Reaction of $Ru_5C(CO)_{15}$ and $Ru_6C(CO)_{17}$ with Nitrogen Heterocyles

3.1 Introduction

The $Ru_5C(CO)_{15}$ cluster **17** was first synthesised in *ca.* 1% yield by the reaction of $Ru_4(\mu\text{-}H)_4(CO)_{12}$ **1** with ethylene and was postulated to be isostructural with the square based pyramidal $Fe_5C(CO)_{15}$ analogue on the basis of its IR spectrum,[1] and was later confirmed by a single crystal X-ray diffraction study. [2] A major feature of the chemistry of $Ru_5C(CO)_{15}$ is the ability it has to accept electron pairs and hence form adducts. This was first observed for the reversible reaction with acetonitrile which led to the formation of $Ru_5C(CO)_{15}(MeCN)$, [3] whose structure is given in Figure 3.1.1. The addition of the acetonitrile ligand causes the cleavage of a metal-metal bond to occur and the reorganisation of the cluster's metal core to form a bridged butterfly structure.

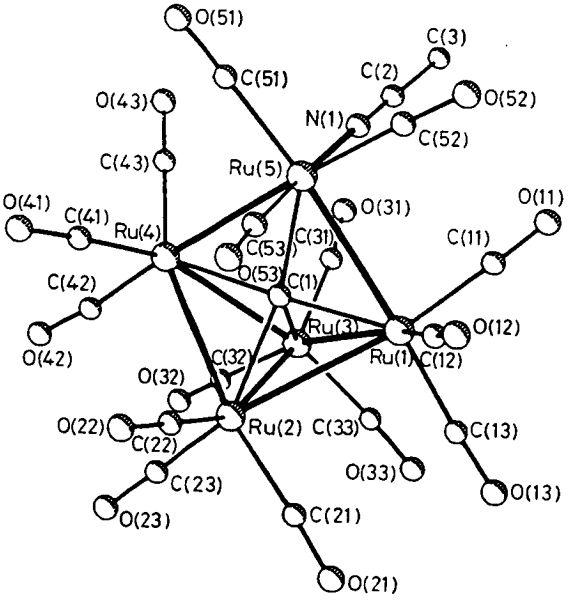

Figure 3.1.1: The solid state molecular structure of $Ru_5C(CO)_{15}(MeCN)$.

The observed structure can be rationalised using electron counting rules [4] as follows:

$Ru_5C(CO)_{15}$		$Ru_5C(CO)_{15}(MeCN)$	
5 Ru	40 e	5 Ru	40 e
15 CO	30 e	15 CO	30 e
1 C	4 e	1 C	4 e
		1 MeCN	2 e
Total =	74 e	Total =	76 e

Subtract 12 electrons per Ru for ligand bonding to give the number of electrons involved in skeletal bonding *i.e.* the electrons holding the metal framework together.

74-60 e = 14 skeletal electrons	76-60 e = 16 skeletal electrons
7 SEPS (n+2)	8 SEPS (n+3)

Note 3.1.1: Prediction of cluster geometries by electron counting.

Cluster geometries are based on *closo* parent polyhedra, with n vertices which possess n+1 skeletal electron pairs (SEPS). Removal of one vertex leads to the formation of a *nido* polyhedron with n+2 SEPS, and the loss of a further vertex produces an *arachno* polyhedron with n+3 SEPS. Hence, $Ru_5C(CO)_{15}$ which possesses 7 SEPS is based on a six vertex parent polyhedron with one vertex removed, and so can be described as a *nido* octahedron, or more simply as a square based pyramid. Likewise, $Ru_5C(CO)_{15}(MeCN)$ can be described as an *arachno* pentagonal bipyramid or simply as a bridged butterfly.

Similarly, the reaction with halides leads to the formation of the 76 electron species $[Ru_5C(CO)_{15}X]^-$ (X= Cl, Br or I), [2] which is proposed to have the bridged butterfly geometry on the basis of its electron count and by analogy with $[Os_5C(CO)_{15}I]^-$ [5] whose structure has been determined, and which shows a comparable IR spectrum. Protonation of $[Ru_5C(CO)_{15}X]^-$ leads to the formation of

the neutral $Ru_5(\mu\text{-}H)C(CO)_{15}X$ complex, which can also be prepared from the parent cluster by direct reaction with HX.

The second pertinent feature of the cluster's reactivity is its ability to undergo substitution reactions *e.g.* reaction with 1.1 equivalents of PPh_3 gives the 74 electron *closo* $Ru_5C(CO)_{14}(PPh_3)$ cluster, which is proposed to form *via* a bridged butterfly adduct intermediate (Scheme 3.1.1). [6]

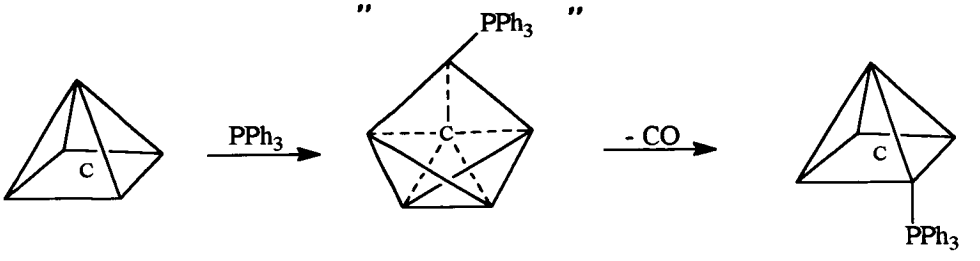

Scheme 3.1.1: The substitution reaction of $Ru_5C(CO)_{15}$ **17** with PPh_3 showing the proposed formation *via* an adduct intermediate.

Attack of the phosphine occurs at the basal ruthenium atom, the site of lowest connectivity, and in the presence of excess phosphine the compound reacts further to produce the disubstituted cluster $Ru_5C(CO)_{13}(PPh_3)_2$. Both of these species have been confirmed by X-ray crystallographic studies and show the expected square based pyramidal structure. [6] The bulk of the PPh_3 groups is sufficient to cause the diphosphine derivative to show co-ordination of the ligands at diagonally opposite basal sites, whilst $Ph_2P(CH_2)_2PPh_2$ chelates to a single basal ruthenium atom only.

In summary, the $Ru_5C(CO)_{15}$ cluster has a tendency to form adducts with nucleophiles which result in the rearrangement of the metal framework from square based pyrimadal (74 e) to bridged butterfly (76 e). These species can then often undergo further reaction with the subsequent loss of a carbonyl ligand, to reproduce the square based pyramidal structural framework.

3.2 Reaction of $Ru_5C(CO)_{15}$ with Pyridine

To date, only Dutton [7,8] has investigated the reactivity of the $Ru_5C(CO)_{15}$ cluster **17** with nitrogen heterocycles. His work concentrated mainly on the thermal reaction with pyridine (Scheme 3.2.1), although the reactions with 2,2-bipyridyl and diazines were also reported.

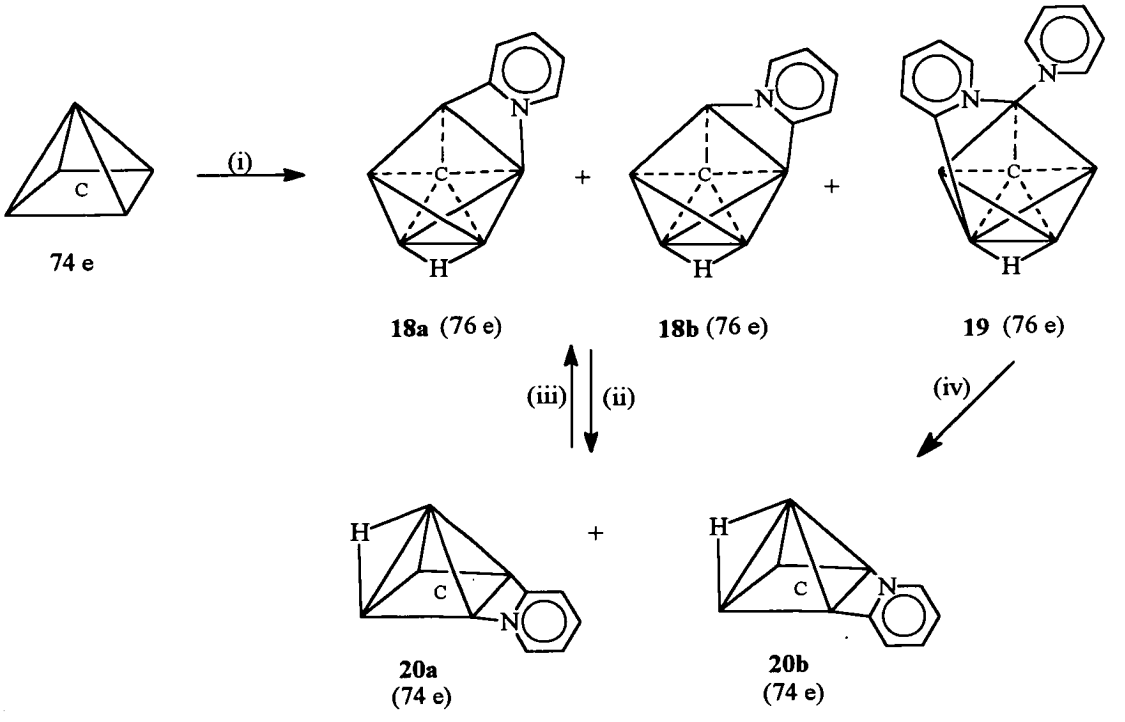

Scheme 3.2.1: The reaction between $Ru_5C(CO)_{15}$ and pyridine in (i) CH_2Cl_2 , 40 °C for 4 hours; (ii) heptane; 98 °C for 24-48 hours; (iii) CO, 80 °C, 10 minutes, or on silica or in air over 3 weeks; (iv) heptane, 90 °C for 2 hours, as reported by Dutton.

The bridged butterfly compound **18**: $Ru_5(\mu\text{-}H)C(CO)_{14}(C_5H_4N)$ was the major reaction product, and was shown to be present in two isomeric forms **a** and **b**, which were separable by tlc, and differed only in the orientation of the *ortho*metalated C-N bond, as shown by X-ray crystallography. These isomers showed only relatively minor changes in their carbonyl IR spectra, but were readily distinguished by ^1H NMR. Refluxing **17** in heptane for between 24 and 48 hours was found to cause the

loss of a second carbonyl ligand to produce $Ru_5(\mu\text{-}H)C(CO)_{13}(C_5H_4N)$ **20**, which showed the reformation of the metal-metal bond to return to the square based pyramidal geometry. It decomposed on silica or in solution to reproduce compound **18** *via* carbonyl scavenging. A second minor product was formed from the reaction between $Ru_5C(CO)_{15}$ **17** and pyridine, and shown to be the disubstituted cluster $Ru_5(\mu\text{-}H)C(CO)_{13}(C_5H_4N)(py)$ **19** by both spectroscopy and X-ray crystallography. It shows a bridged butterfly structure as for **18**, and as expected possesses an electron count of 76. These products were proposed to occur *via* the formation of an intermediate adduct, as for the reaction between $Ru_5C(CO)_{15}$ and PPh_3 discussed earlier (Scheme 3.11).

The reaction between $Ru_5C(CO)_{15}$ and pyridine was repeated, but using chemical rather than thermal activation. Reaction with 2.2 equivalents of Me_3NO proved unsuccessful, producing only major decomposition of the cluster, and so the reaction was repeated using only 1.1 equivalents of Me_3NO. An orange solution was produced at -78 °C which became gradually darker upon warming to room temperature. Two products were isolated from the reaction mixture by tlc: a yellow cluster which was eluted using hexane/dichloromethane (3:2 v/v) and the major product, an orange/yellow cluster eluted using neat dichloromethane.

It is not at all clear from the ^1H NMR spectrum of the orange product what its precise nature is due to the instability of the species. The spectrum of the yellow species is however much more revealing (Figure 3.2.1). It exhibits six aromatic resonances of relative integral 2:1:1:3:1:1 and a single hydride resonance of integral one at -21.32 ppm. This is consistent with the co-ordination of two pyridines, one of which must be *ortho*metallated, and the other terminal, as observed for cluster **19**. However, by comparison with the spectroscopic data reported on cluster **19**, it is apparent that the same product has not been formed. In the absence of X-ray crystallographic data its formulation and structure can only be tentatively proposed on the basis of spectroscopic evidence. Only a relatively weak mass spectral trace was obtained showing the presence of the molecular ion peak at 1011 amu. The IR

spectrum indicates that the cluster possesses only terminal carbonyl ligands, and therefore we suggest the molecule may be $Ru_5(\mu\text{-}H)C(CO)_{12}(C_5H_4N)(py)$ **21**, in which the structure shows the *ortho*metallated pyridine bridging a basal edge (Figure 3.2.1). Its 74 electron count would imply a square based pyramidal structure. However, in the absence of a more definitive mass spectrum or a crystal structure this formulation remains only speculative, and there is no obvious explanation for the loss of three carbonyl ligands under the conditions used. It may be that the structure is analogous to Dutton's $Ru_5(\mu\text{-}H)C(CO)_{13}(C_5H_4N)(py)$ cluster **19**, differing only in the position of the pyridine ring relative to the pyridyl.

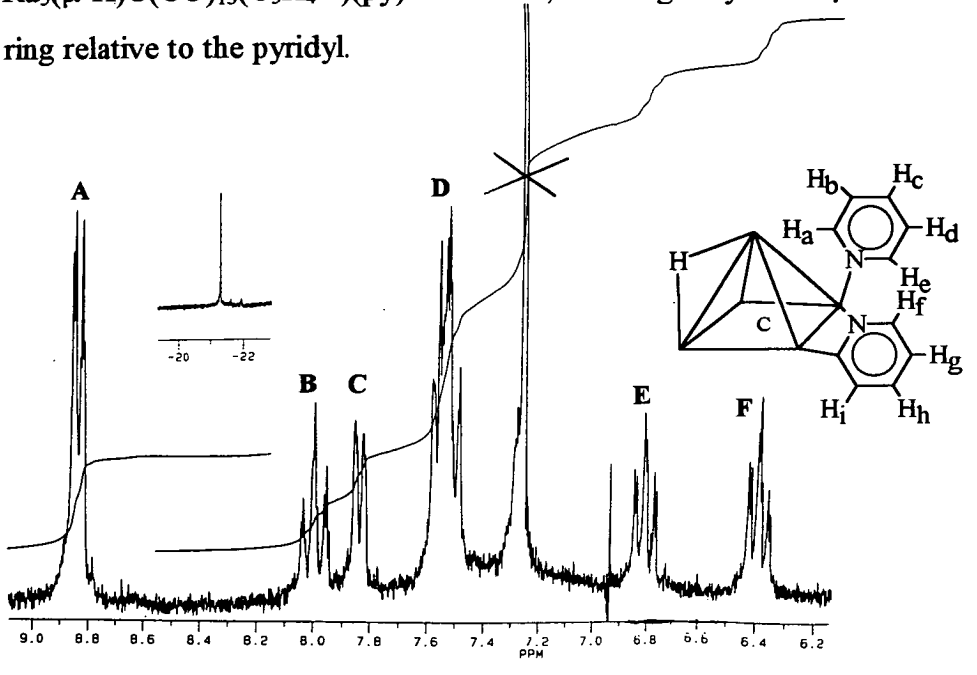

Figure 3.2.1: The ^1H NMR spectrum of the proposed species $Ru_5(\mu\text{-}H)C(CO)_{12}(C_5H_4N)(py)$ **21**.

Interpretation of ^1H NMR

Resonance **A** at 8.83 ppm, an approximate doublet of integral two, is shifted to higher frequency relative to the others and is therefore attributed to the α protons H_a and H_e. The two triplets of doublets **E** and **F** arise from the protons H_g and H_h of the *ortho*metallated pyridine ring, being characteristically shifted to lower frequency. Irradiation of resonance **F** causes the loss of a large coupling to the doublet resonance at 7.83 ppm **C**, which must result from proton H_f, and not H_i which would be predicted at a lower chemical shift. In addition the reduction of **E** from an

approximate triplet to a doublet and the loss of coupling to resonance **D** are observed. Thus, H_f= **C** and H_g= **E**, and consequently H_h= **F**, and H_i must give rise to a resonance hidden amongst the multiplet at 7.53 ppm. Only protons H_b , H_c , and H_d remain to be assigned. H_c must give rise to the triplet of triplets at 7.98 ppm, whilst H_b and H_d contribute to the multiplet **D**.

Resonance	δ/ppm	Proton
A	8.83	H_a, H_e
B	7.98	H_c
C	7.83	H_f
D	7.53	H_b, H_d, H_i
E	6.85	H_h
F	6.39	H_g

Table 3.2.1: Table of proton assignments of $Ru_5(\mu\text{-}H)C(CO)_{12}(C_5H_4N)(py)$ **21**.

3.3 Reaction of $Ru_5C(CO)_{15}$ with 2,2'-Bipyridyl

2,2'-bipyridyl was added to a dichloromethane solution of $Ru_5C(CO)_{15}$ **17** which had been cooled to -78 °C, and was followed by the dropwise addition of 2.2 molar equivalents of Me_3NO to initiate the loss of two carbonyls and cause a similar disubstitution reaction as observed for $M_4(\mu\text{-}H)_4(CO)_{12}$ (M= Ru, Os), which is discussed in Chapter Two. Compound **17** is known to substitute typically at only the basal ruthenium atom sites, although apical substitution has been suggested for a benzene derivative, [9] hence it was predicted that direct substitution of two carbonyls would lead to the formation of $Ru_5C(CO)_{13}$(bipy) **22**, showing a basal connectivity of the ligand (Scheme 3.3.1).

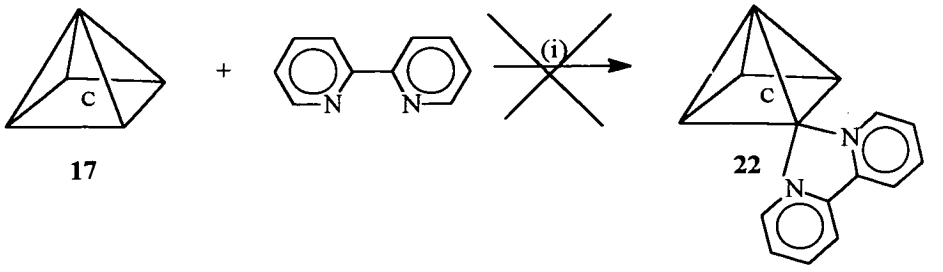

Scheme 3.3.1: The initially proposed reaction scheme for the formation of $Ru_5C(CO)_{13}$(bipy) **22** from the reaction of **17** with 2,2'-bipyridyl in the presence of (i) 2.2 equivalents of Me_3NO at -78 °C.

Results and Discussion

The above reaction was instead found to afford the orange/red bridged butterfly cluster $Ru_5C(CO)_{14}$(bipy) **23** as the major product, and the yellow *ortho*metallated derivative $Ru_5(\mu\text{-}H)C(CO)_{13}(C_{10}H_7N_2)$ **24** as a minor one (Scheme 3.3.2).

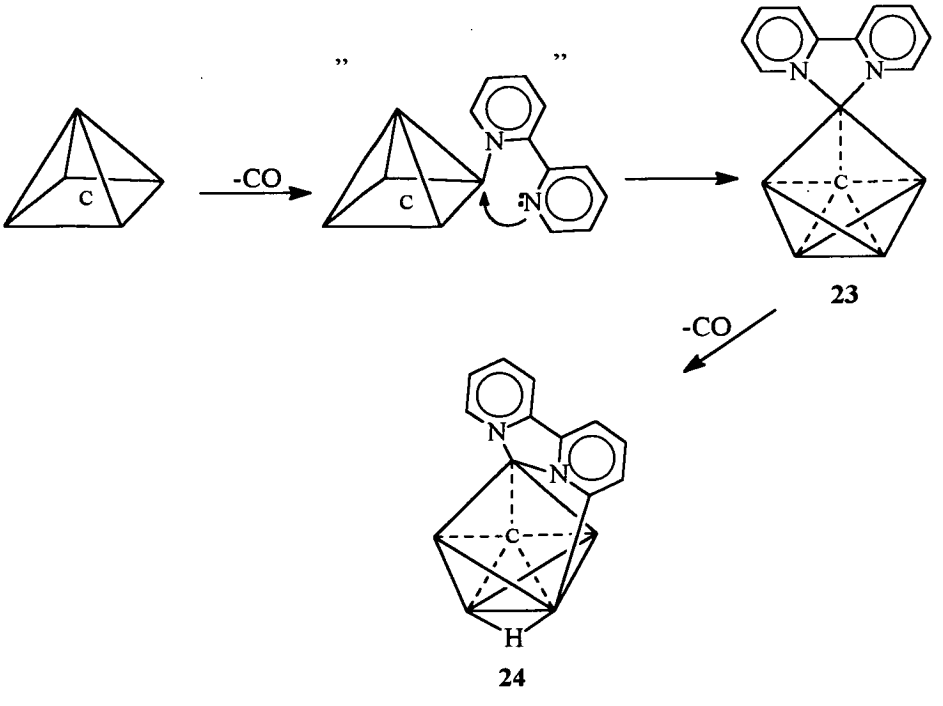

Scheme 3.3.2: Formation of $Ru_5C(CO)_{14}$(bipy) **23** and $Ru_5(\mu\text{-}H)C(CO)_{13}(C_{10}H_7N_2)$ **24** *via* the hypothetical intermediate $Ru_5C(CO)_{14}(\eta^1\text{-bipy})$.

One possible explanation may be that this reaction proceeds *via* the initial formation of the monosubstituted cluster $Ru_5C(CO)_{14}(\eta^1$-bipy), which then undergoes adduct formation to yield $Ru_5C(CO)_{14}$(bipy) **23**. The loss of a second carbonyl ligand from the cluster then leads to the *ortho*metallated product $Ru_5(\mu$-H)$C(CO)_{13}(C_{10}H_7N_2)$ **24**.

Characterisation of $Ru_5C(CO)_{14}$(bipy) 23

The orange/red product **23** was initially characterised by spectroscopy. Its IR spectrum indicated the presence of only terminal carbonyl ligands and the compound was formulated as $Ru_5C(CO)_{14}$(bipy) on the basis of its mass spectrum and was confirmed by both X-ray crystallography and elemental analysis. The cluster produced is clearly not the expected $Ru_5C(CO)_{13}$(bipy) compound **22** (Scheme 3.3.1). Instead only one carbonyl has been lost and a 76 electron bridged butterfly adduct formed by the addition of the second nitrogen lone pair to the basal ruthenium atom, as shown by the X-ray crystal structure (Figure 3.3.4). Dutton [8] had previously suggested the formation of an isomer of cluster **23** (Figure 3.3.3) from the reaction between $Ru_5C(CO)_{15}$ and 2,2'-bipyridyl in refluxing dichloromethane, by analogy with the incorrectly postulated edge bridging structure proposed for $Ru_3(CO)_{10}$(bipy). [10] It is uncertain what the exact nature of this product was, yet by comparison of the ^{1}H NMR data it is apparent that it cannot be either of the products **23** or **24** discussed herein. Furthermore, the air sensitive character of Dutton's product rules it out as both the species formed in this work are air stable.

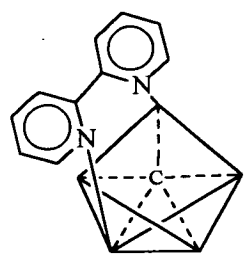

Figure 3.3.3: The suggested structure of Dutton's $Ru_5C(CO)_{14}$(bipy) isomer.

X-ray Structure Determination

The solid state molecular structure of $Ru_5C(CO)_{14}$(bipy) **23** is given in Figure 3.3.4 along with some relevant bond lengths and angles in Table 3.3.1. The metal framework geometry is best described as an approximately bridged butterfly structure akin to those discussed earlier. Formation of the butterfly leads to four 18 electron sites and a 19 electron site at Ru(1). The ligand is bound in a bidentate manner to this apical ruthenium atom, which shows further co-ordination to Ru(2) and Ru(3), the central carbide, and two terminal carbonyl ligands. The remaining ruthenium atoms are each bound to three terminal carbonyl ligands. There is little variation seen between the carbonyl bond lengths which range from 1.127(8) to 1.157(8) Å. The *penta-* co-ordinate carbide atom is asymmetrically bound, showing shorter Ru-C distances between the wing tip atoms Ru(2), Ru(3) than the bridging atoms Ru(4), Ru(5) as observed previously for $[Ru_5C(CO)_{14}(\mu\text{-}AuPPh_3)(\mu\text{-}Br)]$ [11] and $[Ru_5(\mu\text{-}H)C(CO)_{14}(SEt)]$. [12] The bipyridyl ligand is also asymmetrically co-ordinated to the cluster with Ru-N bond lengths of 2.161(6) and 2.124(5) Å, and is tilted somewhat to minimise steric hindrance.

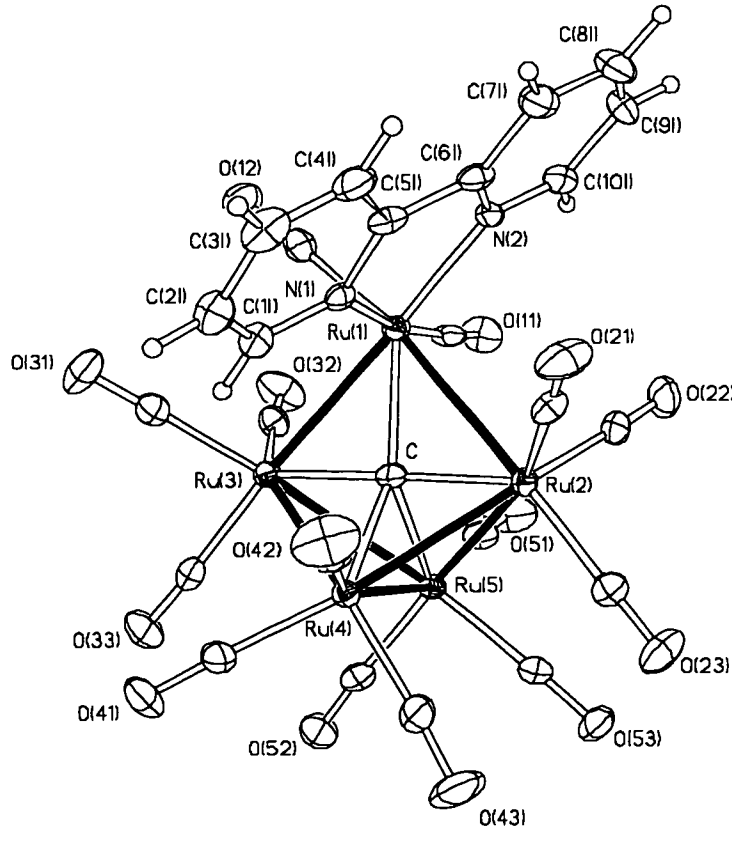

Figure 3.3.4: The thermal ellipsoid plot at 50% probability depicting the molecular structure of $Ru_5C(CO)_{14}$(bipy) **23** at 150K.

Ru(1)-Ru(2) 2.9174(9)	Ru(4)-Ru(5) 2.7212(9)	Ru(4)-C 2.083(6)
Ru(1)-Ru(3) 2.9041(11)	Ru(1)-N(1) 2.161(6)	Ru(5)-C 2.150(6)
Ru(2)-Ru(4) 2.8699(12)	Ru(1)-N(2) 2.124(5)	mean CO 1.14
Ru(2)-Ru(5) 2.8390(10)	Ru(1)-C 2.110(6)	N(1)Ru(1)N(2) 76.2(2)
Ru(3)-Ru(4) 2.9173(10)	Ru(2)-C 1.958 (6)	N(1)Ru(1)Ru(3) 100.67(13)
Ru(3)-Ru(5) 2.8690(11)	Ru(3)-C 1.990(6)	N(2)Ru(1)Ru(2) 95.11(4)

Table 3.3.1: Selected bond lengths (Å) and angles(°) for $Ru_5C(CO)_{14}$(bipy).

Interpretation of ^1H NMR

The ^1H NMR spectrum of compound **23** is presented in Figure 3.3.5 and shows seven resonances of relative integral 1:1:1:2:1:1:1 for the ring protons (H_1-H_4, H_7-H_{10}), indicating that the magnetic environments of the analogous protons of the two rings have become inequivalent. This inequivelance arises from the protons of one of the two aryl rings being brought into closer proximity with carbonyl ligands than the other.

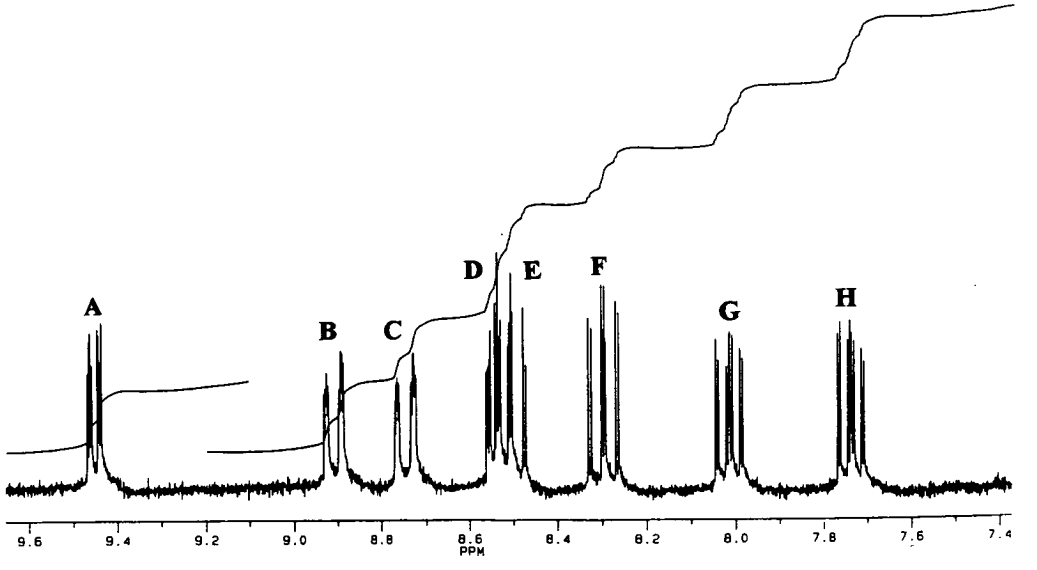

Figure 3.3.5: ^1H NMR of $Ru_5C(CO)_{14}$(bipy) **23** run in CD_2Cl_2.

The resonances have been labelled **A-H** for ease of reference. Four doublets are expected to result from the resonances associated with protons H_1, H_4, H_7, and H_{10}, whilst H_2, H_3, H_8 and H_9 are expected to show a doublet of doublet or a triplet pattern (to a first approximation, ignoring smaller couplings). Obviously two almost identical sets of resonances are expected to arise from the two rings. It is immediately apparent that resonance **A** arises from an α proton adjacent to nitrogen: H_1 or H_{10} but it cannot be unambiguously stated which. The other α proton must give rise to an equivalent resonance with a similar structure and therefore lies hidden amongst the multiplet at *ca.* 8.55 ppm. The remaining doublets **B** and **C** are therefore due to H_4 and H_7. The ddd resonance **F** at *ca.* 8.3 ppm shows two large three bond couplings

(8.7 and 7.6 Hz) and must therefore be attributed to one of the protons H_3 and H_8 rather than protons H_2 and H_9 which are expected to show a characteristically smaller coupling to the α proton in addition to the large coupling to H_3 / H_8. Its equivalent partner must give rise to the resonance which is partially obscured in the multiplet at *ca.* 8.5 ppm. The remaining ddd resonances **G** and **H** are therefore assigned to H_2 and H_9 which show a very similar intensity and structural pattern as expected. These assignments were confirmed by a ^1H COSY experiment which also clearly showed that the resonances **A**, **B**, **E**, and **G** resulted from one of the pyridyl rings and **C**, **D**, **F**, and **H** from the other.

Resonance	δ/ppm	Proton
A / D	9.54, 8.54	H_1 / H_{10}
B / C	8.82, 8.75	H_4 / H_7
E / F	8.48, 8.30	H_3 / H_8
G / H	8.02, 7.74	H_2 / H_9

Table 3.3.1: Table of proton assignments of $Ru_5C(CO)_{14}$(bipy) **23**.

*Characterisation of $Ru_5(\mu\text{-}H)C(CO)_{13}(C_{10}H_7N_2)$ **24***

This yellow cluster was produced as only a minor product in the reaction between $Ru_5C(CO)_{15}$ and 2,2'-bipyridyl, and was formulated initially as $Ru_5(\mu\text{-}H)C(CO)_{13}(C_{10}H_7N_2)$ by a consideration of the spectroscopic evidence only. Its IR spectrum shows the presence of only terminal carbonyl ligands, and the ^1H NMR (Figure 3.3.6) of this minor product implies that *ortho*metallation of the cluster has occurred, and this is confirmed by the crystal structure (Figure 3.3.7). The five aromatic resonances in the spectrum are present in the ratio 1:2:2:1:1 and a sixth metal hydride resonance is observed at -21.42 ppm. A comprehensive analysis of the spectrum has not be undertaken, although further decoupling experiments or a COSY NMR ought to be sufficient to resolve the exact assignments of the resonances. It is

however apparent that the α proton H_{10} gives rise to the resonance which is shifted to highest frequency, and H_3 gives rise to the distinctive triplet at 7.00 ppm. A doublet of doublets at *ca.* 7.23 ppm is partially obscured by the $CHCl_3$ peak and must be due to either H_2 or H_4 , and hence the two multiplets which each result from the overlapping of two proton resonances, originate from H_7, H_8 , H_9, and either H_4 or H_2. The proposed structure perhaps implies that *ortho*metallation occurs in preference to reformation of the metal-metal bond. This may be a direct result of the steric hindrance which would foreseeably be encountered in attempting to bring Ru(1) and Ru(5) close enough to bond.

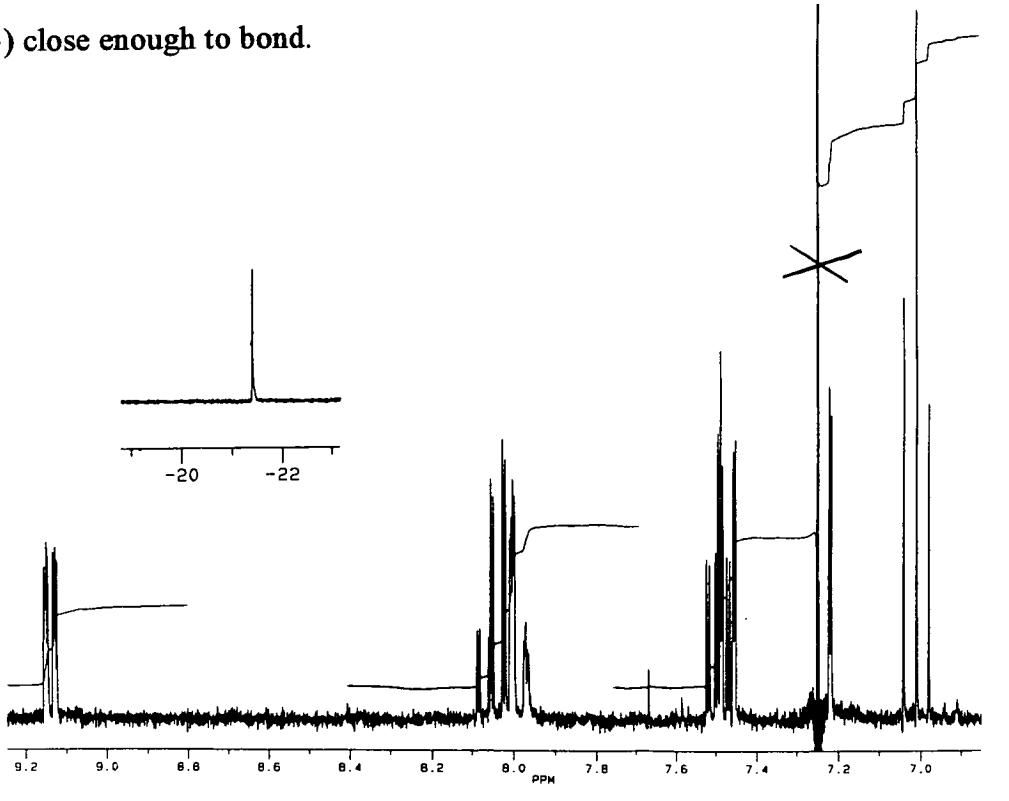

Figure 3.3.6: The ^1H NMR of the $Ru_5(\mu\text{-}H)C(CO)_{13}(C_{10}H_7N_2)$ cluster **24**.

This spectroscopic assignment was confirmed by the growth of single crystals which were found to be suitable for X-ray analysis. The structure was solved by Dr. Ian Scowen (University of North London) and is presented in Figure 3.3.7 below. The structure shows the *ortho*metallated Ru_5 cluster unit to which there are seven metal to metal bonding contacts and is analogous to the structure determined by Dutton [8] for the *bis* pyridine cluster $Ru_5(\mu\text{-}H)C(CO)_{13}(C_5H_4N)(py)$ **19**. It displays a bridged butterfly geometry which is in line with its 76 electron count.

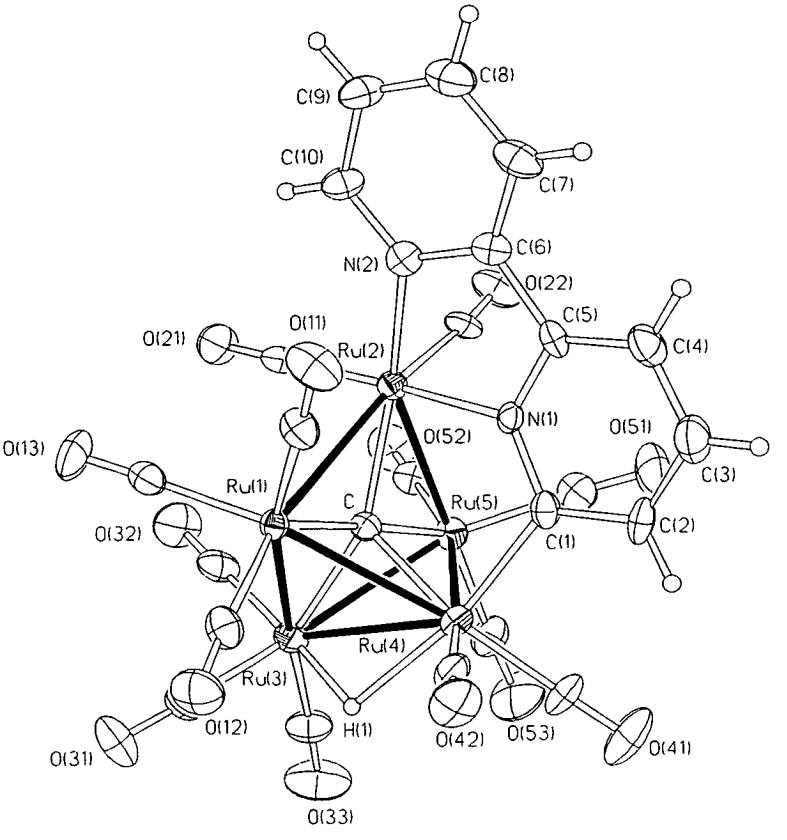

Figure 3.3.7: The thermal ellipsoid plot at 30% probability depicting the molecular structure of $Ru_5(\mu\text{-}H)C(CO)_{13}(C_{10}H_7N_2)$ **24** at 298K.

Ru(1)-Ru(2) 2.9009(10)	Ru(2)-N(1) 2.125(7)	Ru(5)-C 2.006(8)
Ru(1)-Ru(3) 2.8460(10)	Ru(2)-N(2) 2.138(7)	Ru(3)-H(1) 1.5765(8)
Ru(1)-Ru(4) 2.8676(11)	Ru(4)-C(1) 2.053(9)	Ru(4)-H(1) 2.0672(8)
Ru(2)-Ru(5) 2.8826(11)	Ru(1)-C 1.971(8)	mean C-O 1.14
Ru(3)-Ru(4) 2.8959(11)	Ru(2)-C 2.060(8)	N(1)-Ru(2)-N(2) 76.2(3)
Ru(3)-Ru(5) 2.8785(11)	Ru(3)-C 2.096(8)	N(1)C(1)Ru(4) 118.7(6)
Ru(4)-Ru(5) 2.8115(10)	Ru(4)-C 2.053(1)	C(1)N(1)Ru(2) 123.1(6)

Table 3.3.2: Selected bond lengths (Å) and angles (°) of $Ru_5(\mu\text{-}H)C(CO)_{13}(C_{10}H_7N_2)$ **24**.

The Ru(2)-Ru(4) metal-metal bond of the parent cluster $Ru_5C(CO)_{15}$ has been cleaved and shows the atoms lie 3.539(11) Å apart. The 2,2'-bipyridyl ligand is bound

through the lone pair on both of its nitrogens and in addition to the *ortho* carbon atom C(1) of one ring. The proton which was lost from this site has become a bridging hydride, spanning the bond between Ru(3) and Ru(4) and was found directly from the electron density difference map. Its position was confirmed by an examination of a space filling model of the molecule which showed an appropriately sized cavity between these metal atoms (Figure 3.3.8).

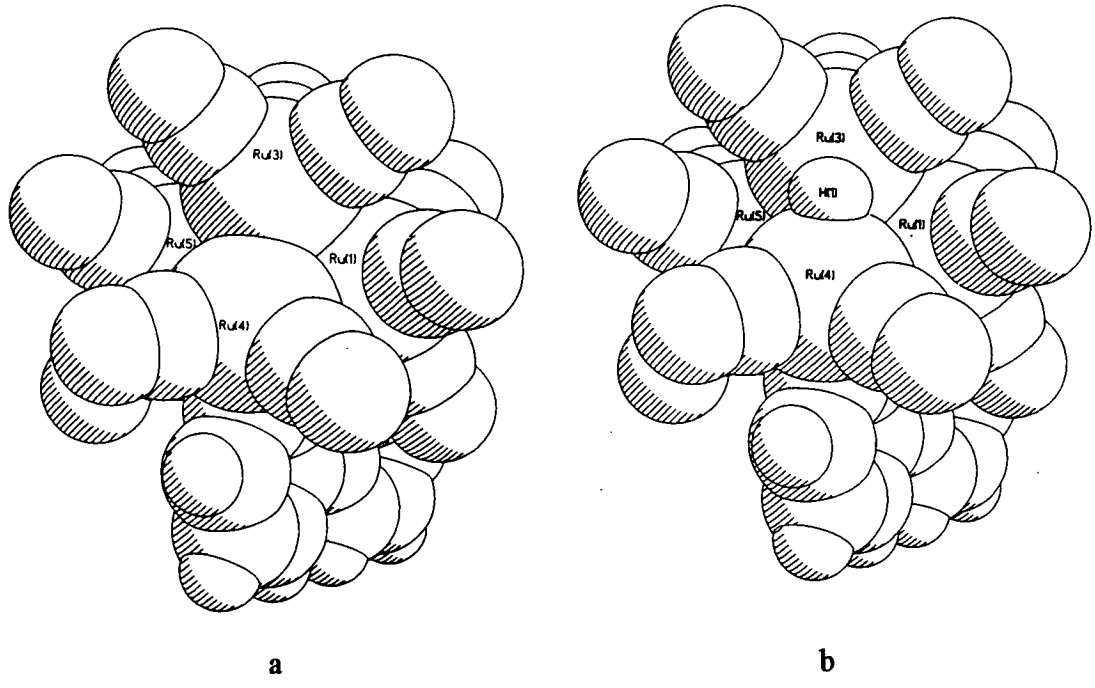

Figure 3.3.8: Molecular packing diagrams showing a) the cavity in the $Ru_5C(CO)_{13}(C_{10}H_7N_2)$ framework, and b) the hydride sitting in this niche for the $Ru_5(\mu\text{-}H)C(CO)_{13}(C_{10}H_7N_2)$ cluster.

The central metal carbide atom is asymmetrically bonded to all five metal metals, showing a longer bond to the Ru(3) and Ru(4) centres of the hinge than to the wing tip rutheniums (1) and (5). All thirteen carbonyl ligands are terminally bonded in agreement with the IR spectrum, and vary in length from 1.128- 1.157 Å, averaging 1.14 Å. Three carbonyl ligands are co-ordinated to each of the ruthenium atoms (1), (3) and (5) whilst the remaining Ru(2) and Ru(4) atoms are co-ordinated to only two carbonyl ligands each.

Because of the somewhat unexpected favoured removal of only one carbonyl ligand in the presence of 2.2 equivalents of Me_3NO, the reaction was repeated using 1.1 equivalents of Me_3NO to see whether cluster **23**: $Ru_5C(CO)_{14}$(bipy) was still formed, but in relatively higher yield. This was indeed found to be the case. The favoured removal of only one carbonyl ligand, whether 1.1 or 2.2 equivalents of Me_3NO were used, is in direct contrast to the reactivity of the $Ru_4(\mu\text{-}H)_4(CO)_{12}$ cluster discussed in Chapter Two, which showed the removal of two carbonyl ligands under analogous conditions.

Conclusions

Despite the use of 2.2 equivalents of Me_3NO the proposed product $Ru_5C(CO)_{13}$(bipy) **22** was not formed during the reaction between the $Ru_5C(CO)_{15}$ cluster **17** and 2,2-bipyridyl. It is suggested that this may be as a result of the steric repulsion between the carbonyl and bipyridyl ligands, which would perceivably occur for this geometry. Hence relatively higher levels of decomposition were observed compared to the reaction using only 1.1 equivalents of Me_3NO. Where the loss of a second carbonyl was successful, the *ortho*metallated cluster $Ru_5(\mu\text{-}H)C(CO)_{13}(C_{10}H_7N_2)$ **24** was formed. However, since the loss of only one carbonyl ligand is favoured, the $Ru_5C(CO)_{14}$(bipy) cluster **23** is formed as the major reaction product. Both clusters $Ru_5C(CO)_{14}$(bipy) **23** and $Ru_5(\mu\text{-}H)C(CO)_{13}(C_{10}H_7N_2)$ **24** show a bridged butterfly arrangement as predicted by their electron count of 76. The inequivalence of the protons of the two pyridyl rings of the 2,2'-bipyridyl ligand in cluster **23** was observed by NMR, and is accounted for by the change in their magnetic environment resulting from the proximity of the ligand to the carbonyls.

3.4 Reaction of $Ru_5C(CO)_{15}$ With 1,10-Phenanthroline

The reaction between $Ru_5C(CO)_{15}$ **17** and 1,10-phenanthroline was carried out in an analogous manner to that reported for the bipyridyl ligand. Initially 2.2 equivalents of Me_3NO were used to activate the cluster, and a dark brown solution

was produced upon warming the solution from -78 °C to room temperature. Product separation by tlc using hexane/dichloromethane (1:1 v/v) as eluent isolated one main orange/red product which was identified as $Ru_5C(CO)_{14}$(phen) **25**, and a second yellow species in lower yield, characterised as $Ru_5(\mu\text{-}H)C(CO)_{13}(C_{12}H_7N_2)$ **26**, analogous to the 2,2'-bipyridyl derivatives (Scheme 3.4.1).

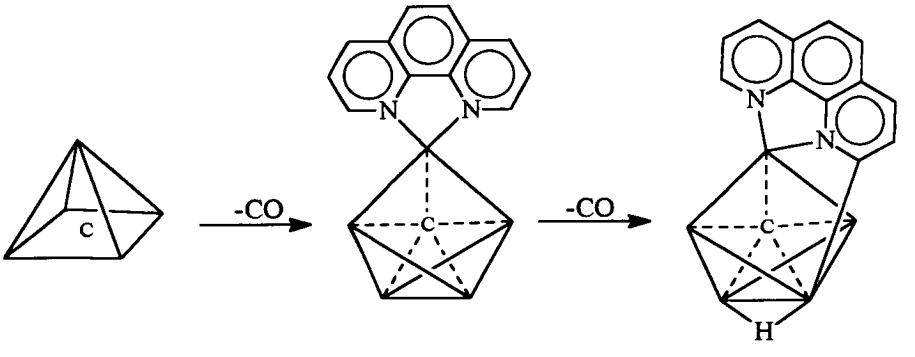

25 **26**

Scheme 3.4.1: Formation of $Ru_5C(CO)_{14}$(phen) **25** and $Ru_5(\mu\text{-}H)C(CO)_{13}(C_{10}H_7N_2)$ **26** from the reaction of $Ru_5C(CO)_{15}$ **17** with (i) 2.2 equivalents of Me_3NO at -78 ° C.

Results and Discussion

Characterisation of $Ru_5C(CO)_{14}$(phen) 25

The IR carbonyl pattern of compound **25** being almost identical to the bipyridyl derivative $Ru_5C(CO)_{14}$(bipy) **23**, implied the formulation $Ru_5C(CO)_{14}$(phen). This was confirmed by further spectroscopy and an X-ray diffraction study on a single crystal grown from a solution of hexane/dichloromethane. Its mass spectrum showed the molecular ion at 1092 (calc. 1089) amu, further confirming the preliminary identification of the cluster. Its molecular structure is presented in Figure 3.4.1. The familiar bridged butterfly skeleton of metal atoms is observed, which shows an outer

shell of fourteen terminal carbonyls, of which three are bound to each of the wing tip and the basal rutheniums Ru(2), Ru(4); and Ru(3), Ru(5) respectively. The remaining two carbonyl ligands are bound to the apical ruthenium Ru(1), which also shows co-ordination to the phenanthroline ligand in a bidentate manner, with a bite angle of 77.3(2) °. The five ruthenium atoms are bound to the central carbido atom, and show an average Ru-C bond length of 1.974 Å to the wing tip atoms, and an average bond length of 2.114 Å to the basal atoms, which is comparable to the Ru-C distance to the apical ruthenium. The carbido atom is therefore intermediate between fully enclosed as in $Ru_6C(CO)_{17}$ **27** [13] and completely exposed as in $Ru_5C(CO)_{15}$ **17**. [2,6]

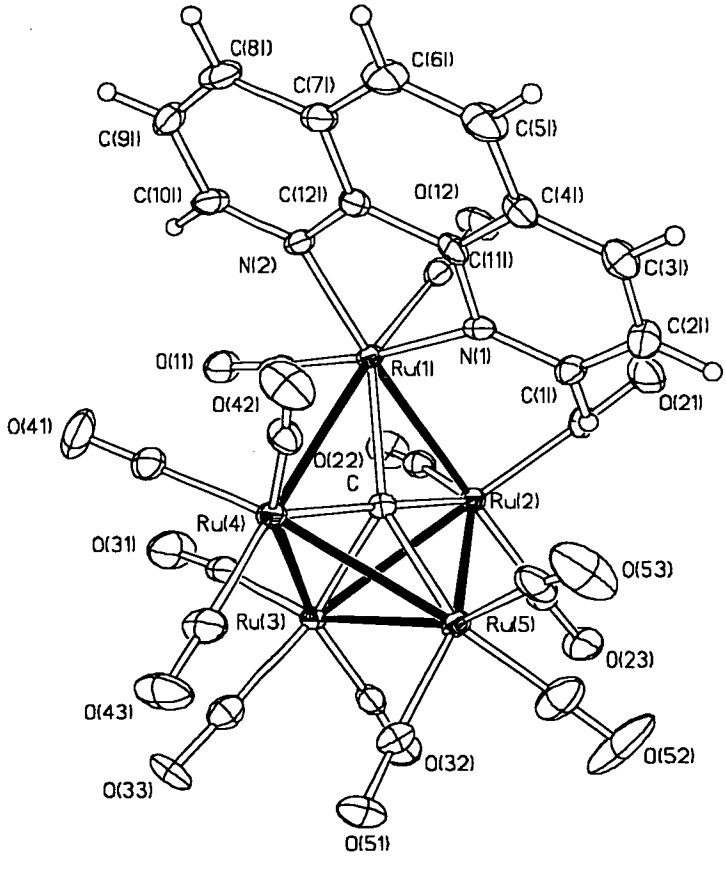

Figure 3.4.1: The thermal ellipsoid plot at 50% probability depicting the molecular structure of $Ru_5C(CO)_{14}$(phen) **25** at 150K.

Ru(1)-Ru(2) 2.8950(14)	Ru(4)-Ru(5) 2.893(2)	Ru(4)-C 1.973(5)
Ru(1)-Ru(4) 2.906(2)	Ru(1)-N(1) 2.166(5)	Ru(5)-C 2.085(6)
Ru(2)-Ru(3) 2.8514(13)	Ru(1)-N(2) 2.130(5)	mean C-O 1.14
Ru(2)-Ru(5) 2.930(2)	Ru(1)-C 2.114(6)	N(1)-Ru(1)-N(2) 77.3(2)
Ru(3)-Ru(4) 2.8469(12)	Ru(2)-C 1.975(5)	N(1)Ru(1)Ru(2) 98.33(13)
Ru(3)-Ru(5) 2.7136(12)	Ru(3)-C 2.144(6)	N(2)Ru(1)Ru(4) 95.14(3)

Table 3.4.1: Selected bond lengths (Å) and angles (°) of $Ru_5C(CO)_{14}$(phen) **25**.

Interpretation of ^1H NMR

The ^1H NMR spectrum of $Ru_5C(CO)_{14}$(phen) exhibits six resonances all of relative intensity one except for the multiplet at 8.04-8.19 ppm which has a relative intensity of three (Figure 3.4.2). The resonances have been labelled **A-F** for ease of reference. It is apparent from our earlier discussions that the doublet of doublets resonance **A** at high frequency results from an α proton, either proton H_1 or H_{10}, although it is not possible to state unambiguously which. From the magnitude of the coupling constants (5.33, 1.33 Hz), resonance **C** at 8.76 ppm can be attributed to proton H_3 or H_8 respectively. Furthermore, either H_2 or H_9 is responsible for the resonance in amongst the "multiplet" at 8.06 ppm, showing one relatively large ^3J coupling of 8.18 Hz to proton H_3 or H_8 and a characteristically smaller one to the α proton of 5.28 Hz. Consequently these resonances result from a set of protons residing on one of the pyridine rings of the phenanthroline ligand. From similar considerations resonances **B** and **F** are assigned to the α and β protons respectively of the other pyridine ring. Thus, only the multiplet between 8.04 and 8.19 ppm remains to be assigned and is obviously the result of the overlap between the resonances of H_5, H_6 and either H_3 or H_8. Expansion of the multiplet allowed the doublet of doublets resonance arising from either H_3 or H_8 to be more readily identified. The exact nature of the remaining resonance was not obvious and hence a further nOe experiment was

carried out. A 3.9% enhancement of resonance **E** at *ca.* 8.1 ppm, attributed to H_5 and H_6 was observed, and appeared as a triplet rather than a doublet, therefore coupling to both H_5 and H_8 must be occurring. Resonance **F** (H_2/H_9) showed a greater enhancement of 12.6%, which is as expected since this proton lies closer in space to H_3 / H_8 than H_5 / H_6. Thus the multiplet shows a closely overlapping set of triplets for H_5 and H_6 which explains the apparent 1:3:3:1 ratio of the resonance. Therefore, these protons are not only coupled to each other but also to H_3 and H_8 respectively.

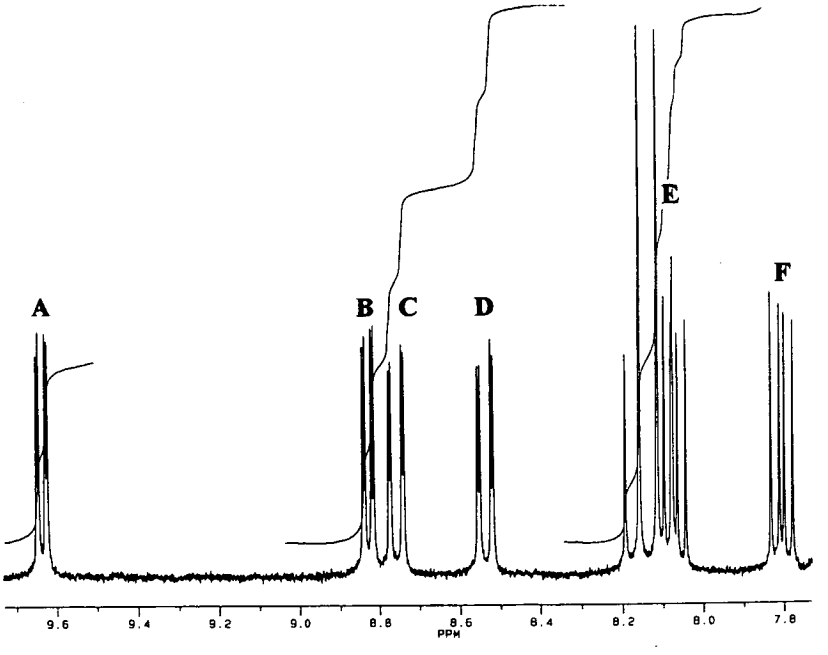

Figure 3.4.2: The ^1H NMR of $Ru_5C(CO)_{14}$(phen) **25** run in d_6-acetone.

Resonance	δ/ppm	Proton
A, B	9.64, 8.83	H_1 / H_{10}
C, D	8.76, 8.54	H_3 / H_8
E	8.13	H_5, H_6
E, F	7.80, 8.06	H_2 / H_9

Table 3.4.2: Table of proton assignments of $Ru_5C(CO)_{14}$(phen) **25**.

Characterisation of $Ru_5(\mu\text{-}H)C(CO)_{13}(C_{12}H_7N_2)$ 26

From the carbonyl IR spectrum of the minor reaction product **26**, it was evident that an analogous species to the *ortho*metallated bipyridyl product **24** had been formed. Its formulation as $Ru_5(\mu\text{-}H)C(CO)_{13}(C_{12}H_7N_2)$ (Figure 3.4.5) was further corroborated by the mass spectrum which showed a strong molecular ion peak at 1061 (calc. 1060) amu followed by the stepwise loss of several carbonyls. Attempts to grow crystals suitable for X-ray diffraction have proven unsuccessful, and hence the structure presented in the figure below is based on spectroscopic evidence alone.

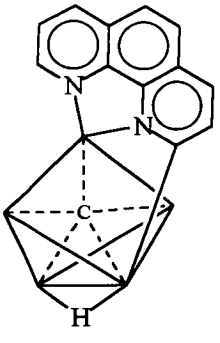

26

Figure 3.4.5: The proposed structure of the cluster $Ru_5(\mu\text{-}H)C(CO)_{13}(C_{12}H_7N_2)$ **26**.

The reaction between $Ru_5C(CO)_{15}$ **17** and phenanthroline was repeated using only 1.1 equivalent of Me_3NO to see whether this affected the resulting products. It was found that as observed previously with the bipyridyl ligand, the same products are formed, and the relative yield of $Ru_5C(CO)_{14}$(phen) **25** was increased whilst the yield of the *ortho*metallated derivative **26** was reduced.

3.5 Photolysis of $Ru_5C(CO)_{14}$(bipy) and $Ru_5C(CO)_{14}$(phen)

The clusters $Ru_5C(CO)_{14}$(bipy) **23** and $Ru_5C(CO)_{14}$(phen) **25** were irradiated both in solution and also as samples embedded in a thin polymethylmethacrylate (PMMA) film. The aim of the photolysis reaction was to attempt to remove a

carbonyl ligand from the cluster and cause the subsequent bond formation to yield a square base pyramidal cluster. However, it was observed that after eight hours irradiation of the film there was no apparent change as monitored by IR spectroscopy. Likewise irradiation in solution proved unsuccessful resulting in product decomposition only. It is suggested that the square based pyramidal compound is not formed as a result of the steric hindrance which would be incurred in attempting to bring the two relevant metal atoms close enough to bond.

3.6 Reaction of $Ru_6C(CO)_{17}$ with 2,2'-Bipyridyl and 1,10-Phenanthroline

The reaction between $Ru_6C(CO)_{17}$ **27** and the 2,2'-bipyridyl or 1,10-phenanthroline ligand was carried out using 2.2 equivalents of Me_3NO at -78 °C in an analogous manner to that described previously for the $Ru_5C(CO)_{15}$ cluster. The resulting dark red/brown solution was separated by tlc using hexane: dichloromethane (1:1 v/v) as eluent. It was found to be necessary to allow the solvent front to run to almost the top of the plate to permit the gradual separation of the two very closely spaced bands, which were orange/yellow and deep red in colour and were present in approximately similar quantities.

Characterisation of the 2,2'-Bipyridyl Derivatives

The IR carbonyl spectrum of the orange band was found to be identical to the spectrum recorded for the $Ru_5C(CO)_{14}$(bipy) cluster **23**, although this was only realised in hindsight because its formation was unexpected. The confirmation of its identity was completed by a) mass spectrometry, which showed the parent ion peak at 1065 (calc. 1065) amu; and b) by X-ray diffraction which showed an isomorphous crystal structure to $Ru_5C(CO)_{14}$(bipy) **23**.

Thus it would appear that the $Ru_6C(CO)_{17}$ cluster has undergone an unexpected degradative elimination reaction under mild conditions, with the resultant loss of an $Ru(CO)_3$ unit. This is in stark contrast to the forcing conditions required to

convert the $Ru_6C(CO)_{17}$ cluster into $Ru_5C(CO)_{15}$ in the autoclave reaction (90 °C, 70 atm CO, 3.5 hours).

The second product isolated from the reaction mixture was a red cluster whose IR spectrum clearly showed the presence of terminal carbonyls and possibly a bridging carbonyl, although this feature was somewhat weak and broad. From the IR pattern and its colour it was immediately apparent that the product was not the *ortho*metallated $Ru_5(\mu\text{-}H)C(CO)_{13}(C_{10}H_7N_2)$ cluster **24**. It was instead assigned as the expected product $Ru_6C(CO)_{15}$(bipy) **28** (Scheme 3.6.1) on the basis of its mass spectrum. The sample was found to be somewhat unstable and decomposed over time to an insoluble black solid.

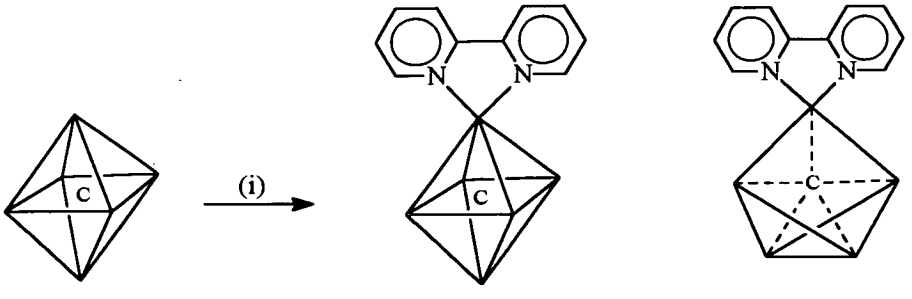

27 **28** **23**

Scheme 3.6.1: Reaction of $Ru_6C(CO)_{17}$ **27** with (i) 2,2'-bipyridyl at -78 °C in the presence of 2.2 equivalents of Me_3NO to form $Ru_5C(CO)_{14}$(bipy) **23** and $Ru_6C(CO)_{15}$(bipy) **28**.

Characterisation of the 1,10-Phenanthroline Derivatives

On the basis of the IR carbonyl pattern the identity of the orange/yellow product was inferred as $Ru_5C(CO)_{14}$(phen) **25**, and this was backed up by the ^1H NMR spectrum. The mass spectrum showed the molecular ion peak at 1092 (calc. 1089) amu followed by the subsequent loss of carbonyl ligands. Single crystals were

grown, and although a full refinement of the structure was not performed, sufficient refinement was carried out to confirm that they were isostructural to $Ru_5C(CO)_{14}$(phen) crystals grown previously.

The similarity in the IR spectrum of the second red product **29**, to the previously determined $Ru_6C(CO)_{15}$(bipy) derivative **28,** implied that an analogous species had been formed which was formulated as $Ru_6C(CO)_{15}$(phen) **29**. Its ^1H NMR spectrum confirmed the presence of the ligand but was somewhat weak owing to the cluster's instability.

3.7 Conclusions

The results of our research into the reactivity of the $Ru_5C(CO)_{15}$ and $Ru_6C(CO)_{17}$ clusters with bidentate nitrogen heterocycles (L-L) has given rise to some rather interesting chemistry. It has been shown that both clusters undergo facile bond cleavage under mild reaction conditions to produce the bridged butterfly cluster $Ru_5C(CO)_{14}$(L-L). For $Ru_6C(CO)_{17}$ this requires in addition the elimination of a metal carbonyl fragment. And it has been shown by NMR studies that the ligand's proton environments become inequivalent on co-ordination to the $Ru_5C(CO)_{14}$ unit. This has been rationalised by the change in the magnetic environments of the two "pyridine" ring's protons due to differences in their proximity to the carbonyl ligands of the cluster. Although the relative yield of this product was found to be much greater from the reaction with the $Ru_5C(CO)_{15}$ cluster **17** the secondary product of the reactions was however found to differ. In the preparation involving cluster **17**, the products were characterised as the *ortho*metallated bridged butterfly derivatives $Ru_5(\mu\text{-H})C(CO)_{13}$(L-L') (L-L'= ligand -H), which were apparently favoured to the alternative square based pyramidal (74 e) $Ru_5C(CO)_{13}$(L-L) cluster because of the steric crowding which would result between the heterocycle and the carbonyl ligands. The $Ru_6C(CO)_{17}$ cluster **27** was found to form the expected product $Ru_6C(CO)_{15}$(L-L) on the basis of spectroscopic results, and was proposed to show the ligand bound to the apical ruthenium atom. It was however found to decompose readily.

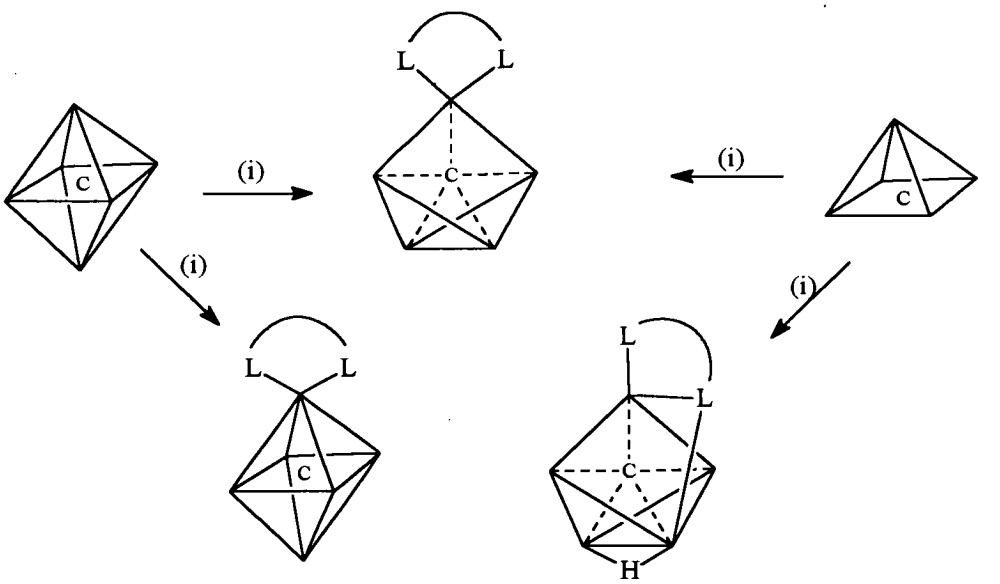

Scheme 3.7.1: The reactivity of $Ru_5C(CO)_{15}$ and $Ru_6C(CO)_{17}$ with (i) 2.2 equivalents of Me_3NO at -78 °C with the bidentate ligands (L-L) 2,2'-bipyridyl and 1,10-phenanthroline.

3.8 References

1. C.R. Eady, B.F.G. Johnson, J. Lewis, T. Matheson, *J. Organomet. Chem.*, 1973, **57**, C 82.
2. D.H. Farrar, P.F. Jackson, B.F.G. Johnson, J. Lewis, J.N. Nicholls, *J. Chem. Soc., Chem. Commun.*, 1981, 415.
3. B.F.G. Johnson, J. Lewis, J.N. Nicholls, I.A. Oxton, P.R. Raithby, M.J. Rosales, *J. Chem. Soc., Chem. Commun.*, 1982, 289.
4. a) K. Wade, *J. Chem. Soc., Chem. Commun.*, 1971, 792; b) K. Wade, *Inorg. Nucl. Lett.*, 1972, **8**, 559; c) R.E. Williams, *Inorg. Chem.*, 1971, **10**, 210; d) D.M.P. Mingos, *Nature (London), Phys. Sci.*, 1972, **236**, 99; e) D.M.P. Mingos, *Acc Chem. Res.*, 1984, **17**, 311.
5. P.F. Jackson, B.F.G. Johnson, J. Lewis, J.N. Nicholls, *J. Chem. Soc., Chem. Commun.*, 1980, 564.
6. B.F.G. Johnson, J. Lewis, J.N. Nicholls, J. Puga, P.R. Raithby, M.J. Rosales, M. McPartlin, W.Clegg, *J. Chem. Soc., Dalton Trans.*, 1983, 277.
7. G. Conole, M. McPartlin, H.R. Powell, T. Dutton, B.F.G. Johnson, J. Lewis, *J. Organomet. Chem.*, 1989, **379**, C 1.
8. T. Dutton, Ph.D Thesis, University of Cambridge, 1989.
9. D. Braga, F. Grepioni, P. Sabatino, P.J. Dyson, B.F.G. Johnson, J. Lewis, P.J. Bailey, P.R. Raithby, D. Stalke, *J. Chem. Soc., Dalton Trans.*, 1993, 985.
10. B.F.G. Johnson, J. Lewis, G.A. Foulds, *J. Organomet. Chem.*, 1985, **294**, 123.
11. B.F.G. Johnson, J. Lewis, J.N. Nicholls, J. Puga, K.H. Whitmire, *J. Chem. Soc., Dalton Trans.*, 1983, 787.
12. A.G. Cowie, B.F.G. Johnson, J. Lewis, J.N. Nicholls, P.R. Raithby, M.J. Rosales, *J. Chem. Soc., Dalton Trans.*, 1983, 2311.
13. A. Sirigu, M. Bianchi, E. Benedetti, *J. Chem. Soc., Chem. Commun.*, 1969, 596.

Chapter Four

Electrochemical, Spectroelectrochemical and UV/Vis Studies on the $Ru_4(\mu\text{-}H)_4(CO)_{10}$(L-L) Clusters (L-L= η^2- Nitrogen Heterocycle)

4.1 Introduction

Earlier electrochemical studies of metal carbonyl clusters have focused primarily on the redox behaviour of the parent clusters $M_3(CO)_{12}$ (M= Ru, [1-4] Os [2]) and their phosphine derivatives, [2,4] although both $Ru_6C(CO)_{17}$ [5] and more recently $Ru_4(\mu\text{-}H)_4(CO)_{12}$ [6] have been reported.

Hartl's group in Amsterdam were the first to investigate the redox and electronic spectroscopic properties of the nitrogen heterocyclic ligands (L-L) 2,2'-bipyridyl, 2,3-*bis*(2-pyridyl)pyrazine, and 2,2'-bipyrimidine bound to the $Os_3(CO)_{12}$ cluster as the $Os_3(CO)_{10}$(L-L) derivatives. [7] In their studies they proposed that a one electron reduction of the cluster was followed by homolytic bond cleavage and subsequent electron transfer to produce zwitterionic species of the formula $Os^-(CO)_4$-$Os(CO)_4$-$Os^+(CO)_2$(L-L), whereas the $Os_3(CO)_{10}$(bpm)$Re(CO)_3Br$ cluster was found to undergo a one electron reduction to form a stable radical anion at room temperature.

Herein we wish to describe the research carried out during our investigation, and that of our collaborators in Amsterdam, into the electrochemistry and UV/Vis spectroscopy of the series of $Ru_4(\mu\text{-}H)_4(CO)_{10}$(L-L) clusters previously discussed in Chapter Two of this thesis, and the subsequent studies into the nature of the reduced species.

4.2 Basic Theory and Principles of Electronic Spectroscopy

The chemistry of metal complexes involving co-ordination of the nitrogen heterocyclic ligands described have been well documented, and it is known that these species possess empty low-lying π^* anti-bonding orbitals. Thus the electronic

transitions induced by UV and visible photons results in either (i) the promotion of an electron from a metal-based orbital to the π^* orbital, a Metal to Ligand Charge Transfer (MLCT), or (ii) an internal ligand based $\pi \rightarrow \pi^*$ transition, or finally (iii) an internal d→d transition between the metal based core orbitals, all of which are shown schematically in Figure 4.2.1. The energy gap between the π and π^* levels of the ligand is somewhat greater than between the metal d and π^* orbitals, and consequently results in a higher energy transition. Typically MLCT bands are observed around 20,000 cm^{-1} whilst $\pi \rightarrow \pi^*$ bands are observed in the region 30-40,000 cm^{-1}. Internal metal based transitions between the d orbitals are usually too weak to be observed in the spectra of transition metal complexes. This is a consequence of the selection rules which govern the electronic transitions: the spin selection rule (there can be no change in the overall spin, $\Delta S = 0$), and the Laporte selection rule (transitions are allowed only between orbitals of different parity, for example g↔u allowed but g↔g is forbidden. Thus, a transition between a t_{2g} and an e_g level would be Laporte forbidden). However neither of these rules appear to be broken for the clusters discussed herein for which the d orbitals are fully delocalised. Consequently Ru_4 core based transitions are relatively intense (*ca.* 10,000 cm^{-1}).

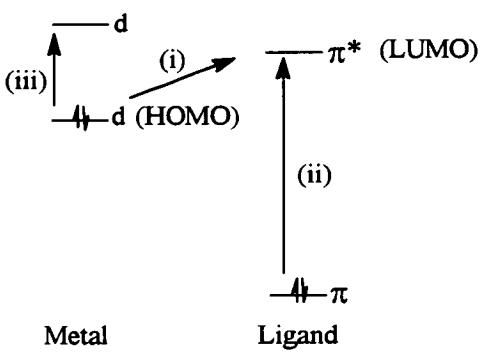

Figure 4.2.1: Schematic representation of (i) MLCT, (ii) $\pi \rightarrow \pi^*$, and (iii) internal d→d electronic transitions in metal complexes.

The intensity of the bands are often quoted in terms of the molar extinction (ε) which is related to the absorption by the Beer Lambert Law:

$$\log\left(\frac{I_o}{I_t}\right) = A = \varepsilon cl$$

I_o= intensity of incident light
I_t= intensity of transmitted light
A= absorbance
ε= molar extinction coefficient / $moldm^{-3}cm^{-1}$
c= concentration of solution / $moldm^{-3}$
l= path length (width of spectral cell) / cm

Equation 4.2.1: The Beer Lambert Law.

The magnitude of ε for the bands is a guide to the interpretation of the electronic transition to which they correspond. A value of less than one typifies a spin forbidden transition, whilst Laporte forbidden d→d transitions show values of between 20-25 $moldm^{-3}cm^{-1}$ respectively. Both spin allowed MLCT and $\pi \rightarrow \pi^*$ transitions typically show values of ε between 1000-50,000 $moldm^{-3}cm^{-1}$. Laporte allowed transitions are of the order of 250 $moldm^{-3}cm^{-1}$. However, although such UV/Vis spectroscopic studies give an insight into the nature of the frontier molecular orbitals, the HOMO and the LUMO, further electrochemical studies are required to understand these system more fully.

4.3 Electrochemistry

The redox potentials were recorded using a three electrode set up, which consisted of a working electrode, a counter electrode and a reference electrode (Figure 4.3.1). The electrochemical response of the system was measured using the technique of cyclic voltammetry. In this technique the potential was increased linearly with time until the ultimate switching potential was achieved, and then the process was reversed to return to the starting potential. The current response was measured as a function of the ramped potential. Because of the very small surface presented to the solution under investigation by the platinum microelectrode used, only minute amounts of products were reduced or oxidised in any one experiment, and so it was

possible to record an electrochemical trace several times over, providing the solution was stirred in between recording times to ensure that the electrode surface was clean. The current response was measured between the counter electrode, a large surface area platinum electrode, and the working electrode. The reference electrode was used to measure the actual potential of the working electrode and was measured against an accepted standard. In these experiments the reference electrode was a Ag|AgCl electrode against which the ferrocene|ferrocinium couple measured + 0.55 V.

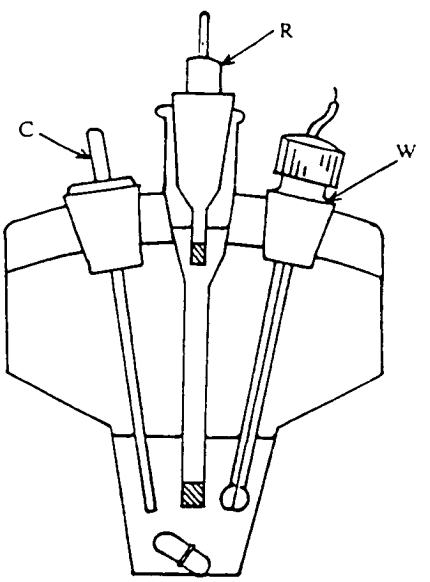

Figure 4.3.1: Diagrammatic representation of the electrochemical cell.
C: counter electrode; W: working electrode; R: reference electrode.

All of the redox processes discussed below are one electron processes and are described as being either a) chemically irreversible *i.e.* leading to the formation of a species which is unstable and undergoes chemical transformation; or b) chemically reversible, that is the redox species is stable and can be converted back to the neutral species. Furthermore, all of the processes are electrochemically reversible *i.e.* there is a rapid electron transfer between the redox species and the electrode, and no apparent geometrical change in this species as a result *e.g.* Jahn Teller distortions on reduction of octahedral d^8 systems.

4.4. Interpretation of Electrochemical and Spectroscopic Results

$Ru_4(\mu\text{-}H)_4(CO)_{12}$

An electrochemical study of the $Ru_4(\mu\text{-}H)_4(CO)_{12}$ cluster **1** showed that it undergoes reduction at -1.13 V which leads to the formation of an unidentified daughter product, and oxidation at 1.30 V, with both redox process being chemically irreversible. This is comparable to a recent report by Osella *et al.* [6] in which the daughter product has been assigned to $[Ru_4(\mu\text{-}H)_2(CO)_{12}]^{2-}$ by *in situ* IR studies. Interestingly, this cluster is postulated to form from the rapid disproportionation of the initial reduction product $[Ru_4(\mu\text{-}H)_3(CO)_{12}]^-$, to give the parent cluster $Ru_4(\mu\text{-}H)_4(CO)_{12}$ **1** and $[Ru_4(\mu\text{-}H)_2(CO)_{12}]^{2-}$ which possesses bridging carbonyl ligands.

Only a single electronic transition at 27473 cm^{-1} was observed for the parent cluster $Ru_4(\mu\text{-}H)_4(CO)_{12}$ and was assigned to an internal electronic transition between the delocalised d- orbitals of the metal core, rather than an MLCT transition to the π^* orbitals of the carbonyl ligands which would be expected to lie to very much higher energy.

$Ru_4(\mu\text{-}H)_4(CO)_{10}(py)_2$

The pyridine ligand is usually considered as electrochemically inert *i.e.* it is neither reduced nor oxidised at modest potentials, although there is evidence that it can be irreversibly reduced at very negative potentials. [8] On co-ordination of the ligand to the $Ru_4(\mu\text{-}H)_4(CO)_{12}$ cluster **1**, electrochemical studies showed that both a chemically irreversible reduction at -1.50 V and oxidation at 0.90 V are observed. Because of the inert nature of the ligand set this redox activity can only be attributed to the metal cluster core itself. This can be compared to the electrochemistry observed for the unsubstituted parent cluster which shows an oxidation process at 1.30 V and a reduction at -1.13 V. The shift of the redox process to more negative

potential on substitution of two carbonyls for two pyridines can be explained in terms of the different π accepting capabilities of these ligands. Because pyridine is a significantly poorer π acceptor in comparison to CO, the metal cluster core will show a higher electron density for $Ru_4(\mu\text{-}H)_4(CO)_{10}(py)_2$ **4** than for the parent cluster **1**. Consequently it should be easier to remove an electron and more difficult to add an electron to the substituted than the parent cluster. The pyridine derivative shows only a single band in the UV/Vis spectral region at a comparable energy to the parent cluster. It is therefore similarly assigned to an internally based electronic transition within the delocalised metal cluster orbitals, and not an MLCT transition which would require substantially higher energy. No pyridine based $\pi \rightarrow \pi^*$ transitions are observed in the spectrum, although this is thought to be a result of it being a high energy process which is masked by solvent effects.

$Ru_4(\mu\text{-}H)_4(CO)_{10}(bipy)$

The cluster $Ru_4(\mu\text{-}H)_4(CO)_{10}(bipy)$ **5** has a much richer absorption spectrum than the pyridine analogue which results from its empty low lying π^* orbital (Figure 4.4.1). Absorption bands are observed at 21,000 and 28,027 cm^{-1} with extinction coefficients of 3211 and 12,063 $mol^{-1}dm^3cm^{-1}$ respectively and are assigned as follows: the band at 28,027 cm^{-1} is attributed to the electronic transition within the Ru_4 core, and is observed at a similar energy to $Ru_4(\mu\text{-}H)_4(CO)_{10}L_2$ (L= CO, py). The band at 21,000 cm^{-1} is assigned to an MLCT transition from the Ru_4 core to the bipy π^* orbital, and this infers that the LUMO of cluster **5** is predominantly located on the bipyridyl ligand, and the HOMO on the metal core. Finally, two bipyridyl based $\pi \rightarrow \pi^*$ transition are observed at 33,200 and 36,604 cm^{-1}, highly characteristic energies for such transitions.

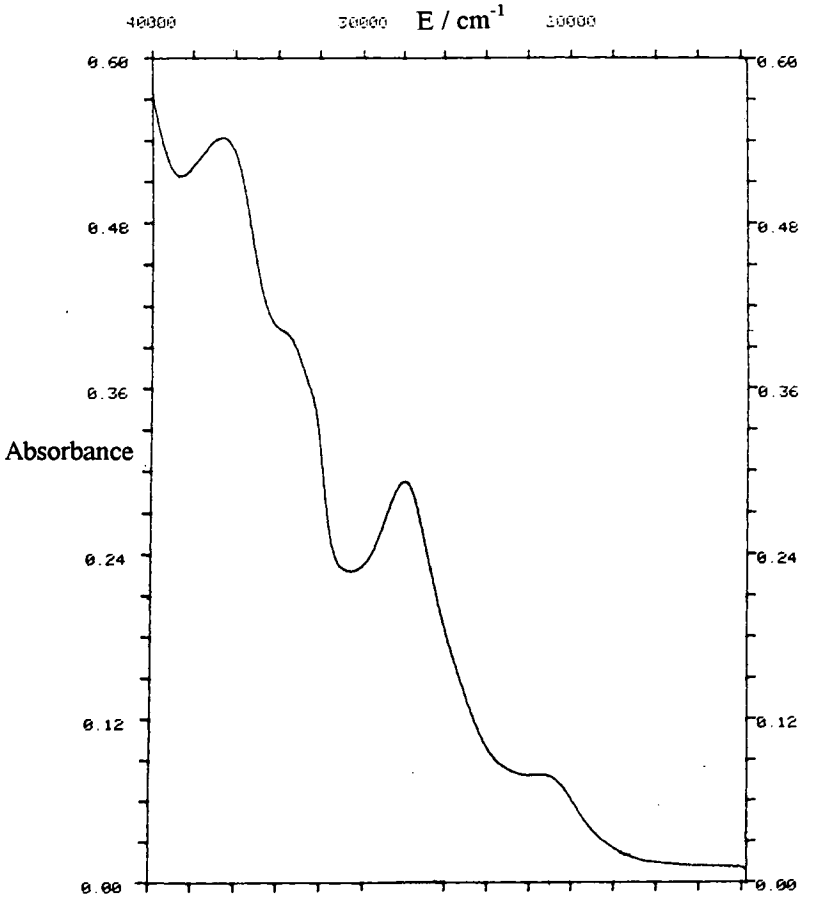

Figure 4.4.1: The UV/Vis spectrum of a 4.9 x10^{-4} M CH_2Cl_2 solution of $Ru_4(\mu\text{-}H)_4(CO)_{10}$(bipy) **5**.

Electrochemical studies carried out on the cluster at room temperature showed both the oxidation and the reduction processes to be chemically irreversible (Figure 4.4.2), and to occur at potentials of 0.77 V and -1.31 V respectively. Thus both processes occur relatively more easily than for the *bis-* pyridine derivative. Following on from the absorption spectrum assignments, it is apparent that the reduction process arises from the addition of an electron into a π^* orbital which is located predominantly on the bipyridyl ligand, whereas the oxidation process occurs on the Ru_4 core. Since bipyridyl is a better π acceptor than pyridine it would be expected that the oxidation of the metal cluster core should occur at more positive potentials than the pyridine analogue. However this was not observed experimentally, and can only be speculatively connected to the enforced geometry of the two clusters. Thus, for $Ru_4(\mu\text{-}H)_4(CO)_{10}(py)_2$ there is no constraint on the angle between the

pyridine ligands, and they will therefore take up a geometry to give the most favourable overlap between these orbitals and those on the metal, which is *ca.* 90 °. However, for the bipyridyl derivative the geometry of the ligand enforces a bite angle of 77.4 ° and hence must result in a less favourable orbital overlap, which will therefore affect its redox properties.

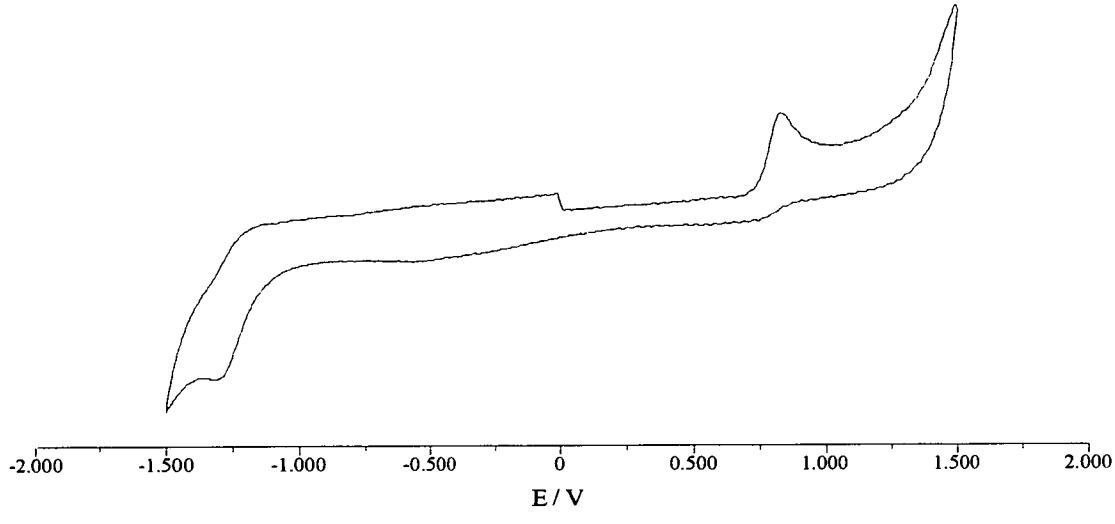

Figure 4.4.2: Cyclic voltammogram of $Ru_4(\mu\text{-}H)_4(CO)_{10}$(bipy) **5** in CH_2Cl_2 / 0.5 M [TBA][BF_4] *vs.* Ag | AgCl.

An *in situ* IR study of the reduction of the cluster was carried out at The University of Amsterdam, and it is apparent from the time resolved spectrum (Figure 4.4.3) that the reduced cluster $[Ru_4(\mu\text{-}H)_4(CO)_{10}(bipy)]^{-\bullet}$ is so unstable that it is not detected. Instead only its transformation to an unidentified species which shows the presence of both terminal and bridging carbonyl ligands is observed. It is tentatively suggested that reduction of the cluster may lead to the loss of hydride ligands and their replacement with bridging carbonyls by comparison with Osella's work on the parent cluster. [6] The almost silent EPR spectrum of the reduced cluster indicates that the final product is not a radical, although the presence of an extremely low concentration of a radical was just detectable.

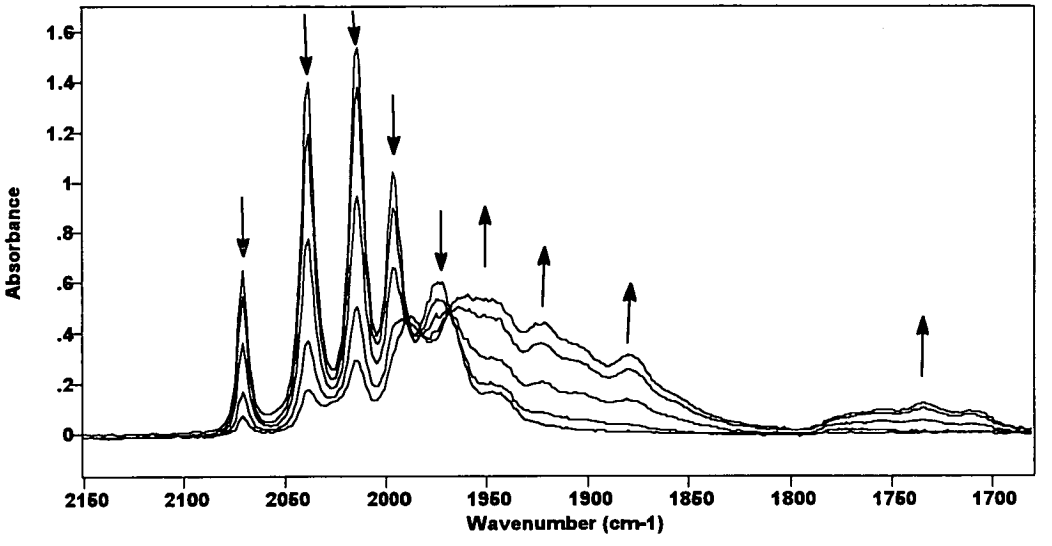

Figure 4.4.3: The *in situ* IR spectra of the reduction of a THF solution of $Ru_4(\mu\text{-}H)_4(CO)_{10}$(bipy) at 293 K.

Cluster	ν (CO) [a] / cm^{-1}
$Ru_4(\mu\text{-}H)_4(CO)_{10}$(bipy)	2071 (m), 2039 (vs), 2015 (vs), 1996 (s), 1974 (m), 1947 (sh).
"$Ru_4(\mu\text{-}H)_4(CO)_{10}$(bipy)$^{-\bullet}$"	2071 (w),[b] 2038 (m),[b] 2015 (m),[b] 1988 (s), 1956 (vs,br), 1923 (s), 1950 (sh), 1880 (m/s), 1735 (w, br).

[a] Measured at 293 K in THF. [b] Peaks associated with the unreduced cluster.

$Ru_4(\mu\text{-}H)_4(CO)_{10}$(phen)

Despite the increased conjugation in the 1,10-phenanthroline ring in comparison with 2,2'- bipyridyl, previous studies [9] have shown that there is little difference in the energy of the π orbitals (HOMO) of the two, and consequently complexes of both ligands show some very similar electrochemical and spectrochemical properties. The two lower energy transitions at 21,400 and

28,091cm^{-1} clearly result from a) an MLCT transition involving the excitation of an electron from a Ru_4 core orbital to a phenathroline π^* orbital, and b) an internal d→d transition based on the metal core respectively. These transitions are comparable in energy to those observed for the bipyridyl substituted cluster. The phenanthroline based $\pi \rightarrow \pi^*$ transitions are observed at 37,204 and 39,600 cm^{-1}, on average 5000 cm^{-1} higher in energy than the bipyridyl transition.

An electrochemical study showed both the oxidation and reduction of the cluster to be chemically irreversible and to occur at potentials of 0.78 V, and -1.33 V respectively, which are very similar to the bipyridyl analogue (Table 4.5.1).

$Ru_4(\mu\text{-}H)_4(CO)_{10}(dmp)$

The introduction of two methyl groups into the 2 and 9 positions of the phenanthroline ring, adjacent to the nitrogen atoms, results in an increase in the electron density on the ring *via* an inductive effect by the methyl groups. Consequently, reduction of the compound becomes more difficult, and can be considered as resulting from an increase in electronic repulsion. This is borne out by experiment which shows a chemically irreversible reduction at -1.41 V *cf.* -1.33 V for the phenanthroline derivative. Oxidation is chemically irreversible at room temperature and occurs at 0.77 V, which is not so different to the phenanthroline derivative (0.78 V), and therefore indicates that it must be occurring at the Ru_4 core.

Its UV/Vis spectrum shows a familiar pattern, with the bands arising at 21,500 and 27,871 cm^{-1} being assigned to the MLCT d→π^* and d→d transitions respectively, and the $\pi \rightarrow \pi^*$ transition based on the heterocyclic ligand arising at 35,921 cm^{-1}.

$Ru_4(\mu\text{-}H)_4(CO)_{10}(bpm)$

Electrochemical studies on the $Ru_4(\mu\text{-}H)_4(CO)_{10}$(bpm) derivative 9 again showed a chemically irreversible oxidation at 0.82 V, but a chemically reversible reduction at -0.89 V (Figure 4.4.4). This redox activity is due to a) oxidation of the

metal cluster core; and b) reduction of the bipyrimidine ligand. The chemical reversibility of the reduced cluster implies that it is a relatively stable species.

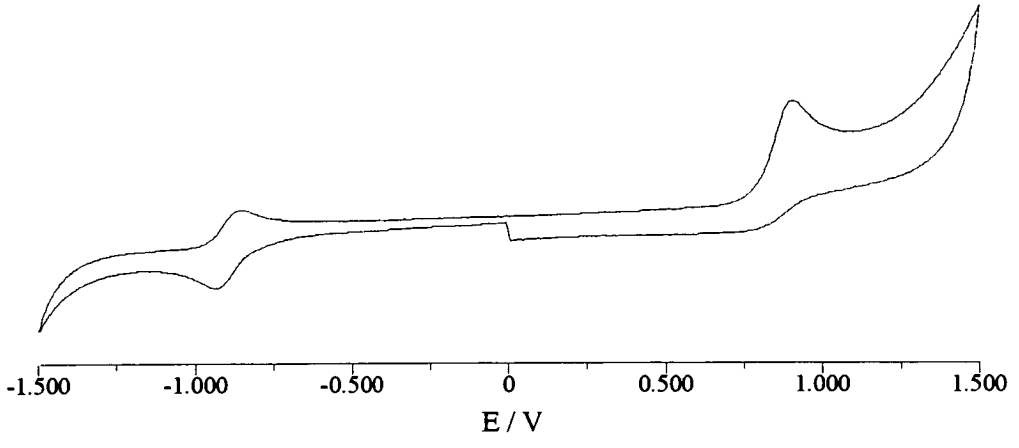

Figure 4.4.4: Cyclic voltammogram of $Ru_4(\mu\text{-}H)_4(CO)_{10}(bpm)$ **9** in CH_2Cl_2 / 0.5M [TBA][BF_4] *vs.* Ag | AgCl.

This stability has been confirmed by an *in situ* IR study of the reduction process, carried out at The University of Amsterdam. The spectral changes are presented in Figure 4.4.5 and clearly show the collapse of the carbonyl bands arising from compound **9** and the simultaneous growth of similar bands to lower energy. This is consistent with the formation of the stable radical anion $[Ru_4(\mu\text{-}H)_4(CO)_{10}(bpm)]^{-\bullet}$, and the presence of the clearly observable isobestic points in the spectrum implies that there is a simple conversion between the redox pairs. The similarity in the spectra of the parent and the radical anion indicate that the structure of the cluster is unaffected by reduction. It is shifted by *ca.* 8 cm^{-1} to lower energy because of an increase in π back bonding from the metal centre to the carbonyl ligands, and this in turn is a result of the increased charge donation from the $(bpm)^{-\bullet}$ radical anion to the metal atom. This behaviour is analogous to that reported by van Outersterp [7] for the $Os_3(CO)_{10}(L\text{-}L)$ clusters (L-L= bpm, dpp, dpb, and bipy).

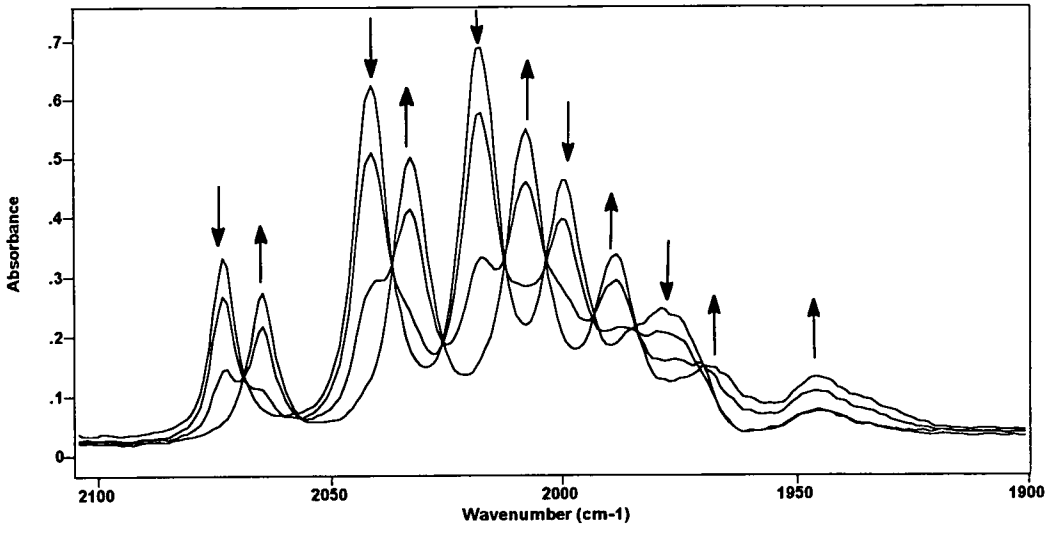

Figure 4.4.5: The *in situ* IR spectra of the reduction of a THF solution of $Ru_4(\mu\text{-}H)_4(CO)_{10}(bpm)$ **9** at 293 K.

Cluster	ν (CO) [a] / cm^{-1}
$Ru_4(\mu\text{-}H)_4(CO)_{10}(bpm)$	2073 (m), 2042 (s), 2018 (s), 2000 (m), 1979 (m), 1945 (w).
$Ru_4(\mu\text{-}H)_4(CO)_{10}(bpm)^{-\bullet}$	2065 (m), 2033 (s), 2008 (s), 1989 (m), 1970 (w), 1945 (w), 1905 (w,sh), 1771 (w, v br).

[a] Measured at 293 K in THF.

The radical anion shows a very gradual decomposition over time to an unidentified product. The intensity of all of the carbonyl IR bands associated with the neutral cluster decrease and a very broad band begins to grow at *ca.* 1905.5 and also a broad band at 1771 cm^{-1} (not shown) which is indicative of a bridging carbonyl ligand. These bands lie to higher energy than the $[Ru_4(\mu\text{-}H)_2(CO)_{12}]^{2-}$ dianion discussed earlier and therefore do not seem to result from a bipyrimidine analogue. Substitution of two carbonyl ligands for a bipyrimidine should result in a lowering of the carbonyl frequencies as a direct result of the greater electron donation from the bipyrimidine to

the metal and subsequent increased π back donation. What the exact nature of the product is, remains open to speculation.

The EPR spectrum of the radical anion has a total spectral width of 200 G and shows hyperfine structure which results from coupling to the nitrogen and also probably to the protons on the ligand (Figure 4.4.6). No attempts have been made to simulate the spectrum due to lack of time, and consequently individual couplings cannot be stated. The magnitude of the g value is 2.0016 which is comparable to the free electron value, g_e (2.0023), and hence indicates that the unpaired electron is predominantly ligand based, in agreement with both the electrochemical and UV/Vis spectroscopic studies which are now discussed.

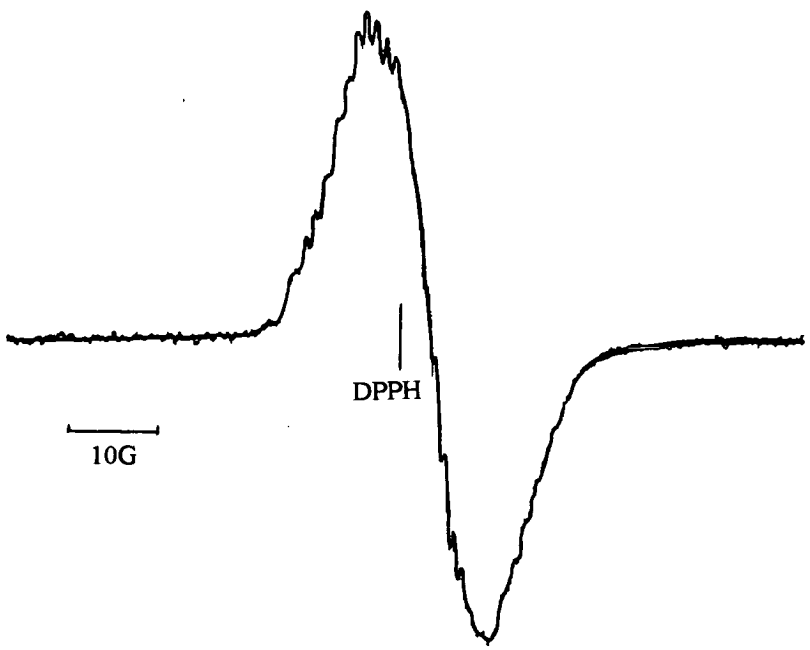

Figure 4.4.6: The EPR spectrum of $[Ru_4(\mu\text{-}H)_4(CO)_{10}(bpm)]^{-\bullet}$ recorded in THF at 293 K, *vs.* DPPH as the internal standard (95G).

The electrochemical studies show that the cluster's reduction is shifted by several hundred mV less negative relative to the bipyridyl derivative. This results from the lower energy of the π^* orbital of bipyrimidine which makes reduction easier. It can also be thought of as adding further electron sinks (nitrogen sites) which will accept extra electron density more readily. Oxidation occurs at 0.85 V and implies that the Ru_4 based HOMO lies at a slightly lower energy than for the bipyridyl

to lower energy relative to the neutral cluster. Additional bands at 1935, 1890 and *ca.* 1723 (br) cm^{-1} are seen to grow which do not seem to be assignable to the radical anion, and may be an indication of the formation of a breakdown product possessing bridging carbonyl ligands. The position of these bands is somewhat different to those observed for the bipyrimidine derivative and so imply the formation of an unrelated product.

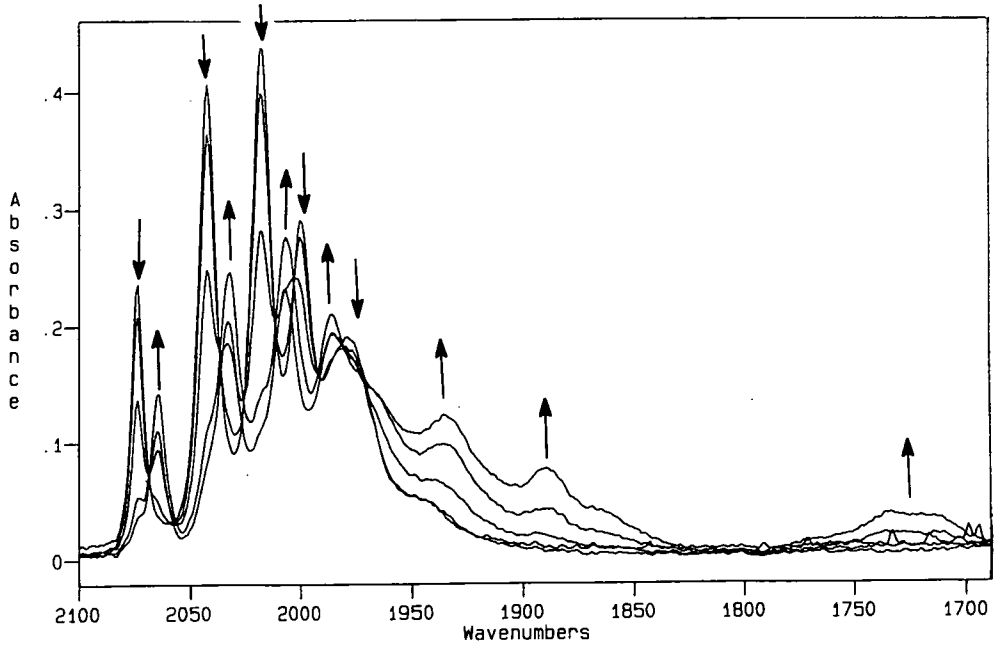

Figure 4.4.7: The *in situ* IR spectra of the reduction of a CH_2Cl_2 solution of $Ru_4(\mu\text{-}H)_4(CO)_{10}(bpp)$ **10** at 293 K.

Cluster	ν (CO) [a] / cm^{-1}
$Ru_4(\mu\text{-}H)_4(CO)_{10}(bpp)$	2074 (m), 2043 (s), 2018 (s), 2000 (m), 1980 (m).
$Ru_4(\mu\text{-}H)_4(CO)_{10}(bpp)^{-\bullet}$	2064 (m), 2033 (s), 2007 (s), 1985 (m), 1935 (m), 1890 (w), 1723 (w, v br).

[a] Measured at 293 K in CH_2Cl_2.

On repeating the experiment at -50 °C, again in dichloromethane, no bridging carbonyl bands were observed on reduction and the reduction was shown to be fully chemically reversible by the reformation of the carbonyl bands associated with the neutral cluster on oxidation. Furthermore, the broad band centred at 1935 cm^{-1} was

analogue thus making removal of the electron more difficult. Presumably this is a reflection of the increased π accepting capabilities of bipyrimidine compared to bipyridyl.

The compound shows only two electronic transitions: an MLCT at 20,200 cm^{-1}, assignable to a $d\rightarrow\pi^*$ transition, and a transition at 27,871 cm^{-1} which is attributed to an internally based Ru_4 $d\rightarrow d$ excitation because of its similarity in energy to the band observed for the parent cluster $Ru_4(\mu\text{-}H)_4(CO)_{12}$. The assignment of the band at 20,200 cm^{-1} to a $d\rightarrow\pi^*$ transition is consistent with the lowering in energy of the bipyrimidine's π^* orbital as inferred from the electrochemistry, and is lower in energy than all of the previously discussed MLCT transitions of the other cluster derivatives. It can only be tentatively suggested that no apparent $\pi\rightarrow\pi^*$ transition is observed because it lies at such high energy that it is therefore obscured by the solvent band's absorption.

$Ru_4(\mu\text{-}H)_4(CO)_{10}(bpp)$

Although both bipyrimidine and 2,3-*bis*(2-pyridyl)pyrazine (bpp) have four nitrogen sites, the latter has an increased delocalisation of its π system through three rather than two rings and hence is more stable *i.e.* its orbitals lie lower in energy. Therefore, oxidation is a little more difficult, as shown by the chemically irreversible electron loss at 0.90 V, assigned to the removal of an electron from the Ru_4 core, and by the chemically reversible reduction at -0.92 V on an orbital predominantly located on the bpp ligand. These shifts are not substantial and indicate that the effect is relatively minor in comparison with these two ligands, but is more significant when compared to the other ligands (Table 4.5.1).

One electron reduction of the ligand has again been shown to lead to the formation of a comparatively stable radical anion, $[Ru_4(\mu\text{-}H)_4(CO)_{10}(bpp)]^{-\bullet}$. Its reduction was followed by *in situ* IR at room temperature (Figure 4.4.7), and clearly shows the gradual formation of the radical anion whose carbonyl bands lie *ca.* 10 cm^{-1}

observed and can therefore be assigned to the radical anion and not the breakdown product as had been previously thought.

The EPR spectrum of the radical anion of the cluster is presented in Figure 4.4.8 below. The hyperfine structure shows twelve lines with an average splitting of 4.25 G which may result from coupling to the four nitrogens. No attempts have been made to simulate the spectrum owing to a lack of time, however the splitting pattern has been tentatively proposed to result from coupling to all four nitrogen sites on the ligand. The magnitude of the g value, 2.0015, is almost identical to that observed for the bipyrimidine derivative, and again implies that the unpaired electron is predominantly ligand based, in line with the observed electrochemistry.

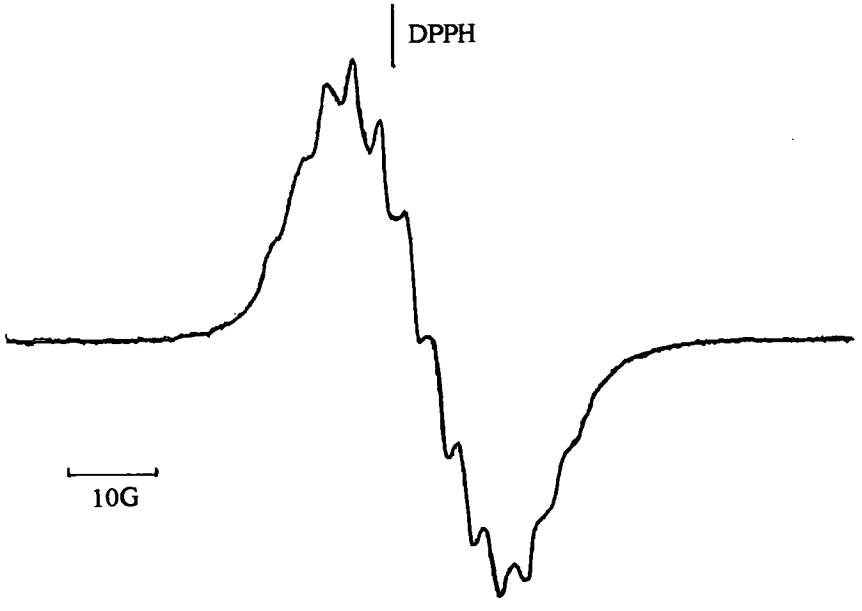

Figure 4.4.8: The EPR spectrum of $[Ru_4(\mu\text{-}H)_4(CO)_{10}(bpp)]^{-\bullet}$ recorded in THF at 293 K, *vs.* DPPH as the internal standard (95G).

The UV/Vis spectrum of the neutral cluster shows an MLCT at 19,493 cm^{-1} which arises from the $d\rightarrow\pi^*$ transition, and is lower in energy than the bipyrimidine analogue because of the lowering in energy of the π_{bpp}^* orbital as discussed above. The band at 28,011 cm^{-1} is assigned to a d→d orbital based transition within the Ru_4 core, whilst the remaining transition at 36,232 cm^{-1} is assigned to a $\pi\rightarrow\pi^*$ transition

on the bpp ligand. Thus, the LUMO of the cluster is the ligand based π^* orbital, in agreement with the EPR data.

Interpretation of OTTLE Studies

To further confirm that the reduction process above is indeed ligand rather than cluster based, *in situ* UV/Vis measurements were carried out on the bipyrimidine derivative whilst the cluster was reduced by means of an OTTLE cell. The experiment was carried out at -20 °C to minimise any possibility of side reactions occurring. The time resolved spectrum of this reduction process is shown in Figure 4.4.8. The observed spectral changes can all be rationalised by the electronic structure of the cluster proposed earlier. Thus the absorption at 27,871 cm^{-1} assigned to a transition within the Ru_4 core on the neutral cluster can still be observed at approximately the same energy in the reduced cluster. The visible region of the spectrum undergoes a dramatic change on reduction, as the broad and featureless MLCT band is replaced by two sharp absorptions and a weak, broad absorption grows in at very low energy. These sharp bands result from intraligand transitions of the reduced bipyrimidine ligand on the basis of comparative studies of similar reduced ligands. The reduced cluster should therefore be formulated as $[Ru_4(\mu\text{-}H)_4(CO)_{10}(bpm^{-\bullet})]^{-\bullet}$ in which the added electron is based primarily in a low lying π^* ligand orbital.

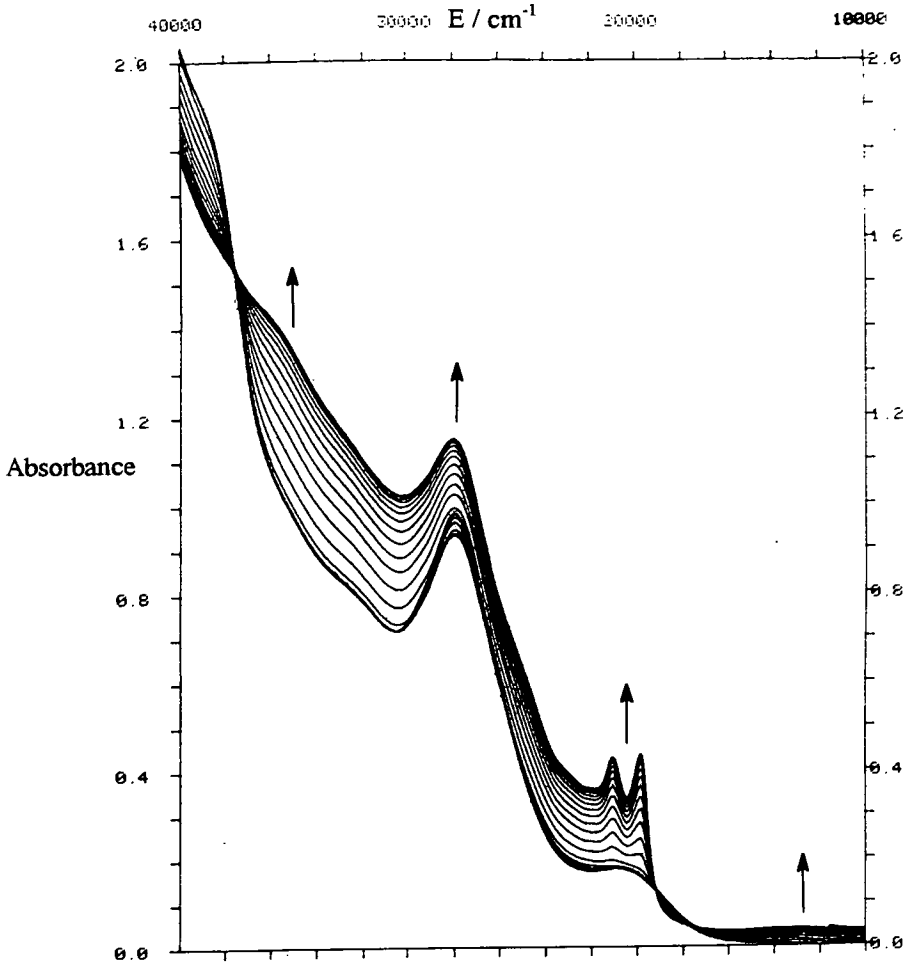

Figure 4.4.8: The *in situ* UV/Vis spectra on reduction of $Ru_4(\mu\text{-}H)_4(CO)_{10}$(bpm) at 253 K.

The chemical reversibility of this radical anion was confirmed by the reproduction of the neutral cluster's spectrum on reoxidation. Had the reduction involved metal based orbitals, such large changes in the electronic spectrum would not have been observed. The growth of analogous bands was observed during the chemically reversible reduction of the dpp derivative, however these were rather broad and featureless in comparison.

4.5 Conclusions and Summary of Results

The comparative electrochemical and UV/Vis absorption spectral studies of the disubstituted $Ru_4(\mu\text{-}H)_4(CO)_{10}(L\text{-}L)$ clusters suggests that the HOMO is predominantly located on the Ru_4 metal core and the LUMO on the nitrogen heterocyclic ligand, with the exception of the pyridine derivative, where the LUMO is thought to be predominantly on the metal core. An examination of the trends in the observed electrochemistry (Table 4.5.1) reveals that bipyridyl and phenanthroline are reduced at similar potentials, which is as expected from previous studies of these ligands, whilst addition of methyl groups at the 2 and 9 positions of phenanthroline is sufficient to cause a 100 mV shift towards more negative potential. This is readily explainable on the basis of the inductive effect of the methyl groups which introduces a higher electron density into the phenanthroline ring system, therefore making it less favourable for reduction to occur. Because of the electronegative character of nitrogen, increasing the number of nitrogen sites within a ligand results in reduction being more favourable, with "excess" electron density residing on these sites. Consequently, reduction of the $Ru_4(\mu\text{-}H)_4(CO)_{10}(bpm)$ and $Ru_4(\mu\text{-}H)_4(CO)_{10}(bpp)$ clusters occurs at a somewhat less negative potential, with the latter being most easily reduced as a result of the increased conjugation between the rings. *In situ* IR studies have shown the radical anion of the bipyrimidine and bpp derivatives of the $Ru_4(\mu\text{-}H)_4(CO)_{10}(L\text{-}L)$ to be relatively stable, decomposing only slowly over time. They show a similar carbonyl IR pattern to the parent cluster but are shifted by *ca.* 10 cm^{-1} to lower energy as a result of increased π back bonding on reduction (Table 4.5.3). Their relative stability is in contrast to that found for the $Os_3(CO)_{10}(L\text{-}L)$ analogues, [7] and can be traced to two principal factors: a) higher cluster nuclearity; and b) a higher metal-metal bond connectivity for the tetrahedral *cf.* triangular cluster. The radical anion of the bipyridyl analogue was however unstable and therefore not detected. Reduction caused the cluster to decompose rapidly to an unidentified species (or perhaps several species).

Cluster [a,b]	E_{red}/V [c]	E_{ox}/V [c]
$Ru_4(\mu\text{-}H)_4(CO)_{12}$	-1.13 (irr.)	1.30 (irr.), 0.05 (irr.)[d]
$Ru_4(\mu\text{-}H)_4(CO)_{10}(py)_2$	-1.50 (irr.)	0.90 (irr.)
$Ru_4(\mu\text{-}H)_4(CO)_{10}$(bipy)	-1.31 (irr.)	0.77 (irr.)
$Ru_4(\mu\text{-}H)_4(CO)_{10}$(phen)	-1.33 (irr.)	0.78 (irr.)
$Ru_4(\mu\text{-}H)_4(CO)_{10}$(dmp)	-1.41 (irr.)	0.78 (irr.)
$Ru_4(\mu\text{-}H)_4(CO)_{10}$(bpm)	-0.89 (rev.), E_c-E_a 66 mV	0.85 (irr.)
$Ru_4(\mu\text{-}H)_4(CO)_{10}$(bpp)	-0.92 (rev.), E_c-E_a 75 mV	0.88 (irr.)

Table 4.5.1: Redox potentials for the $Ru_4(\mu\text{-}H)_4(CO)_{10}$(L-L) clusters *vs.* Ag|AgCl.

[a] Measured at 293 K. [b] Measured in CH_2Cl_2. [c] Chemical reversibility is indicated by rev. and irrev. respectively. [d] Daughter product. E_{red}= reduction potential, E_{ox}= oxidation potential, E_c= cathodic potential, E_a= anodic potential.

Cluster [a,b]	E/cm^{-1}	ε/$mol^{-1}dm^3cm^{-1}$
$Ru_4(\mu\text{-}H)_4(CO)_{12}$	27473	14605
$Ru_4(\mu\text{-}H)_4(CO)_{10}(py)_2$	27788	15062
$Ru_4(\mu\text{-}H)_4(CO)_{10}$(bipy)	21000	3211
	28027	12063
	33200	32606
$Ru_4(\mu\text{-}H)_4(CO)_{10}$(phen)	21400	2794
	28091	10522
	37204	24220
	39600	24135
$Ru_4(\mu\text{-}H)_4(CO)_{10}$(dmp)	21500	4695
	27871	11828
	35921	27404
$Ru_4(\mu\text{-}H)_4(CO)_{10}$(bpm)	20200	3350
	27871	13672
$Ru_4(\mu\text{-}H)_4(CO)_{10}$(bpp)	19493	3641
	28011	15461
	36232	26708

Table 4.5.2: Electronic spectroscopic data, showing the energy of the electronic transitions (E/ cm^{-1}) and their relative intensities (molar absorption coefficients, ε / $mol^{-1}dm^3cm^{-1}$).

[a] Measured at 293 K. [b] Measured in CH_2Cl_2.

Cluster	ν (CO) / cm^{-1}

Cluster	ν (CO) / cm^{-1}
$Ru_4(\mu\text{-}H)_4(CO)_{10}(bipy)$ [a]	2071 (m), 2039 (vs), 2015 (vs), 1996 (s), 1974 (m), 1947 (sh).
$Ru_4(\mu\text{-}H)_4(CO)_{10}(bipy)^{-\bullet}$ [a]	1988 (m), 1956 (m, br), 1923 (m), 1950 (m), 1880 (m), 1735 (w, ν br).
$Ru_4(\mu\text{-}H)_4(CO)_{10}(bpm)$ [a]	2073 (m), 2042 (s), 2018 (s), 2000 (m), 1979 (m), 1945 (w).
$Ru_4(\mu\text{-}H)_4(CO)_{10}(bpm)^{-\bullet}$ [a]	2065 (m), 2033 (s), 2008 (s), 1989 (m), 1970 (w), 1945 (w), 1906 (w, sh), 1771 (w, ν br).
$Ru_4(\mu\text{-}H)_4(CO)_{10}(bpp)$ [b]	2074 (m), 2043 (s), 2018 (s), 2000 (m), 1980 (m).
$Ru_4(\mu\text{-}H)_4(CO)_{10}(bpp)^{-\bullet}$ [b]	2064 (m), 2033 (s), 2007 (s), 1986 (m), 1935 (m), 1890 (w), 1723 (w, ν br).

Table 4.5.3: IR vibrational data for the reduced and neutral $Ru_4(\mu\text{-}H)_4(CO)_{10}$(L-L) clusters.

[a] Measured in THF at 293K. [b] Measured in CH_2Cl_2 at 293K.

4.6 References

1. J.C. Cyr, J.E. DeGray, D.K. Gosser, E.S. Lee, P.H. Rieger, *Organometallics*, 1985, **4**, 950.
2. A.J. Downard, B.H. Robinson, J. Simpson, *J. Organomet. Chem.*, 1987, **320**, 363.
3. J.E. Cyr, P.H. Rieger, *Organometallics*, 1991, **10**, 2153.
4. D. Osella, J. Hanzlik, *Inorg. Chim. Acta*, 1993, **213**, 311.
5. S.R. Drake, B.F.G. Johnson, J. Lewis, *Dalton Trans.*, 1989, 243.
6. D. Osella, C. Nervi, M. Ravera, J. Fiedler, V.V. Strelets, *Organometallics* 1995, **14**, 2501.
7. a) J.W.M. van Outersterp, Ph.D. Thesis, Universiteit van Amsterdam, van't Hoff Research Institut, 1995; b) J.W.M. van Outersterp, F. Hartl, D.J. Stufkens, *Inorg. Chem.*, 1994, **33**, 2711.
8. L.J. Yellowlees, Ph.D. Thesis, The University of Edinburgh, 1983.
9. A.B.P. Lever, *Inorg. Elec. Spec.*, Elsevier, 1984, 211.

Chapter Five

Experimental

5.1 General Experimental Procedures and Instrumentation

Syntheses

Autoclave reactions were carried out in a magnetically stirred Burghoff (250ml) autoclave fitted with a PTFE liner to prepare $Ru_3(CO)_{12}$, $Ru_4(\mu\text{-}H)_4(CO)_{12}$,[1] $Os_4(\mu\text{-}H)_4(CO)_{12}$,[2] $Ru_5C(CO)_{15}$ and $Ru_6C(CO)_{17}$.

$Ru_3(CO)_{12}$ Preparation

The autoclave was first flushed three times with CO before a methanol solution of $RuCl_3$ hydrate (4g in 150 ml) was pressurised to 55 atm and heated for 9 hours at 125 °C to yield orange crystals of $Ru_3(CO)_{12}$ on cooling.

$Ru_5C(CO)_{15}$ Preparation

The autoclave was first flushed three times with ethylene before a heptane solution of $Ru_3(CO)_{12}$ (1g in 150 ml) was pressurised to 30 atm and heated for 3.5 hours at 145 °C to yield dark red crystals of $Ru_6C(CO)_{17}$ on cooling.

$Ru_6C(CO)_{17}$ Preparation

The autoclave was first flushed three times with CO before a heptane solution of $Ru_6C(CO)_{17}$ (1g in 50 ml) was pressurised to 70 atm and heated for 3.5 hours at 90 °C to yield the dark red cluster $Ru_5C(CO)_{15}$ which precipitates on cooling. A large amount of the cluster remains in solution and should be extracted *in vaccuo* and followed by washing with boiling hexane.

General

Trimethylamine-N-oxide dihydrate ($Me_3NO.2H_2O$), purchased from Aldrich, was carefully dried by first refluxing the sample (15 g) in benzene (250 ml), typically overnight, to remove the water of crystallisation *via* a Dean and Stark distillation. The benzene was then decanted and the sample dried under vacuum on a Schlenk line, and sublimed prior to use. Addition of Me_3NO to the reaction solutions was carried out under an atmosphere of dry nitrogen, although no strict measurements were taken to completely exclude air from the reaction systems.

Dichloromethane was dried using CaH_2 and freshly distilled prior to reaction. All other reagents were used as supplied without further purification. Pyridine, 2,2'-bipyridyl, 1,10-phenathroline, 2,3-*bis*(2-pyridyl)pyrazine, 2,9-dimethyl-1,10-phenanthroline were purchased from Aldrich, and 2,2'-bipyrimidine from Lancaster Chemicals.

Separations

All separations were achieved chromatographically on silica, on the open bench without any precautions to exclude air. Thin layer chromatography (tlc) was carried out using glass plates (20 cm x 20 cm) coated with a 0.25 cm layer of silica gel 60 F_{254}, which were supplied by Merck. Column chromatography was carried out using a 50 cm long glass column with an internal diameter of 3 cm, fitted with a 100 ml solvent reservoir, and a facility for pressurisation. 60 mesh silica was used to pack the column, and the eluents used for both column and thin layer chromatography were mixed from standard grade laboratory solvents.

Crystallisations

Single crystals of high quality were required for the collection of X-ray diffraction data and were typically grown from dichloromethane-hexane at low temperature, unless otherwise stated.

Infra-red Spectroscopy

Infra-red spectra were recorded in dichloromethane in NaCl cells (0.5 mm path length) supplied by Specac Ltd, using a Perkin-Elmer Series 1600 fourier transform instrument.

Mass Spectroscopy

Fast atom bombardment mass spectra were obtained on a Kratos MS50TC spectrometer which was run in positive mode. Samples were run as a matrix in 3- NOBA. (*meta*- nitrobenzyl alcohol)

NMR Spectroscopy

^{1}H NMR were recorded for samples in deuterated solvents on Bruker WH 200 or 250 MHz fourier transform instruments. All spectra described herein were recorded in deuterated solvents, $CDCl_3$ in most instances, and were referenced to an internal trimethylsilane (TMS) standard.

Single Crystal X-ray Diffraction Studies

Diffraction data were collected on a Stoë Stadi 4-circle diffractometer. An Oxford Cryosystems device was used for low temperature data collection. [3] The appropriate crystal data, data collection and structure refinement parameters are presented in the text, and full crystallographic listings are given in the appendices. All refinements were carried out using the crystallographic program SHELXL 93, [4] and all figures were produced using SHELXTL PC. [5]

5.2 Experimental Details for Chapter Two

Reaction of $Ru_4(\mu\text{-}H)_4(CO)_{12}$ 1 with Pyridine and 1.1 Equivalents of Me_3NO

The compound $Ru_4(\mu\text{-}H)_4(CO)_{12}$ **1** (150 mg) was dissolved in dichloromethane (100 ml) and cooled to -78 °C in a dry ice/acetone bath, which resulted in slight precipitation and the solution looking pale orange/yellow in colour. An excess of the pyridine ligand (*ca.* 1 ml) was then added before Me_3NO (17.6 mg, 1.2 mol. equiv.) in CH_2Cl_2 (25 ml) was added dropwise to the solution over a period of 15 minutes. The mixture was then stirred for a further 15-20 minutes, over which time the solution was allowed to warm up to room temperature and was observed to change colour from yellow to orange to finally red/orange. The solvent and excess pyridine were removed under vacuum on a Schlenk line, and the residue separated by tlc using hexane-dichloromethane (7:3 v/v) as eluent. (It was found that without high temperatures, the vacuum produced by a water pump was insufficient to remove the pyridine, and caused problems with the separation). Three products were isolated and characterised. The major orange/red product was identified as $Ru_4(\mu\text{-}H)_4(CO)_{10}(py)_2$ **4** on the basis of spectroscopic and single crystal X-ray crystallographic data, with a relatively high yield of the unreacted cluster **1** also being recovered. The predicted product $Ru_4(\mu\text{-}H)_4(CO)_{11}(py)$ **3** was assigned by mass spectroscopy and represents the minor product of the reaction. It is important to note that this species appears to only be produced when undistilled CH_2Cl_2 is used, with dried CH_2Cl_2 the product is apparently not formed.

Spectroscopic data for $Ru_4(\mu\text{-}H)_4(CO)_{11}(py)$ **3**: IR (CH_2Cl_2): ν(CO) 2087 (vw, sh), 2080 (m), 2066 (s), 2056 (m), 2029 (m), 2022 (m, sh), 2006 (w), 1989 (vw, br) cm^{-1}; MS: M^+= 796 (calc. 795) amu.

Spectroscopic data for $Ru_4(\mu\text{-}H)_4(CO)_{10}(py)_2$ **4**: IR (CH_2Cl_2): ν(CO) 2075 (m), 2043 (s), 2020 (s), 1999 (s), 1976 (m), 1958 (sh) cm^{-1}; ^1H NMR (CD_2Cl_2): δ 8.39 (dd, 4H), 7.75 (tt, 2H), 7.29 (ddd, 4H), -14.30 (s, 2H), -21.45 (s, 2H) ppm; MS: M^+= 847 (calc. 846) amu.

Crystal measurement and details for $Ru_4(\mu\text{-}H)_4(CO)_{10}(py)_2$ **4**: Formula $C_{20}H_{14}N_2O_{10}Ru_4$, M.Wt. 846.61 amu, crystal size/mm 0.27 x 0.16 x 0.08, crystal system Monoclinic, space group $P2_1/c$, a= 8.6732 (12) Å, b= 19.054 (2) Å, c= 16.275 (2) Å, β= 92.70 (2) °, Volume= 2686.7 (6) $Å^3$, Z= 4, F(000)= 1616, ρ_{calc}= 2.093 gcm^{-3}, λ (Mo-K_α)= 0.71073 Å, temperature 298 (2) K, 2θ range= 5.0 to 50.0 °, measured reflections 4731, unique observed reflections [I>2σ(I)] 4715, No. of refined parameters 338, goodness of fit on F^2 1.132, final refinement factor indices (R) [I>2σ(I)] R1= 0.0469, wR2= 0.0820, R indices (all data) R1= 0.0808, wR2= 0.1044. A final difference electron density Fourier synthesis revealed maximum and minimum residual electron density peaks of 0.641 and -0.679 e $Å^{-3}$, which were located in close proximity to ruthenium atoms.

Reaction of $Ru_4(\mu\text{-}H)_4(CO)_{12}$ 1 with Pyridine and 2.2 Equivalents of Me_3NO

To a solution of the $Ru_4(\mu\text{-}H)_4(CO)_{12}$ cluster **1** (210 mg, 150 ml CH_2Cl_2) at -78 °C was added an excess of pyridine (*ca.* 1 ml). The solution was then chemically activated by the dropwise addition of 2.2 molar equivalents of Me_3NO (44 mg, 25ml CH_2Cl_2) over a 20 minute period. On slowly warming to room temperature the solution changed colour from yellow to red/orange as the reaction proceeded. The sample was then treated as before and the cluster $Ru_4(\mu\text{-}H)_4(CO)_{10}(py)_2$ **4** isolated by tlc in a higher yield than previously, when only 1.1 molar equivs. were used. Only a trace of the unreacted parent cluster was found to be present.

Reaction of $Ru_4(\mu\text{-}H)_4(CO)_{12}$ 1 with Pyridine and 4.2 Equivalents of Me_3NO

Treatment of a solution of **1** (150 mg) at -78 °C in dichloromethane (150 ml) with Me_3NO (64 mg, 4.2 mol. equivs., 25 ml CH_2Cl_2) in the presence of excess pyridine (*ca.* 3 ml) gave cluster **4** $Ru_4(\mu\text{-}H)_4(CO)_{10}(py)_2$ in 34% yield from a tlc separation using hexane:dichloromethane (7:3 v/v) as previously.

*Attempted Orthometallation of $Ru_4(\mu\text{-}H)_4(CO)_{10}(py)_2$ **4***

Cluster **4** (20 mg) was suspended in octane (10 ml) and a slight excess of pyridine (ca. 0.5 ml) added to inhibit the possible elimination of pyridine from the cluster. The solution was then heated under a nitrogen atmosphere and became bright yellow in colour, although some decomposition to a dark brown unidentified insoluble precipitate did occur. The solution, although hot, never reached reflux when this changed was observed. A single yellow/green product was separated by column chromatography using acetone-hexane (7:3 v/v) as eluent. Attempts to gain mass spectral data proved unsuccessful, and the crystals grown were not of sufficiently high quality for single X-ray diffraction studies to be carried out.

Spectroscopic data: IR (CH_2Cl_2): ν(CO) 2078 (vw, sh), 2067 (m/w), 2061 (m/w), 2006 (vw), 1992 (m/w, br), 1982 (w, br), 1958 (m) cm^{-1}.

*Synthesis of $Ru_4(\mu\text{-}H)_4(CO)_{10}(bipy)$ **5***

An excess of 2,2'-bipyridyl (96 mg) in CH_2Cl_2 (10 ml) was added to a solution of the $Ru_4(\mu\text{-}H)_4(CO)_{12}$ cluster **1** (200 mg, in 150 ml CH_2Cl_2) and reacted in the presence of both 1.1 and 2.2 equivalents of Me_3NO as previously described. The reaction mixture was observed to change in colour from yellow/orange to green on gradual warming and finally to deep red/brown on reaching room temperature. Two products were separated and characterised as unreacted starting material, and $Ru_4(\mu\text{-}H)_4(CO)_{10}(bipy)$ **5** as the major product. The relative yield of cluster **5** was found to increase when 2.2 equivalents of Me_3NO were used.

Product separation was achieved after the removal of solvent *in vaccuo* using either tlc with hexane-dichloromethane (3:7 v/v) as eluent or by column chromatography using initially hexane-dichloromethane (1:9 v/v) to remove unreacted cluster, followed by stepwise elution with increasingly more concentrated dichloromethane solutions to remove the red product band **5**.

Spectroscopic data for $Ru_4(\mu\text{-}H)_4(CO)_{10}$(bipy) **5**: IR ($CH_2Cl_2$): ν(CO) 2074 (m), 2042 (s), 2018 (s), 1999 (m), 1977 (m) cm^{-1}; ^1H NMR ($CDCl_3$): δ 8.92 (dd, *J*= 5.78 Hz, 2H), 8.11 (dd, *J*= 6.6 Hz, 2H), 7.76 (td, *J*= 7.52, 1.55 Hz, 2H), 7.44 (ddd, *J*= 7.49, 5.61, 1.49 Hz, 2H), -15.00 (s, 2H), -21.45 (s, 2H) ppm; MS: M^+= 845 (calc. 844) amu.

Crystal measurement and details for $Ru_4(\mu\text{-}H)_4(CO)_{10}$(bipy) **5**: Formula $C_{20}H_{12}N_2O_{10}Ru_4.¼CH_2Cl_2$, M.Wt. 865.83 amu, crystal size/mm 0.66 x 0.47 x 0.47, crystal system Triclinic, space group P-1, a= 8.6204 (10) Å, b= 9.9099 (12) Å, c= 16.431 (2) Å, α= 73.625 (10) °, β= 84.345 (10) °, γ= 88.371 (9) °, Volume= 1340.1 (3) $Å^3$, Z= 2, F(000)= 825, ρ_{calc}= 2.146 gcm^{-3}, λ (Mo-K_α)= 0.71073Å, temperature 298 (2) K, 2θ range= 5.2 to 50.1 °, measured reflections 4728, unique observed reflections [I>2σ(I)] 4720, No. of refined parameters 351, goodness of fit on F^2 1.199, final refinement factor indices (R) [I>2σ(I)] R1= 0.0347, wR2= 0.0994, R indices (all data) R1= 0.0376, wR2= 0.1054. A final difference electron density Fourier synthesis revealed maximum and minimum residual electron density peaks of 2.566 and -0.545 e $Å^{-3}$, which were located in close proximity to ruthenium atoms.

Preparation of $Ru_4(\mu\text{-}H)_4(CO)_{10}$(phen) 6

To a dichloromethane solution of $Ru_4(\mu\text{-}H)_4(CO)_{12}$ **1** (140mg in 150 ml solvent) cooled to -78 °C, was added an excess of 1,10-phenanthroline (40mg in 10 ml CH_2Cl_2) and the reaction activated by the dropwise addition of Me_3NO (30 mg, 2.1 mol. equivs., in 25 ml CH_2Cl_2) over a 20 minute period. The reaction was then allowed to warm gradually to room temperature to give an orange/red solution. Removal of solvent under vacuum followed by product separation by tlc using initially hexane-dichloromethane (1:1 v/v) as eluent, followed by 100% dichloromethane to shift the band further from the baseline was carried out. A small amount of the unreacted cluster was recovered, but the major product was characterised as $Ru_4(\mu\text{-}H)_4(CO)_{10}$(phen) **6**. Single crystals suitable for diffraction were grown from a solution of hexane-dichloromethane at 5 °C.

Spectroscopic data for $Ru_4(\mu\text{-}H)_4(CO)_{10}$(phen) **6**: IR ($CH_2Cl_2$): ν(CO) 2074 (m), 2042 (s), 2018 (s), 1998 (m), 1976 (m) cm^{-1}; ^1H NMR ($CDCl_3$): δ 9.22 (dd, *J*= 1.3, 5.2 Hz, 2H), 8.48 (dd, *J*= 1.3, 8.2 Hz, 2H), 8.02 (s, 2H), 7.79 (dd, *J*= 5.2, 8.2 Hz, 2H), -15.65 (s, 2H), -21.03 (s, 2H) ppm; MS: M^+= 870 (calc. 868) amu.

Crystal measurement and details for $Ru_4(\mu\text{-}H)_4(CO)_{10}(phen)$ **6**: Formula $C_{22}H_{12}N_2O_{10}Ru_4.\frac{1}{2}CH_2Cl_2$, M.Wt. 911.08 amu, crystal size/mm 0.19 x 0.12 x 0.12, crystal system Triclinic, space group P-1, a= 9.113 (2) Å, b= 10.022 (2) Å, c= 15.674 (3) Å, α= 105.77 (2) °, β= 96.94 (1) °, γ= 93.52 (2) °, Volume= 1360.9 (5) $Å^3$, Z= 2, F(000)= 870, ρ_{calc}= 2.223 gcm^{-3}, λ (Mo-K_α)= 0.71073 Å, temperature 150 (2) K, 2θ range= 5.4 to 45.0 °, measured reflections 3561, unique observed reflections [I>2σ(I)] 3551, No. of refined parameters 383, goodness of fit on F^2 1.056, final refinement factor indices (R) [I>2σ(I)] R1= 0.0256, wR2= 0.0675, R indices (all data) R1= 0.0330, wR2= 0.0744. A final difference electron density Fourier synthesis revealed maximum and minimum residual electron density peaks of 0.758 and -1.035 e $Å^{-3}$, which were located in close proximity to ruthenium atoms.

Synthesis of $Ru_4(\mu\text{-}H)_4(CO)_{10}(dmp)$ 7

Neocuproine dihydrate (69 mg) in CH_2Cl_2 (10 ml) was added to a solution of the parent $Ru_4(\mu\text{-}H)_4(CO)_{12}$ cluster **1** (200 mg, in 150 ml CH_2Cl_2) at -78 °C before adding Me_3NO (30 mg, 2.1 mol. equivs., in 25 ml CH_2Cl_2) dropwise over a 30 minute period. The orange/red solution thus produced on warming to room temperature was then reduced in volume under vacuum and separated by column chromatography. A little of the unreacted cluster was eluted by hexane-dichloromethane (9:1 to 8.5:1.5 v/v), followed by elution with a more polar mixture (3:2 v/v) to isolate the major orange product which was characterised as $Ru_4(\mu\text{-}H)_4(CO)_{10}(dmp)$ **7**.

Spectroscopic data for $Ru_4(\mu\text{-}H)_4(CO)_{10}(dmp)$ **7**: IR (CH_2Cl_2): ν(CO) 2074 (m), 2043 (s), 2018 (s), 1999 (m), 1977 (m), 1955 (sh) cm^{-1}; ^1H NMR ($CDCl_3$): δ 8.26 (d, *J*= 8.31 Hz, 2H), 7.82 (s, 2H), 7.67 (d, *J*= 8.32 Hz, 2H), 3.15 (s, 6H), -16.04 (s, 2H), -21.03 (s, 2H) ppm; MS: M^+= 899 (calc. 896) amu. Analytical data, $C_{24}H_{16}N_2O_{10}Ru_4$ found (calc.): 31.84 (32.15) %C, 1.77 (1.80) %H, 2.73 (3.12) %N.

Crystal measurement and details for $Ru_4(\mu\text{-}H)_4(CO)_{10}(dmp)$ **7**: Formula $C_{24}H_{16}N_2O_{10}Ru_4$, M.Wt. 896.67 amu, crystal size/mm 0.47 x 0.47 x 0.35, crystal system Triclinic, space group P-1, a= 8.798 (4) Å, b= 12.745 (7) Å, c= 13.147 (6) Å, α= 95.73 (7) °, β= 108.93 (3) °, γ= 94.31 (4) °, Volume= 1378.4 (1) $Å^3$, Z= 2, F(000)= 860, ρ_{calc}= 2.160 gcm^{-3}, λ (Mo-K_α)= 0.71073 Å, temperature 150 (2) K, 2θ range= 6.2 to 50.0 °, measured reflections 4933, unique observed reflections [I>2σ(I)] 4326, No. of refined parameters 376, goodness of fit on F^2 1.257, final refinement factor indices (R) [I>2σ(I)] R1= 0.0214, wR2= 0.0559, R indices (all data) R1= 0.0242, wR2= 0.0860. A final difference electron density Fourier synthesis revealed maximum and minimum residual

electron density peaks of 0.486 and -0.635 e $Å^{-3}$, which were located in close proximity to ruthenium atoms.

Preparation of $Ru_4(\mu\text{-}H)_4(CO)_{10}(bpm)$ 9

To a dichloromethane solution of $Ru_4(\mu\text{-}H)_4(CO)_{12}$ **1** (190mg in 150 ml solvent) cooled to -78 °C, was added an excess of 2,2'-bipyrimidine (122 mg in 10 ml CH_2Cl_2) and the reaction activated by the dropwise addition of Me_3NO (41 mg, 2.2 mol. equivs., in 25 ml CH_2Cl_2) over a 20 minute period. Initially the solution was observed to turn green before warming completely to room temperature to give a dark red/brown solution. It was necessary to keep the green solution cooled to minimise conversion to the final red/brown product **9**. Rapid transfer to an IR cell allowed its spectrum to be recorded. On the basis of its spectrum and comparison with that for $Ru_4(\mu\text{-}H)_4(CO)_{11}(py)$ **3**, this species was tentatively assigned as $Ru_4(\mu\text{-}H)_4(CO)_{11}(bpm)$ **8**.

Removal of solvent under vacuum followed by product separation by tlc using 100% CH_2Cl_2 as eluent allowed one product to be isolated, which was characterised by both spectroscopy and a single crystal X-ray diffraction study as $Ru_4(\mu\text{-}H)_4(CO)_{10}(bpm)$ **9**. Single crystals suitable for diffraction were grown from a solution of hexane-dichloromethane at -20 °C.

Spectroscopic data for $Ru_4(\mu\text{-}H)_4(CO)_{11}(bpm)$ **8**: IR (CH_2Cl_2): ν(CO) 2080 (m), 2066 (s), 2053 (m), 2029 (m), 2022 (m), 2005 (w) cm^{-1}.

Spectroscopic data for $Ru_4(\mu\text{-}H)_4(CO)_{10}(bpm)$ **9**: IR (CH_2Cl_2): ν(CO) 2076 (m), 2045 (s), 2020 (s), 2002 (m), 1981 (m/w) cm^{-1}; ^1H NMR ($CDCl_3$): δ 9.16 (dd, *J*= 2.17, 4.74 Hz, 2H), 9.07 (dd, *J*= 2.15, 5.66 Hz, 2H), 7.62 (dd, *J*= 4.80, 5.61 Hz, 2H), -15.9 (s, 2H), -21.5 (s, 2H) ppm; MS: M^+= 848 (calc. 846) amu. Analytical data, $C_{17}H_{10}N_4O_{10}Ru_4$ found (calc.): 25.68 (25.53) %C, 1.37 (1.18) %H, 6.18 (6.62) %N.

Crystal measurement and details for $Ru_4(\mu\text{-}H)_4(CO)_{10}(bpm)$ **9**: Formula $C_{18}H_8N_4O_{10}Ru_4.CH_2Cl_2$, M.Wt. 929.49 amu, crystal size/mm 0.27 x 0.19 x 0.08, crystal system Monoclinic, space group $P2_1/c$, a= 8.474 (2) Å, b= 18.897 (4) Å, c= 18.400 (5) Å, β= 92.15 (2) °, Volume= 2944.4 (1) $Å^3$, Z= 4, F(000)= 1768, ρ_{calc}= 2.097 gcm^{-3}, λ (Mo-K_α)= 0.71073 Å, temperature 150 (2) K, 2θ range= 5.2 to 45.0 °, measured reflections 4549, unique observed reflections [I>2σ(I)] 3842, No. of refined parameters 395, goodness of fit on F^2 1.056, final refinement factor indices (R) [I>2σ(I)] R1= 0.0431, wR2= 0.1024, R indices (all data) R1= 0.0623, wR2= 0.1151. A final difference electron density Fourier synthesis revealed maximum and minimum residual electron density peaks of 1.885 and -0.529 e $Å^{-3}$, which were located in close proximity to ruthenium atoms.

Attempted Synthesis of $Ru_4(\mu\text{-}H)_4(CO)_8(bpm)_2$

A solution of the parent carbonyl cluster $Ru_4(\mu\text{-}H)_4(CO)_{12}$ **1** (155 mg dissolved in 150 ml CH_2Cl_2) was cooled to -78 °C before the addition of bipyrimidine (91 mg, 2.8 mol. equivs., dissolved in 10 ml CH_2Cl_2). Me_3NO (66mg, 4.2 mol. equivs. in 25 ml CH_2Cl_2) was then dripped into the reaction mixture over a 20 minute period. The solution was observed to change colour from dark green to deep red on gradual warming to room temperature. A large amount of insoluble material, considered to be decomposition products, was formed in addition to a red product which was purified by tlc (100 % dichloromethane as eluent) and identified by IR and mass spectroscopy as $Ru_4(\mu\text{-}H)_4(CO)_{10}(bpm)$ **9** and not $Ru_4(\mu\text{-}H)_4(CO)_8(bpm)_2$.

*Synthesis of $Ru_4(\mu\text{-}H)_4(CO)_{10}(bpp)$ **10***

An excess of 2,3-bis(2-pyridyl)pyrazine (204 mg) in CH_2Cl_2 (10 ml) was added to a solution of the $Ru_4(\mu\text{-}H)_4(CO)_{12}$ cluster **1** (210 mg, in 150 ml CH_2Cl_2) at -78 °C and Me_3NO (48 mg, 2.2 mol. equivs., in 25 ml CH_2Cl_2) dripped slowly into the reaction flask over a 20 minute period. The sample was then allowed to gradually warm to room temperature. The resulting dark red solution was then reduced in volume under vacuum and separated by tlc. 100% CH_2Cl_2 was found to be the most effective eluent in moving the major red product band from the baseline. Again a trace of unreacted cluster was also detected. The red product was characterised as

$Ru_4(\mu\text{-}H)_4(CO)_{10}$(bpp) **10** on the basis of spectroscopic evidence only. Despite repeated attempts, single crystals suitable for diffraction were never grown.

Spectroscopic data for $Ru_4(\mu\text{-}H)_4(CO)_{10}$(bpp) **10**: IR ($CH_2Cl_2$): ν(CO) 2075 (m), 2044 (s), 2020 (s), 2001 (m/s), 1979 (m), 1944 (sh) cm^{-1}; ^1H NMR ($CDCl_3$): δ 8.92 (d, *J*= 2.96 Hz, 1H), 8.89 (d, 1H), 8.68 (d, 2H), 8.66 (d, *J*= 2.90 Hz, 1H), 8.04 (td, *J*= 1.75, 7.71 Hz, 1H), 7.94 (ddd, *J*= 1.11, 1.21, 7.90 Hz, 1H), 7.56 (m, 2H), 7.34 (ddd, *J*= 1.45, 5.45, 7.62 Hz, 1H), 7.04 (d, *J*= 8.37 Hz, 1H), -16.0 (vw, br) ppm; MS: M^+= 925 (calc. 922) amu.

*Reaction of $Os_4(\mu\text{-}H)(CO)_{10}(MeCN)_2$ **11** with Pyridine*

$Os_4(\mu\text{-}H)(CO)_{10}(MeCN)_2$ **11** was prepared from $Os_4(\mu\text{-}H)(CO)_{12}$ (150 mg) as previously described by Chen *et al.* [6] The solution was then filtered through silica to remove any decomposition products, the solvent removed *in vaccuo* and a CH_2Cl_2 solution (30 ml) prepared to which an excess of pyridine (*ca.* 0.5 ml) was added. The solution was then heated at reflux for one hour and allowed to cool. Reduction of the solvent volume followed by separation by tlc using 7:3 (v/v) dichloromethane/hexane as eluent allowed the separation of three products: $Os_4(\mu\text{-}H)(CO)_{11}$(py) **12** (major product), unreacted $Os_4(\mu\text{-}H)(CO)_{10}(py)_2$ **13** in similar yield, and $Os_4(\mu\text{-}H)(CO)_{10}(MeCN)_2$ **11** as a minor product.

Spectroscopic data for $Os_4(\mu\text{-}H)_4(CO)_{10}(MeCN)_2$ **11**: IR (MeCN): ν(CO) 2080 (w), 2051 (m), 2019 (s), 1998 (vs), 1983 (s), 1944 (w) cm^{-1}; MS: M^+= 1124 (calc. 1126) amu.

Spectroscopic data for $Os_4(\mu\text{-}H)_4(CO)_{11}$(py) **12**: IR ($CH_2Cl_2$): ν(CO) 2090 (w), 2058 (s), 2050 (s), 2029 (s), 2003 (m, sh), 1994 (m), 1986 (m, sh), 1960 (vw), 1945 (vw) cm^{-1}; ^1H NMR ($CDCl_3$): δ 8.72 (d, *J*= 5.12 Hz, 2H), 7.93 (ddd, *J*=1.59, 3.00, 7.64 Hz, 1H), 7.63 (dd, *J*= 6.70, 7.53 Hz, 2H), -17.89 (s, br, 3H), -24.3 (s, vw, br, 1H) ppm; MS: M^+= 1152 (calc. 1151) amu.

Spectroscopic data for $Os_4(\mu\text{-}H)_4(CO)_{10}(py)_2$ **13**: IR (CH_2Cl_2): ν(CO) 2080 (m), 2049 (vs), 2020 (s), 1998 (s), 1976 (m, br) cm^{-1}; MS: M^+= 1254 (calc. 1253) amu.

*Reaction of $Os_4(\mu\text{-}H)_4(CO)_{11}(MeCN)$ **14** and Pyridine*

The yellow cluster $Os_4(\mu\text{-}H)_4(CO)_{11}(MeCN)$ **14** was prepared by the dropwise addition of 1.2 equivalents of Me_3NO (7.9 mg) in MeCN (25 ml) to $Os_4(\mu\text{-}H)_4(CO)_{12}$ (99.2 mg, in 25ml MeCN) over 20 minutes. The solvent was then removed *in vaccuo* and the cluster dissolved in CH_2Cl_2 (20 ml) and heated under reflux for 18 hours in the presence of an excess of pyridine (0.5 ml). The products were separated by tlc using 3:2 (v/v) dichloromethane-hexane as eluent, and $Os_4(\mu\text{-}H)_4(CO)_{10}(py)_2$ **13** was identified on the basis of spectroscopy.

Spectroscopic data for $Os_4(\mu\text{-}H)_4(CO)_{11}(MeCN)$ **14**: IR (MeCN): ν(CO) 2081 (vw, sh), 2058 (m), 2052 (m), 2027 (m, sh), 2020 (s), 1999 (s), 1983 (m), 1955 (sh) cm^{-1}; MS: M^+= 1115 (calc. 1113) amu.

*Reaction of $Os_4(\mu\text{-}H)(CO)_{10}(MeCN)_2$ **11** with 2,2'-Bipyridyl*

An excess of 2,2'-bipyridyl (33 mg) in CH_2Cl_2 (10 ml) was added to a CH_2Cl_2 solution of the $Os_4(\mu\text{-}H)_4(CO)_{10}(MeCN)_2$ cluster **11** (prepared as previously described using 100 mg $Os_4(\mu\text{-}H)_4(CO)_{12}$ in 25 ml MeCN) and heated at reflux for 18 hours. Product separation was achieved after the removal of solvent *in vaccuo* using tlc with dichloromethane-hexane (1:1 v/v) as eluent initially. The desired red/brown product was then isolated and purified further by tlc using dichloromethane-hexane(7:3 v/v) as eluent.

Spectroscopic data for $Os_4(\mu\text{-}H)_4(CO)_{10}(bipy)$ **15**: IR (CH_2Cl_2) ν(CO): 2078 (m), 2048 (w), 2017 (s), 1996 (s), 1980 (m), 1972 (m), 1954 (w, sh), 1931 (w, sh) cm^{-1}; ^1H NMR ($CDCl_3$): δ 9.27 (s, br, 2H), 8.17 (dd, *J*=7.92 Hz, 2H), 8.06 (d, *J*= 7.42 Hz, 2H), 7.46 (dd, *J*= 6.45Hz, 2H), *ca.* -18.3 (vw), *ca.* -21.5 (vw), ppm; MS: M^+= 1203 (calc. 1200) amu.

Note: Where only one coupling constant has been quoted in *e.g.* a doublet of doublet resonance, it is the result of the other coupling being too small to measure, although it is apparent by eye.

Reaction of $Os_4(\mu\text{-}H)(CO)_{10}(MeCN)_2$ 11 with 1,10-Phenanthroline

$Os_4(\mu\text{-}H)_4(CO)_{10}(MeCN)_2$ was prepared from 129 mg of the parent cluster **2** as previously described and refluxed in CH_2Cl_2 (30 ml) in the presence of excess phenanthroline (40 mg) for 20 minutes. The resulting dark brown was then reduced in volume and separated into its fractions by tlc using initially hexane/dichloromethane (1:1 v/v) as eluent. The desired red product was then isolated and purified further by tlc using hexane/dichloromethane (3:2 v/v) as eluent.

Spectroscopic data for $Os_4(\mu\text{-}H)_4(CO)_{10}(phen)$ **16**: IR (CH_2Cl_2) ν(CO): 2078 (m), 2048 (vs), 2017 (s), 1996 (s), 1978 (w, sh), 1972 (m), 1931 (w, sh) cm^{-1}; ^1H NMR ($CDCl_3$): δ 9.55 (s, br, 2H), 8.55 (dd, *J*=8.17 Hz, 2H), 8.07 (s, 2H), 7.80 (dd, *J*= 5.36, 8.14 Hz, 2H), -18.13 (s, br, 1H), -18.76 (s, br, 1H), -20.69 (s, br, 1H), -21.28 (s, br, 1H) ppm; MS: M^+= 1225 (calc. 1224) amu.

5.3 Experimental Details for Chapter Three

Reaction of $Ru_5C(CO)_{15}$ 17 with Pyridine

A solution of $Ru_5C(CO)_{15}$ (108 mg, 100 ml CH_2Cl_2) was cooled to -78 °C and an excess of pyridine (*ca.* 1 ml) added. Chemical activation of the cluster was then carried out at this temperature by the dropwise addition of 1.1 molar equivalents of Me_3NO (10 mg in 25 ml CH_2Cl_2) to give an orange solution. On gradual warming to room temperature the solution became darker: ultimately red/ brown in colour. The solution was then filtered through a short silica column and washed first with dichloromethane and then acetone. Reduction of the solvent volume under vacuum followed by separation by tlc using hexane-dichloromethane (3:2 v/v) allowed product separation.

Spectroscopic data for $Ru_5(\mu\text{-}H)C(CO)_{12}(C_5H4N)(py)$ **21**: IR (CH_2Cl_2) ν(CO): 2102 (w), 2085 (m), 2076 (w, sh), 2048. (vs), 2041 (vs, sh), 2029 (s), 1988 (m, br) cm^{-1}; IR (Hexane) ν(CO): 2100 (w), 2086 (m), 2073 (m/w), 2056 (m), 2051 (vs), 2042 (m), 2031 (m), 2016 (w), 2007 (w), 2000 (m), 1991 (m), 1971 (m/w), 1966 (m/w, sh) cm^{-1};

^{1}H NMR ($CDCl_3$): δ 8.83 (dd, *J*= 1.41, 5.78 Hz, 2H), 7.98 (td, *J*= 1.50 ,7.58 Hz, 1H), 7.83 (dd, *J*= 5.48 Hz, 1H), 7.53 (m, 3H), 6.85 (dddd, *J*= 1.77, 7.34, 7.97 Hz, 1H), 6.39 (dddd, 1.52, 6.02 Hz,1H), -21.32 (s, 1H) ppm; MS: M+= 1011 (calc. 1011) amu.

Reaction of $Ru_5C(CO)_{15}$ 17 with 2,2'-Bipyridyl

The compound $Ru_5C(CO)_{15}$ **17** (88 mg) was dissolved in dichloromethane (50 ml), and cooled to -78 °C before the addition of an excess of 2,2'-bipyridyl (44 mg in 10 ml CH_2Cl_2). A solution of Me_3NO (15.4 mg, 2.1 mol. equivs.) in 25 ml dichloromethane was added dropwise over a period of 20 minutes, before being allowed to warm to room temperature gradually. The solution became dark red/brown in colour and was reduced *in vaccuo* and the residue separated by column chromatography. Initially 7:3 hexane:dichloromethane was used as the eluent and a gradient elution followed to remove first the yellow cluster $Ru_5(\mu\text{-}H)C(CO)_{13}(C_{10}H_7N_2)$ **24** and then the major red cluster $Ru_5C(CO)_{14}$(bipy) **23** which were identified from both spectroscopic and X-ray crystallographic data. Single crystals of compound **23** were grown from a hexane/dichloromethane at 5 °C, and compound **24** was crystallised from a solution of chloroform/hexane at -20 °C.

Spectroscopic data for $Ru_5C(CO)_{14}$(bipy) **23**: IR (CH_2Cl_2): ν(CO) 2074 (m), 2040 (s), 2032 (s), 2013 (m, sh), 2008 (s), 1981 (m), 1960 (m/w, br) cm^{-1}; ^{1}H NMR (d_6-acetone): δ 9.45 (ddd, *J*= 0.75, 1.46, 5.68 Hz, 1H), 8.91 (d, *J*= 0.76, 1.35, 8.43 Hz, 1H), 8.75 (d, *J*= 0.73, 1.3, 8.45 Hz, 1H), 8.56-8.48 (m, 2H), 8.33 (ddd, *J*= 1.60, 7.65, 8.70 Hz, 1H), 8.02 (ddd, *J*= 1.40, 5.72, 7.62 Hz, 1H), 7.74 (ddd, *J*= 1.34, 5.64, 7.65 Hz, 1H) ppm; M^+= 1068 (calc. 1065) amu. Analytical data, $C_{25}H_8N_2O_{14}Ru_5.CH_2Cl_2$ found (calc.): 27.10 (27.14) %C, 0.87 (0.56) %H, 2.43 (2.30) %N.

Crystal measurement and details for $Ru_5C(CO)_{14}$(bipy) **23**: Formula $C_{25}H_8N_2O_{14}Ru_5.CH_2Cl_2$, M.Wt. 1150.61 amu, crystal size/mm 0.85 x 0.45 x 0.20, crystal system Monoclinic, space group $P2_1/c$, a= 10.615 (3) Å, b= 17.967 (5) Å, c= 17.696 (6) Å, β= 100.63 (3) °, Volume= 3317 (2) $Å^3$, Z= 4, F(000)= 2184, ρ_{calc}= 2.304 gcm^{-3}, λ (Mo-K_α)= 0.71073 Å, temperature 150 (2) K, 2θ range= 5.1 to 50.0 °, measured reflections 6083, unique observed reflections [I>2σ(I)] 4796, No. of refined parameters 442, goodness of fit on F^2 1.270, final refinement factor indices (R) [I>2σ(I)] R1= 0.0333, wR2= 0.1048, R indices (all data) R1= 0.0365, wR2= 0.1071.

A final difference electron density Fourier synthesis revealed maximum and minimum residual electron density peaks of 1.199 and -1.391 e $Å^{-3}$, which were located in close proximity to ruthenium atoms.

Spectroscopic data for $Ru_5(\mu\text{-}H)C(CO)_{13}(C_{10}H_7N_2)$ **24**: IR (CH_2Cl_2): ν(CO) 2085 (m), 2046 (s), 2028 (s), 2007 (w), 1992 (sh), 1987 (w/m), 1944 (w, br) cm^{-1}; ^1H NMR ($CDCl_3$): 9.14 (ddd, *J*= 0.81, 1.51, 5.61 Hz, 1H), 8.03 (m, 2H), 7.49 (m, 2H), 7.23 (dd, *J*= *ca.* 7.54, 1H {resonance partially obscured by $CHCl_3$ solvent peak}, 1.26 Hz), 7.01 (t, *J*= 7.76 Hz, 1H) ppm.

Crystal measurement and details for $Ru_5(\mu\text{-}H)C(CO)_{13}(C_{10}H_7N_2)$ **24**: Formula $C_{24}H_8N_2O_{13}Ru_5$, M.Wt. 1037.67 amu, crystal size/mm 0.56 x 0.10 x 0.10, crystal system Monoclinic, space group $P2_1/n$, a= 10.297 (2) Å, b= 17.162 (2) Å, c= 16.803 (2) Å, β= 92.76 (2) °, Volume= 2965.8 (7) $Å^3$, Z= 4, F(000)= 1960, ρ_{calc}= 2.324 gcm^{-3}, λ (Mo-K_α)= 0.71073 Å, temperature 298 K, 2θ range= 3.4 to 50.0 °, measured reflections 6591, unique observed reflections [I>2σ(I)] 5209, No. of refined parameters 398, goodness of fit on F^2 1.132, final refinement factor indices (R) [I>2σ(I)] R1= 0.0436, wR2= 0.0718, R indices (all data) R1= 0.0852, wR2= 0.0964. A final difference electron density Fourier synthesis revealed maximum and minimum residual electron density peaks of 0.573 and -0.657 e $Å^{-3}$, which were located in close proximity to ruthenium atoms.

Reaction of $Ru_5C(CO)_{15}$ 17 with 1,10-Phenanthroline

The compound $Ru_5C(CO)_{15}$ **17** (97 mg) was dissolved in dichloromethane (75ml), and cooled to -78 °C before the addition of an excess of 1,10-phenanthroline (72 mg in 10 ml CH_2Cl_2). A solution of Me_3NO (17.5 mg, 2.2 mol. equivs. in 25 ml dichloromethane) was then added dropwise over a period of 20 minutes. The reactants were then stirred for a further 20 minutes whilst warming to room temperature, producing a dark red/brown solution. Removal of the solvent under reduced pressure followed by tlc separation using a solution 1:1 hexane/dichloromethane as eluent allowed 2 major products to be isolated and characterised. The red cluster $Ru_5C(CO)_{14}$(phen) **25** was formed in relatively higher yields than the yellow cluster $Ru_5(\mu\text{-}H)C(CO)_{13}(C_{12}H_7N_2)$ **26**.

Spectroscopic data for $Ru_5C(CO)_{14}$(phen) **25**: IR (CH_2Cl_2): ν(CO) 2085 (vw), 2074 (m), 2040 (s), 2032 (s), 2013 (m, sh), 2008 (s), 1981 (m), 1961 (m/w, br) cm^{-1};

^{1}H NMR (CD_2Cl_2): δ 9.64 (dd, *J*= 5.33, 1.33 Hz, 1H), 8.83 (dd, *J*= 5.25, 1.46 Hz, 1H), 8.76 (dd, *J*= 8.22, 1.32 Hz, 1H), 8.54 (dd, *J*= 8.25, 1.44 Hz, 1H), 8.13 (dd, *J*= 8.25, 1.44 Hz, 2H), 8.06 (dd, *J*= 8.18, 5.28 Hz, 2H), 7.80 (dd, *J*= 5.24, 8.21 Hz, 1H) ppm; MS: M^+= 1091 (calc. 1089) amu.

Crystal measurement and details for $Ru_5C(CO)_{14}$(phen) **25**: Formula $C_{27}H_8N_2O_{14}Ru_5.½CH_2Cl_2$, M.Wt. 1132.17 amu, crystal size/mm 0.15 x 0.12 x 0.06, crystal system Triclinic, space group P-1 , a= 9.087 (4) Å, b= 13.005 (5) Å, c= 15.597 (7) Å, α= 105.48(3)°, β= 92.96 (3) °, γ= 104.53 (3) °, Volume= 1705.6 (13) Å^3, Z= 2, F(000)= 1074, ρ_{calc}= 2.205 gcm^{-3}, λ (Mo-K$_\alpha$)= 0.71073 Å, temperature 150 (2) K, 2θ range= 5.10 to 50.08 °, measured reflections 6406, unique observed reflections [I>2σ(I)] 6007, No. of refined parameters 455, goodness of fit on F^2 1.062, final refinement factor indices (R) [I>2σ(I)] R1= 0.0338, wR2= 0.0844, R indices (all data) R1= 0.0415, wR2= 0.0907. A final difference electron density Fourier synthesis revealed maximum and minimum residual electron density peaks of 1.532 and -1.005 e Å^{-3}, which were located in close proximity to ruthenium atoms.

Spectroscopic data for $Ru_5(\mu\text{-}H)C(CO)_{13}(C_{12}H_7N_2)$ **26**: IR (CH_2Cl_2): ν(CO) 2085 (m), 2047 (s), 2042 (sh), 2029 (s), 2010 (w), 1993 (sh), 1986 (m), 1945 (w) cm^{-1}; MS: M^+= 1061 (calc 1061) amu.

Reaction of $Ru_6C(CO)_{17}$ 27 with 2,2'-Bipyridyl

To a 150 ml solution of $Ru_6C(CO)_{17}$ **27** (122mg) cooled to -78 °C was added an excess of 2,2'-bipyridyl (60 mg in 10 ml CH_2Cl_2) and Me_3NO (18.7 mg, 2.2 equivalents in 25 ml CH_2Cl_2) added steadily dropwise over a 20 minute period. The solution was then allowed to slowly warm to room temperature and was left to stir for a further 10 minutes on reaching this temperature. Removal of solvent *in vaccuo* and subsequent product separation by tlc using a 1:1 hexane/dichloromethane mixture as eluent led to the isolation of two major products: $Ru_5C(CO)_{14}$(bipy) **23**, and $Ru_6C(CO)_{15}$(bipy) **28**, which were characterised spectroscopically. In addition, single crystals of **23** were grown from a pentane/ethyl acetate solution at 5 °C, and their composition confirmed by their unit cell dimensions.

Crystallographic symmetry and unit cell dimensions for $Ru_5C(CO)_{14}$(bipy) **23**: Crystal system Monoclinic, space group $P2_1/c$, a= 10.633 (1) Å, b= 18.276 (2) Å, c= 17.956 (2) Å, β= 99.04 (1) °, Volume= 3446 $Å^3$.

Spectroscopic data for $Ru_6C(CO)_{15}$(bipy) **28**: IR (CH_2Cl_2): ν(CO) 2070 (m/w), 2018 (s), 1978 (m/w), 1826 (vw, br) cm^{-1} ; MS: M^+= 1165 (calc. 1166) amu.

Reaction of $Ru_6C(CO)_{17}$ 27 with 1,10-Phenanthroline

A solution of $Ru_6C(CO)_{17}$ **27** was dissolved in dichloromethane with rapid stirring over 10 minutes (74 mg in 50 ml) and cooled to -78 °C before the addition of an excess of the 1,10-phenanthroline ligand in dichloromethane (204 mg in 5 ml). 2.2 molar equivalents of a Me_3NO solution (11 mg in 15 ml CH_2Cl_2) was then dripped into the reaction mixture over a 20 minute period and then leaving to stir for a further 10 minutes. The solution became a deeper red colour on gradually warming to room temperature. Reduction of the solvent volume followed by tlc using 1:1 hexane/dichloromethane as eluent allowed the successful separation of two major products which were characterised spectroscopically as $Ru_5C(CO)_{14}$(phen) **25** and $Ru_6C(CO)_{15}$(phen) **29**. In addition the identification of cluster **25** was confirmed from the successful growth of single crystals from a hexane/dichloromethane solution at 5°C, and the determination of their unit cell dimensions.

Crystallographic symmetry and unit cell dimensions for $Ru_5C(CO)_{14}$(phen) **25**: Crystal system Triclinic, space group P-1, a= 9.145 (1) Å, b= 13.102 (1) Å, c= 15.769 (1) Å, α= 104.917 (3) °, β= 92.992 (8) °, γ= 104.817 (8) °, Volume= 3501.8 $Å^3$.

Spectroscopic data for $Ru_6C(CO)_{15}$(phen) **29**: IR (CH_2Cl_2): ν(CO) 2071 (m/w), 2018 (m), 1979 (m/w) cm^{-1}; ^1H NMR ($CDCl_3$): 8.52 (dd, 2H), 8.44 (dd, 2H), 7.98 (s, 2H), 7.70 (q, 2H) ppm. Due to decomposition of the cluster in solution over time the resonances in the NMR were too weak to determine all couplings precisely.

5.4 Experimental Details for Chapter Four

Edinburgh:

Electrochemical Measurements

Cyclic voltammetry studies were carried out using a standard three electrode configuration with a Pt micro- working and counter electrodes, and a Ag|AgCl reference electrode against which the ferrocene|ferrocinium couple was measured at +0.55 V. All data was collected at a scan rate of 100 mVs^{-1} CH_2Cl_2 / $[Bu_4N][BF_4]$ electrolyte solutions of 0.5 M concentration. The solution was purged with a stream of nitrogen gas for *ca.* 20 minutes to ensure the removal of oxygen before measurements were taken.

Spectroelectrochemical Measurements

In situ UV/Vis reduction of $Ru_4(\mu\text{-}H)_4(CO)_{10}$(bpm) **9** was carried out at -20 °C and at a potential of -1.048 V using an Optically Transparent Thin Layer Electrode (OTTLE) cell (Figure 5.4.1). [7] The working electrode is made of a fine platinum gauze which is reinforced with 10% rhodium and has an optical transparency of around 40%. This reduction in transmittance is compensated for by background correction. In the cell the platinum wire counter and Ag|AgCl reference electrodes are isolated from the working electrode by sintered frits. The cell assembly is located within a gas tight, double glazed PTFE block in which the temperature was controlled by a constant flow of precooled nitrogen between the inner windows of the block. Spectra were recorded at 5 minute intervals on a Pekin-Elmer Lamda 9 spectrophotometer, and the chemical reversibility of the system tested by regeneration of the starting material at 0 V.

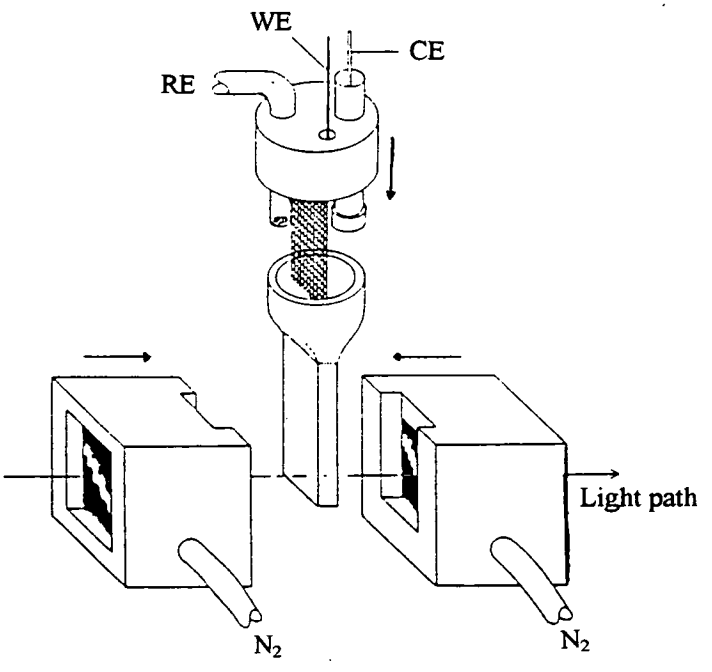

Figure 5.4.1: A schematic representation of the OTTLE cell.
WE= Working Electrode, CE= Counter Electrode, RE= Reference Electrode.

Amsterdam:

Spectroscopic Measurements

IR spectra were recorded on a BioRad FTS-7-FTIR spectrometer (resolution 2 cm^{-1}). Low temperature IR measurements were performed using an Oxford Instrument DN 1704/54 liquid nitrogen cooled cryostat. EPR spectra were recorded on a Varian E6 EPR spectrometer at room temperature and were referenced to DPPH (2,2'-diphenyl-1-picrylhydrazyl) as an internal standard(95 G).

EPR instrument settings for $Ru_4(\mu\text{-}H)_4(CO)_{10}$(bpm) **9**, P= 5 mW; R.G.= 4 x10^3; H_o= 3390 G, ΔH= 200 G; I= 0.1 μA; τ= 0.3s; acquisition time, t= 300 s.

EPR instrument settings for $Ru_4(\mu\text{-}H)_4(CO)_{10}$(bpp) **10**, P= 5 mW; R.G.= 2.5 x10^3; H_o= 3390 G, ΔH= 200 G; I= 0.25 μA; τ= 0.3s; acquisition time, t= 300 s.

Spectroelectrochemical Measurements

An OTTLE cell, [8] equipped with a Pt-minigrid working electrode (32 wires/cm) was used for IR and UV/Vis spectroelectrochemical experiments at room temperature. Spectroelectrochemistry at low temperatures was performed in a home made cryostated OTTLE cell, which has been described in detail elsewhere. [9] NaCl/CaF_2 windows were employed for the IR OTTLE experiments respectively. The working electrode surroundings were masked carefully to avoid the spectral beam passing through the non-electrolysed solution. Cyclic voltammetry and controlled potential electrolysis within the OTTLE cells were carried out using PAR Model 174 and PA4 (Ekom, Czech republic) potentiostats. For all spectroelectrochemical samples the concentration of the complexes and $[Bu_4N][PF_6]$ were 5 $x10^{-3}$ M and 4 $x10^{-1}$ M respectively.

5.5 References

1. M.I. Bruce, M.L. Williams, G. Lavigne, T. Arliguie, *Inorg. Synth,* **26**, 263.
2. C. Zuccaro, G. Pamploni, F. Calderazzo, *Inorg. Synth.*, **26**,293.
3. J. Cosier, A.M. Glazer, *J. Appl. Crystallogr.*, 1986, **19**, 105.
4. G.M. Sheldrick, SHELXL 93, Program for crystal structure refinement, University of Göttingen, Germany, 1993.
5. G.M. Sheldrick, SHELXTL PC, University of Göttingen and Siemens Analytical X-ray Instruments, Madison, 1990.
6. H. Chen, B.F.G. Johnson, J. Lewis, D. Braga, F. Grepioni, E. Parisini, *J. Chem. Soc., Dalton Trans.*, 1991, 215.
7. S.A. MacGregor, E. McInnes, R.J. Sorbie, L.J. Yellowlees, *Moleular Electrochemistry of Inorganic, Bioinorganic, and Organometallic Compounds*, (A.J.L. Pombeiro and J.A. McCleverty eds.), 1993, 503.
8. M. Krejcik, M. Danek, F. Hartl, *J. Electroanal. Chem., Interfacial Electrochem.*, 1991, **317**, 719.
9. F. Hartl, H. Luyten, H.A. Nieuwenhuis, G.C. Schoemaker, *Appl. Spectrosc.*, 1994, **48**, 1522